ABSTRACT

PENDLETON, TERRANCE LAMAR. An Analytical and Numerical Study of a Class of Nonlinear Evolutionary PDEs. (Under the direction of Dr. Alina Chertock.)

This thesis concerns itself with an analytical and numerical study of a family of evolutionary partial differential equations (PDEs) which supports peakon solutions for special values of a given bifurcation parameter. Here, the bifurcation parameter describes the balance between convection and stretching for small viscosity in the dynamics of one dimensional (1D) nonlinear waves in fluids.The first portion of this thesis is to provide global existence and uniqueness results for the considered family of evolutionary PDEs by establishing convergence results for the particle method applied to these equations. This particular class of PDEs is a collection of strongly nonlinear equations which yield traveling wave solutions and can be used to model a variety of flows in fluid dynamics. We apply a particle method to the studied evolutionary equations and provide a new self-contained method for proving its convergence. The latter is accomplished by using the concept of space-time bounded variation and the associated compactness properties. From this result, we prove the existence of a unique global weak solution in some special cases and obtain stronger regularity properties of the solution than previously established.

The second portion of this thesis is dedicated to studying the dynamics of the interaction among a special class of solutions of the one-dimensional Camassa-Holm (CH) equation which are a particular example of such a PDE which supports peakon solutions. The equation yields soliton solutions whose identity is preserved through nonlinear interactions. These solutions are characterized by a discontinuity at the peak in the wave shape and are thus called peakon solutions. We apply a particle method to the CH equation and show that the nonlinear interaction among the peakon solutions resembles an elastic collision, i.e., the total energy and momentum of the system before the peakon interaction is equal to the total energy and momentum of the system after the collision. From this result, we provide several numerical illustrations which supports the analytical study, as well as showcase the merits of using a particle method to simulate solutions to the CH equation under a wide class of initial data.

The final portion of this thesis seeks to investigate the possibility of the two component Camassa-Holm (2CH) equation as a relevant model for the long time propagation of tsunami-like waves. The (2CH) equation is a generalization of the Camassa Holm equation

for which a continuity component for density is incorporated. We show how the 2CH equation can be derived in the context of shallow water wave theory. Furthermore, we solve the considered equations using both a central upwind scheme, and a hybrid particle-finite volume scheme which combines the strengths of both the particle method and central upwind scheme using physically relevant initial data. Our preliminary results show that for a certain range of values of a length scale associated with the CH equation, the shape and amplitude of the waves are preserved for a longer period of time compared with the classical Saint-Venant system for shallow water waves. Furthermore, we show that we can capture these dynamics on a coarser grid by using a hybrid finite volume particle scheme.

An Analytical and Numerical Study of a Class of Nonlinear Evolutionary PDEs

by
Terrance Lamar Pendleton

A dissertation submitted to the Graduate Faculty of
North Carolina State University
in partial fulfillment of the
requirements for the Degree of
Doctor of Philosophy

Applied Mathematics

Raleigh, North Carolina

2013

APPROVED BY:

Dr. Michael Shearer	Dr. Mark Hoefer
Dr. Pierre Gremaud	Dr. Alina Chertock Chair of Advisory Committee

DEDICATION

In memory of my father, Howard L. Pendleton who gave me opportunities he never had.
To my mother, my family and my friends for making sure that I did not lose my mind
in the process.

BIOGRAPHY

Terrance Pendleton was born in New Jersey in March 5, 1986 but was raised in Phenix City, AL, where he is the oldest of two sisters and a brother. He received a B.S. from Alabama Agricultural and Mechanical University in Secondary Mathematics Education. Quickly realizing that being a high school mathematics teacher was not his true calling in life, he immediately enrolled in the Applied Mathematics Ph.D program at North Carolina State University. Following his graduate work, he will join Iowa State University as postdoctoral associate in the Mathematics department.

ACKNOWLEDGEMENTS

It is difficult to find the right combination of a finite number of words to express my gratitude for my advisor, Dr. Alina Chertock. I am eternally grateful for the knowledge, mentoring, care, and patience she bestowed on me. Without her assistance, this endeavor would remain but a dream. I am equally grateful for the contagious love for PDEs that she help instilled in me. I look forward to spreading the same joy and love for this subject to others.

Many other professors and advisors have helped paved the way to obtaining my goal here at NC State. I am thankful for having such a supportive group of members on my thesis committee. With kind words, and constructive feedback, Dr. Mark Hoefer, Dr. Pierre Gremaud, and Dr. Michael Shearer have helped better me as a graduate student, and for this I am forever grateful. Special thanks also goes to professors Dr. Robert Martin and Dr. Sandra Paur for teaching me the tools for not only surviving graduate school but flourishing.

To my parents Howard and Phyllis who have invested so much into me. At every step of the way, they were with me even though they were physically hundred of miles away. Since the instant I was born, they loved and cared for me in a way that I can never fully understand. It is an honor to be their son and to carry their name.

While there can never be a comprehensive list of all of the people on this earth who made this degree a reality, I feel obligated to mention the name of a few friends whose support and guidance meant beyond what they realize. To Kaska Adoteye, George Lankford, Daisy Sudparid, Cre'Shannon Thompson, Karmethia Thompson, Cleveland Waddell, Nakeya Williams, thank you for your friendship. You have offered motivational words and support when I have needed it most and you have helped keep me grounded and in check when appropriate. You have been willing to listen and offer advice when needed, and even laugh at my never ending flow of corny jokes.

Finally, to North Carolina State University, thanks for giving me a great six years.

TABLE OF CONTENTS

LIST OF FIGURES

Chapter 1

Introduction

This thesis concerns itself with an analytical and numerical study of a family of evolutionary partial differential equations (PDEs) which supports a special class of solitary traveling waves for special values of a given bifurcation parameter (b). To this extent, we are are interested in studying

$$m_t + m_x u + bmu_x = 0 \qquad u = G * m, \quad x \in \mathbb{R}, \qquad t > 0, \tag{1.1}$$

with the parameter $b \in \mathbb{R}$ and is considered subject to the initial condition

$$m(x, 0) = m_0(x) \quad x \in \mathbb{R}. \tag{1.2}$$

Here the momentum m and velocity u are functions of the time variable t and the spatial variable x, and $G(x)$ is the Green's kernel which relates m with u through a convolution. The parameter b describes the balance between convection ($m_x u$) and stretching (bmu_x) for small viscosity in the dynamics of one-dimensional (1-D) nonlinear waves in fluids. In other words, the real dimensionless constant b is the ratio of stretching to convection transport. b can also be seen as the number of covariant dimensions associated with the momentum density m as was shown in [80] and provides a balance for the nonlinear solution behavior. We remark that for the remainder of this thesis, we will focus our efforts on (1.1) with $b > 1$ which generates stable solitary traveling waves.

The aim of the first portion of this thesis focuses on establishing global weak solutions and analyzing special solutions for (1.1)-(1.2). In this chapter we provide background information and motivation which is pertinent to the numerical and analytical methods

developed in this thesis. We also provide an outline for the remainder of the thesis.

An important research area in the field of PDEs involves the study and establishment of global solutions for a variety of equations. The equations given by (1.1) (b-equations) are a family of first-order hyperbolic problems and have been studied in a variety of contexts. Moreover, they have been shown to possess several interesting properties. For instance, the b-equations' invariance under space and time translations ensures that it admits traveling wave solutions for $b > 1$ (although this is true for any $b \in \mathbb{R}$). In particular, the traveling wave solutions assume the form $u(x,t) = aG(x-ct)$, with speed $c = -aG(0)$, which is proportional to the solution amplitude and G is the kernel in (1.1). The kernel $G(x)$ relates the velocity with the momentum through the convolution product

$$u = G * m = \int_{\mathbb{R}} G(x-y)m(y,t)\,dy, \tag{1.3}$$

and determines the shape of the traveling wave and the length scale for (1.1); see e.g., [81].

The derivation of traveling wave solutions associated with (1.1) can be found in [80] where

$$u = u(z) \quad \text{and} \quad m = m(z), \quad \text{where} \quad z = x - ct, \tag{1.4}$$

and c is the wave speed. In what follows, we will let $'$ denote d/dz and rewrite (1.1) in the form of the conservation law

$$\left(m^{1/b}\right)_t + \left(m^{1/b}u\right)_x = 0. \tag{1.5}$$

For $b \neq 0$, the conservation law (1.5) for traveling waves becomes

$$\left((u-c)m^{1/b}\right)' = 0, \tag{1.6}$$

which after integrating gives

$$(u-c)^b\, m = K. \tag{1.7}$$

For $b > 0$, (1.1) has nontrivial solutions ($m(x,t)$) vanishing as $|z| \to \infty$ so that $K = 0$ in (1.7). Thus, one obtains

$$(u-c)^b\, m = 0, \tag{1.8}$$

which yields the generalized function solutions

$$m = c\delta(z) \quad \text{and} \quad u = G * m = cG(z),$$

matched by $u - c = 0$ at $z = 0$ and where $\delta(x)$ is the Dirac delta-function. This gives a traveling wave, whose shape in u is given by the kernel G. Nonlinear interactions among these solutions are governed by the following superposition of solutions:

$$u(x,t) = \sum_{i=1}^{N} p_i(t)G(x - q_i(t)). \tag{1.9}$$

This class of solutions satisfy a finite dimensional dynamical system for the amplitudes denoted by $p_i(t)$, and the associated locations denoted by $q_i(t)$.

The family of evolutionary PDEs given by (1.1)–(1.2) arises in diverse scientific applications such as shallow water waves, computational anatomy, mechanical vibrations and turbulent fluid flows (see, e.g. [20, 73, 76, 77, 78]). These equations also enjoys several remarkable properties both in the 1-D and multi-dimensional cases, see, e.g. [16, 110]. The quadratic terms in (1.1) represents the balance in fluid convection between nonlinear transport and amplification due to b-dimensional stretching. If one considers G as the Green's function associated with the modified 1-D Helmholtz operator, $I - \alpha^2\partial_{xx}$, then

$$G(x) = \frac{1}{2\alpha}e^{-|x|/\alpha}, \tag{1.10}$$

and (1.1) reduces to

$$m_t + m_x u + bmu_x = 0 \qquad m = u - \alpha^2 u_{xx}, \quad x \in \mathbb{R}, \qquad t > 0, \tag{1.11}$$

where α is some length scale. If, for example, we consider m as the fluid momentum in (1.11) then we have $b = 2$; see e.g., [81]. It turns out that this case $b = 2$ coincides with the dispersionless case of the Camassa-Holm (CH) equation for shallow water waves. Furthermore, the case for $b = 3$ coincides with the Degasperis-Procesi (DP) equation used to model the propagation of nonlinear dispersive waves, see [55].In this special case, the corresponding traveling wave solutions assume the form $u(x,t) = ae^{-|x-ct|/\alpha}$, with speed c, amplitude a and length α. The traveling wave solutions to (1.11) are characterized by a discontinuity in the first derivative at their peaks since $u_x(x,t) = -\frac{a}{\alpha}\text{sgn}(x-ct)e^{-|x-ct|/\alpha}$ and are thus referred to as peakon solutions. Both the CH and DP

equations are completely integrable as Hamiltonian systems and their peakon solutions are true solitary waves that emerge from the initial data. Peakons for either $b = 2$ or $b = 3$ exhibit a remarkable stability–their identity is preserved through nonlinear interactions, see, e.g. [16, 129] and [53, 54, 55, 110, 117]. Peakons corresponding to $b = 2$ and $b = 3$ are also orbitally stable–i.e. their shape is maintained under small perturbations, see, e.g. [47, 58, 103]. We note that peakons can also be considered as waves of largest amplitude that are exact solutions of the governing equations for irrotational water waves, see [140]. For a more complete discussion on the hydrodynamical properties of peakons generated from the CH or DP equation, we refer the reader to [45, 86].

The two-dimensional (2-D) version of (1.11) with $b = 2$, the so-called EPDiff equation (Euler-Poincaré equation associated with the diffeomorphism group) is given by

$$\frac{\partial \mathbf{m}}{\partial t} + \mathbf{u} \cdot \nabla \mathbf{m} + \nabla \mathbf{u}^{\mathbf{T}} \cdot \mathbf{m} + \mathbf{m}(\operatorname{div} \mathbf{u}) = 0, \quad \mathbf{m} = \mathbf{u} - \alpha^2 \Delta \mathbf{u}, \tag{1.12}$$

and appears in the theory of fully nonlinear shallow water waves [78, 79, 80, 81]. Applying viscosity to the incompressible, three-dimensional analog of this equation produces the Navier-Stokes α-model for the averaged fluid equations (see, e.g., [20]). The equation (1.1) has many further interpretations beyond fluid applications. For instance, in 2D, it coincides with the averaged template matching equation (ATME) for computer vision (see, e.g., [73, 76, 77]). One could also use (1.1) to quantify growth and other changes in shape, such as occurs in a beating heart, by providing the transformative mathematical path between the two shapes, (see, e.g, [78]).

The Cauchy problems for both the CH ($b = 2$) and DP ($b = 3$) equations have been extensively studied in the literature. We refer the reader to a review paper [121], where a survey of recent results on well-posedness and existence of local and global weak solutions for the CH equation is presented. In particular, the local well-posedeness results for the CH equation in $H^s(\mathbb{R}), s > 3/2$, were established in [40, 108, 133]. The continuation of solutions to the CH equation after wave breaking in $L^\infty(\mathbb{R}_+, H^1(\mathbb{R}))$ was established in [11, 12]. The existence of a global weak solution to the CH equation in $L^\infty(\mathbb{R}_+, H^1(\mathbb{R}))$ was proven in [11, 41, 145] and in [46], it was shown that this global solution is unique.

Recent results related to well-posedness and existence of local and global weak solutions of the DP equation can be found, e.g., in [37, 60, 116, 147, 148], where it was proven that the global weak solutions of the DP equation belong to $L^\infty(\mathbb{R}_+, H^1(\mathbb{R}))$ and global entropy weak solutions are in $L^\infty(\mathbb{R}_+, L^1(\mathbb{R}) \cap \mathrm{BV}(\mathbb{R}))$ and $L^\infty(\mathbb{R}_+, L^2(\mathbb{R}) \cap L^4(\mathbb{R}))$. The

local well-posedeness and several global existence results were obtained in [61] for a general case of the initial-value problem (IVP) (1.11), (1.2) with different values of the parameter b.

Capturing peakon solutions numerically poses quite a challenge–especially if one considers a peakon-antipeakon (a peakon with negative initial weight) interaction. Several numerical methods have been proposed for simulating peakon interactions for the CH equation such as finite-difference [38, 74, 75], finite-volume [3] finite-element [119, 132, 146], and spectral [34, 39, 62, 88, 89] methods. A few numerical methods, such as conservative finite-difference schemes, have been used to study the DP equation (see [118]). Many of these methods are computationally intensive and require very fine grids along with adaptivity techniques in order to simulate the peakon behavior.

Solutions of (1.1), (1.2) can be accurately captured by using a particle method as it was shown in our paper [31] as well as in [17, 18, 22] for the CH equation and in [22] for the EPDiff equation. In the particle method, described in our paper [31] and in [22], the solution is sought as a linear combination of Dirac distributions, whose positions and coefficients represent locations and weights of the particles, respectively. The solution is then found by following the time evolution of the locations and the weights of these particles according to a system of ODEs obtained by considering a weak formulation of the problem. The particle methods presented in [17, 18] have been derived using a discretization of a variational principle and provide the equivalent representation of the ODE particle system. The main advantage of particle methods is their (extremely) low numerical diffusion that allows one to capture a variety of nonlinear waves with high resolution, see, e.g., [25, 29, 30, 131] and references therein.

A convergence analysis for the particle method applied to the CH equation was studied in [129] and in our paper [31]. In [129], the authors used the Hamiltonian structure of the CH equation and its complete integrability to establish error estimates for the particle method when the solutions are smooth. In our paper [31], the convergence of the particle method for the CH equation has been proven using the concept of space-time bounded variation. Properties of the particle method were also studied in the context of the DP equation in [53, 54, 55, 81].

The thesis is organized as follows. For the remainder of this chapter, we develop the numerical and analytical techniques that will be pertinent to our study as well as provide background information for the considered equations that we wish to study. In

Chapter 2, we provide global existence and uniqueness results for the family of fluid transport equations given by (1.1) by establishing convergence results for the particle method applied to these equations. In Chapter 3, we study the dynamics of the interaction among a special class of solutions of the 1-D CH equation as well as showcase the merits of using particle methods to simulate solutions to the CH equation using arbitrary smooth initial data. In Chapter 4, we consider a two-component generalization of the CH equation as a possible model for the long time propagation of tsunami waves by implementing a variety of numerical methods with pertinent initial data. In Chapter 5, we conclude the thesis by providing some future goals related to our study.

1.1 Camassa Holm Equation and Its Generalizations

Completely integrable nonlinear evolutionary partial differential equations often arise in various applications in shallow water wave theory. By completely integrable, we mean that there is some change of variables such that the given evolution equation in the new variables is equivalent to a linear flow at constant speed. The Korteweg-de Vries (KdV) equation is perhaps one of the most famous and extensively studied examples in this particular class of equations (see e.g. [90]). The KdV equation is typically regarded as the prototypical example of a nonlinear evolutionary PDE whose solutions can be exactly specified and are given by solitons– localized solutions which undergo a strongly nonlinear complex interaction but retain their form after the interaction, with the possible exception of a phase shift [102]. This thesis concerns itself with the CH equation (and one of its generalizations) which describes surface waves in shallow water.

In 1993, Roberto Camassa and Darryl Holm proposed a new completely integrable dispersive shallow water equation by using an asymptotic expansion directly in the Hamiltonian for Euler's equations in the shallow water regime [129]:

$$m_t + um_x + 2u_x m = -c_0 u_x - \gamma u_{xxx}, \quad m = u - \alpha^2 u_{xx}. \tag{1.13}$$

Here $m = u - \alpha^2 u_{xx}$ is the momentum variable, α^2 and γ/c_0 are squares of length scales, and $c_0 = \sqrt{g'h}$ is the linear wave speed for undisturbed water of depth h at rest under gravity g' at infinity. We note that any constant value $u = u_0$ is also a solution of (1.13).

With an appropriate Galilean transformation and a velocity shift ($t \to t + t_0, x \to x + x_0 + ct, u \to u + c + u_0, m \to m + c + u_0$), one may absorb the linear dispersive terms

as seen in [80]. In this scenario, we are left with the following *dispersionless* CH equation:

$$m_t + um_x + 2u_x m = 0, \quad m = u - \alpha^2 u_{xx}. \tag{1.14}$$

Indeed, one can derive a dispersion relation for (1.1) to understand why (1.1) corresponds to the dispersionless CH equation (for the case $b = 2$). To this extent, we assume a plane wave solution for the momentum m of the form:

$$m(x,t) = m_0 + Ae^{i(kx-\omega t)} = m_0 + v(x,t). \tag{1.15}$$

Here, m_0 is the background uniform momentum, k is the wave number, $|A| \ll 1$ is a small complex parameter (necessary for the linearizion) and ω is the frequency. By a dispersion relation, we seek a relationship between k and ω of the form

$$\omega = \omega(k). \tag{1.16}$$

We calculate u from (1.3) and (1.15) to obtain

$$\begin{aligned} u &= G * (m_0 + v(x,t)) \\ &= G * m_0 + G * v(x,t) \\ &= m_0 \int_{-\infty}^{\infty} G(x-y)\,dy + Ae^{-i\omega t} \int_{-\infty}^{\infty} G(x-y)e^{iky}\,dy \\ &= m_0 \int_{-\infty}^{\infty} G(x-y)\,dy + Ae^{ikx-i\omega t} \int_{-\infty}^{\infty} G(z)e^{-ikz}\,dz \\ &= m_0 \mathscr{F}[G](0) + \mathscr{F}[G](k)v, \end{aligned} \tag{1.17}$$

where $\mathscr{F}[G](k)$ is the Fourier transform of $G(x)$ and is given by

$$\mathscr{F}[G](k) = \int_{-\infty}^{\infty} G(x)e^{-ikx}\,dx. \tag{1.18}$$

We substitute (1.15) and (1.17) into (1.1) to obtain

$$v_t + \left(m_0 \mathscr{F}[G](0) + \mathscr{F}[G](k)v\right) v_x + b\left(m_0 + v\right) \mathscr{F}[G](k) v_x = 0. \tag{1.19}$$

To derive a dispersion relation, we linearize (1.19) to obtain

$$v_t + (m_0 \mathscr{F}[G](0) + b m_0 \mathscr{F}[G](k))\, v_x = 0. \tag{1.20}$$

Using v as was given in (1.15) to calculate v_t and v_x, we obtain the following dispersion relation

$$\omega(k) = k m_0 \left(\mathscr{F}[G](0) + b\mathscr{F}[G](k)\right). \tag{1.21}$$

Assuming that $b \neq 0$, from (1.21), we see that if $m_0 = 0$, then the linearized flow is dispersionless (i.e. $w''(k) = 0$). This is what is meant by the *dispersionless* CH equation.

We recall that traveling waves, associated with differential equations, are solutions of the form

$$u(x,t) = f(x - ct), \tag{1.22}$$

which represents waves of a permanent shape f that propagates at some constant speed c. The waves given by (1.22) are *solitary* if they are localized in the sense that the wave profile decays at infinity. If in addition, these solitary waves retain their shape and speed after interacting with other waves of the same type, then these waves are referred to as solitons. The traveling wave solutions to (1.14) are given by (1.22) with $f(x) = \frac{1}{2\alpha} e^{-|x|/\alpha}$ and are hence referred to as peakons–solitons with a sharp peak that is characterized by a discontinuity in the first derivative. We remark that these particular traveling wave solutions may be easily deduced by taking $G(x)$ as given in (1.10). The interactions among N peakons are given by

$$u(x,t) = \frac{1}{2\alpha} \sum_{i=1}^{N} p_i(t) e^{-|x - q_i(t)|/\alpha}, \tag{1.23}$$

where the amplitudes $p_i(t)$ and the locations $q_i(t)$ are given by a $2N$ dimensional dynamical system (c.f. [129]) to be determined by substituting (1.23) into (1.14). This forms the basis for applying a particle method for numerically simulating solutions to the considered equations. We further discuss the particle method in the sections that follow.

The CH equation models breaking waves as was shown in [18] and [129]. In the situation of a breaking wave, we consider a solution which remains bounded but its slope becomes unbounded in finite time. It was shown in [129] that the only way singularities may arise in solutions to the CH equation is in the form of breaking waves. Moreover,

from the knowledge of a smooth initial profile it is possible to predict the occurrence of wave breaking. If wave breaking occurs, then one can proceed with the continuation of solutions in one of two ways. One may consider either the conservative case which is characterized by the conservation of energy or the dissipative case which accounts for the the loss of energy due to breaking.

In [129], Camassa and Holm first observed that (1.13) was bi-Hamiltonian; that is, the equation can be expressed in Hamiltonian form in two different ways. Recalling that $m = u - \alpha^2 u_{xx}$, the two compatible Hamiltonian descriptions of the CH equations are given by

$$m_t = -\left(m\partial_x + \partial_x m\right)\frac{\delta H_1}{\delta m} = -\partial_x\left(1 - \alpha^2\partial_x^2\right)\frac{\delta H_2}{\delta m} = -\partial_x\frac{\delta H_2}{\delta u}, \tag{1.24}$$

with the following conserved quantities:

$$H_1 = \frac{1}{2}\int_{\mathbb{R}}\left(u^2 + \alpha^2 u_x^2\right)\,dx \quad \text{and} \quad H_2 = \frac{1}{2}\int_{\mathbb{R}}\left(u^3 + \alpha^2 u u_x^2\right)\,dx.$$

Because of this unique property, the CH equation possesses an infinite number of conservation laws. Given the fact that both the KdV equation and the CH equation are completely integrable, it is no surprise that the KdV equation and CH equation are related in some formal way. Indeed, the KdV equation appears at linear order in an asymptotic expansion for unidirectional shallow water waves in a free surface under gravity. The expansion is made in terms of two small dimensionless ratios for small-amplitude long waves in shallow water. At quadratic order in the same asymptotic expansion, the Camassa-Holm equation is derived. We note that the KdV equation may be recovered if we take $\alpha^2 \to 0$. Additional information regarding the derivation and associated properties of the CH equation may be found in [43, 44, 51].

Recently, the CH equation has been extended to a two-component integrable system (2CH) which includes both velocity and density variables in the dynamics. In particular, the CH equation has been extended so as to combine its integrability property with compressibility, or free-surface elevation dynamics in its shallow-water interpretation. This extension involves adding a continuity equation for the scalar density, or total depth, ρ for real functions and including a pressure term involving ρ in the equation for the fluid momentum, as well as the fluid velocity u (see e.g. [42, 82, 84, 107]). To this regard, the 2CH equation is given by the following system of equations

$$\begin{aligned} m_t + um_x + 2mu_x &= -g\rho\rho_x, \\ \rho_t + (\rho u)_x &= 0. \end{aligned} \tag{1.25}$$

Similar to the CH equation, one may derive a dispersion relation for (1.25). To this extent, we assume a plane wave solution for the momentum m and the density ρ of the forms:

$$\begin{aligned} m(x,t) &= m_0 + Ae^{i(kx-\omega t)} = m_0 + v(x,t), \\ \rho(x,t) &= \rho_0 + Be^{i(kx-\omega t)} = \rho_0 + w(x,t). \end{aligned} \tag{1.26}$$

Here, m_0 is the background uniform momentum, ρ_0 is the background uniform density, k is the wave number, $|A|, |B| \ll 1$ are small complex parameters (necessary for the linearizion) and ω is the frequency. By substituting (1.26) and (1.17) into (1.25) and linearizing the results we obtain

$$\begin{aligned} v_t + \left(m_0\mathscr{F}[G](0) + 2m_0\mathscr{F}[G](k)\right) v_x &= -g\rho_0 w_x, \\ \rho_t + \rho_0\mathscr{F}[G](k)v_x + m_0\mathscr{F}[G](0)w_x &= 0. \end{aligned} \tag{1.27}$$

Using our definition for v and w in (1.26), we obtain the following system of equations written in matrix form

$$\begin{bmatrix} -\omega + km_0\left(\mathscr{F}[G](0) + 2\mathscr{F}[G](k)\right) & kg\rho_0 \\ k\rho_0\mathscr{F}[G](k) & -\omega + m_0k\mathscr{F}[G](0) \end{bmatrix} \begin{bmatrix} A \\ B \end{bmatrix} = \begin{bmatrix} 0 \\ 0 \end{bmatrix}$$

Since $A, B \neq 0$, we must have that $\det(M) = 0$ where

$$M = \begin{bmatrix} -\omega + km_0\left(\mathscr{F}[G](0) + 2\mathscr{F}[G](k)\right) & kg\rho_0 \\ k\rho_0\mathscr{F}[G](k) & -\omega + m_0k\mathscr{F}[G](0) \end{bmatrix}.$$

Thus, to find the dispersion relation, we must solve

$$\left(-\omega + km_0\left(\mathscr{F}[G](0) + 2\mathscr{F}[G](k)\right)\right)\left(-\omega + m_0k\mathscr{F}[G](0)\right) - gk^2\rho_0^2\mathscr{F}[G](k) = 0, \tag{1.28}$$

for ω. Solving this quadratic equation for ω yields the following results:

$$\omega(k) = m_0k\mathscr{F}[G](0) + m_0k\mathscr{F}[G](k) \pm \sqrt{m_0^2k^2(\mathscr{F}[G](k))^2 + gk^2\mathscr{F}[G](k)\rho_0^2}. \tag{1.29}$$

This particular multicomponent generalization of the CH equation has been studied extensively and was shown to be completely integrable in [42]. Additionally in [42], it was shown that similar to the CH equation, (1.25) has a Lax pair formulation and is bi-Hamiltonian. Many others studied a modified version of (1.25) which supports peakon solutions (see e.g. [59, 123] and references therein). However, a hallmark feature of (1.25) is that the system was shown to be physically relevant in [42]. There, it was shown how the system given by (1.25) arises in shallow water theory, where it is derived from the Green-Naghdi [69] equations using appropriate expansions in terms of physical parameters. The Green-Naghdi equations themselves are approximate models to the full governing equations [69] and are commonly used in coastal oceanography to describe the propagation of large amplitude surface waves. The shallow water scaling ($\mu \ll 1$), gives rise to the Green-Naghdi equations where μ is a dimensionless parameter given by

$$\mu = \frac{h^2}{\lambda^2},$$

where h is the mean depth and λ is the typical wavelength of the waves under consideration. In [42], it was also shown that the only way for singularities to occur in smooth solutions is through wave breaking–a similar occurrence for the 1-D CH equation. In addition, they were able to establish the global existence of small amplitude solutions of (1.25) and large amplitude traveling wave solutions with initial data that has a sufficient rate of decay. From their investigation, it was determined that unlike the CH equation, the solitary waves generated form (1.25) must be smooth and hence cannot be referred to as peakon solutions. In Chapter 4, we show how the 2CH equation may be derived in the context of shallow water wave theory and from there determine its potential as a relevant model for the long time propagation of tsunami waves.

1.2 Numerical Methods

Because exact answers to mathematical problems derived from real world considerations are usually impossible to find, we employ numerical tools in an attempt to provide adequate approximations to solutions of these problems. Numerical methods are rich and varied and have been used for centuries to approximate solutions and other mathematical quantities of interest. In the field of numerical PDEs, one may consider a variety of numerical methods/tools to approximate a solution to a PDE. For example, one may con-

sider using a finite difference method, for which a function is represented by its values at certain grid points and derivatives are approximated through differences in these values. Another popular numerical tool involves the method of lines, where all but one variable is discretized. The result is a system of ODEs in the remaining continuous variable. One may also consider a finite volume method, where the computational domain is divided into regions or volumes and the change within each volume is computed by considering the flux (flow rate) across the surfaces of the volume. In this thesis, we focus our attention on two particular methods for obtaining a numerical solution for the b-equation of fluid transport equations and its generalizations.

1.2.1 Finite Volume Method For Systems of Conservation Laws

In this section, we describe an important class of numerical methods for solving systems of hyperbolic conservation laws. Finite Volume methods (FV) are typically useful for solving these types of problems thanks to their ability to capture (possibly) discontinuous solutions in an accurate and non-oscillatory manner. To begin the process for formulating a finite volume method for a system of conservation laws, we consider the following (for simplicity) 1-D version of a system of conservation laws:

$$\frac{\partial}{\partial t}\mathbf{q}(x,t) + \frac{\partial}{\partial x}\mathbf{f}(\mathbf{q}(x,t)) = 0, \tag{1.30}$$

where $\mathbf{q} := (q_1, \ldots, q_n)$ and $\mathbf{f} := (f_1, \ldots, f_n)$ are mappings from $\mathbb{R}^n$ into $\mathbb{R}^n$ and (1.30) is subjected to some initial condition of the form

$$\mathbf{q}(x,0) = \mathbf{q}_0(x). \tag{1.31}$$

Here, $\mathbf{q}(x,t)$ is the quantity under consideration, $\mathbf{f}(\mathbf{q})$ is the flux function, and x and t are the spatial and time variables respectively. If we let $\mathbf{A}(\mathbf{q})$ denote the $n \times n$ Jacobian of $\mathbf{f}$ then we may express (1.30) in the following quasilinear form

$$\mathbf{q}_t + \mathbf{A}(\mathbf{q})\mathbf{q}_x = 0, \tag{1.32}$$

with

$$\mathbf{A} := \begin{pmatrix} \frac{\partial f_1}{\partial q_1} & \cdots & \frac{\partial f_1}{\partial q_n} \\ \vdots & \ddots & \vdots \\ \frac{\partial f_n}{\partial q_1} & \cdots & \frac{\partial f_n}{\partial q_n} \end{pmatrix}.$$

The system given by (1.30) is said to be strictly hyperbolic if its Jacobian matrix $\mathbf{A}(\mathbf{q})$ has n real, distinct eigenvalues that can be ordered in such a way: $\lambda_1(\mathbf{q}) < \ldots < \lambda_n(\mathbf{q})$. In general, if we are given smooth initial conditions and $\mathbf{A}$ is sufficiently smooth, then a smooth solution exists for at least a short time. However, it is well known that for systems of nonlinear conservation laws, a solution may develop a singularity in finite time, even if $\mathbf{A}$ and $\mathbf{g}$ are infinitely differentiable functions. Thus, while (1.30) is in the *conservation form* of the conservation law, it is usually advantageous to consider a weak solution to (1.30) in order to study the associated singularities that may arise in the solution. Indeed we say that $\mathbf{q}(x,t)$ is a weak/distributional solution to (1.30)–(1.31) if and only if

$$\int_0^\infty \int_{-\infty}^\infty \mathbf{q}(x,t)\phi_t(x,t) + \mathbf{f}(\mathbf{q}(x,t))\phi_x(x,t)\,dx\,dt = -\int_{-\infty}^\infty \mathbf{q}(x,0)\phi(x,0)\,dx, \tag{1.33}$$

for every C^1 function $\phi : \Omega \subset \mathbb{R} \times \mathbb{R}^+ \to \mathbb{R}^n$ with compact support. We remark that using integration by parts, one could show that if $\mathbf{q}$ and $\mathbf{A}$ are C^1 functions, then (1.33) implies that $\mathbf{q}$ is a solution to (1.30). We also note that from this definition, we only require $\mathbf{q}$ to be locally integrable in $\mathbb{R}$. To investigate weak solutions for (1.30), we typically solve Riemann problems which are conservation laws of the form (1.30) coupled with the following special class of initial conditions:

$$\mathbf{q}_o(x) = \begin{cases} \mathbf{q}_l & : x < 0 \\ \mathbf{q}_r & : x > 0 \end{cases}. \tag{1.34}$$

Characteristic curves are curves in the solution space along which the PDE becomes an ordinary differential equation (ODE). The union of the solutions, or the integral surface, of the ODEs that pass through the initial curve is the solution to the PDE. One can visualize this process as flowing out from each point of the initial curve along the characteristic curve that passes through this point. For example, in linear problems these curve are necessarily parallel and their slopes (or characteristic speeds) are given by the

coefficient matrix $A(\mathbf{q}) = A$. For nonlinear problems, the eigenvalues of the Jacobian matrices depend on the solution, and thus the possibility exists that as we evolve the solution, we will observe regions on the wave that propagate faster or slower than other regions. If two characteristics intersect at any given time, then we have a solution that has different values at the same point. That is, the integral surface has folded over on itself. Thus, the solution is discontinuous and we can no longer consider derivatives at this point. To avoid such a situation, we consider the weak form of the PDE (i.e. we look for a solution which satisfies (1.33)). Shocks occur in our solution whenever two characteristic curves carry conflicting information and meet. To investigate the development of shocks in our solution, we let Λ be a surface which separates our considered domain Ω into two separate regions, say Ω_1 and Ω_2. Suppose that $\mathbf{q}|_{\Omega_1} = \mathbf{q}_1$, and $\mathbf{q}|_{\Omega_2} = \mathbf{q}_2$ are the initial states in the given regions. Then $\mathbf{q}$ satisfies (1.33) if any only if $\mathbf{q}$ is a classical solution (i.e $\mathbf{q}$ solves (1.30)) in each region Ω_1 and Ω_2 and the Rankine-Hugoniot (R-H) jump condition holds along Λ. The R-H jump condition is given by

$$n_t \left[\mathbf{q}\right] + n_x \left[f\left(\mathbf{q}\right)\right] = 0, \tag{1.35}$$

where the unit normal vector is given by $\mathbf{n} = (n_t, n_x)$. In our example, we have that the jump across the solution $\mathbf{q}$ is given by

$$\left[\mathbf{q}\right] = \mathbf{q}_2 - \mathbf{q}_1, \tag{1.36}$$

and the jump across the flux function is given by

$$\left[\mathbf{f}\left(\mathbf{q}\right)\right] = \mathbf{f}\left(\mathbf{q}_2\right) - \mathbf{f}\left(\mathbf{q}_1\right). \tag{1.37}$$

For additional information regarding hyperbolic PDEs and hyperbolic systems of conservation laws, we refer the reader to [64, 104, 120, 136, 137, 141]. For more information about the general theory of PDEs, we refer the reader to [64, 83, 120, 128, 138, 142, 149].

We now turn our attention to the formation of finite volume schemes. To this extent, we consider the integral form of a conservation law which takes on the following form:

$$\frac{d}{dt}\int_{C_i} \mathbf{q}(x,t)\,dx = \mathbf{f}(\mathbf{q}(x_{i-1/2},t)) - \mathbf{f}(\mathbf{q}(x_{i+1/2},t)). \tag{1.38}$$

where C_i is the ith subdomain (grid cell) denoted by

$$C_i = \left[x_{i-1/2}, x_{i+1/2}\right]. \tag{1.39}$$

In the 1-D case, finite volume methods involve dividing a computational domain into subdomains (sometimes called finite volumes and/or grid cells) and then approximating the integral of $\mathbf{q}(x,t)$ over these subdomains. We use the fluxes through the endpoints of the intervals to update the approximation at each time step. To this extent, we define our grid cells given in (1.39) by subdividing our computational domain and letting $\Delta x = x_{i+1/2} - x_{i-1/2}$, $x_i = i\Delta x$, and $x_{i+1/2} = x_i + \frac{\Delta x}{2}$, $i = 1, \ldots, N$, where N denotes the size of each subinterval. In each cell average, we denote the approximation of the integral of $\mathbf{q}(x,t)$ by $\bar{\mathbf{q}}(x,t)$ given by

$$\bar{\mathbf{q}}_i^n \approx \frac{1}{\Delta x}\int_{C_i} \mathbf{q}(x,t^n)\,dx, \tag{1.40}$$

at time t^n and $\Delta x = x_{i+1/2} - x_{i-1/2}$. We note that if $\mathbf{q}(x,t)$ is a smooth function, then one may obtain a second-order approximation of the integral given in (1.40) through the midpoint rule. To evolve this cell average in time, we integrate (1.38) from t^n to t^{n+1} to obtain:

$$\int_{C_i} \mathbf{q}(x,t^{n+1})\,dx - \int_{C_i} \mathbf{q}(x,t^n)\,dx = \int_{t^n}^{t^{n+1}} \mathbf{f}\left(\mathbf{q}(x_{i-1/2},t)\right)\,dt - \int_{t^n}^{t^{n+1}} \mathbf{f}\left(\mathbf{q}(x_{i+1/2},t)\right)\,dt. \tag{1.41}$$

By rearranging terms and dividing by Δx we obtain

$$\begin{aligned}\frac{1}{\Delta x}\int_{C_i} \mathbf{q}\left(x,t^{n+1}\right)\,dx = \\ \frac{1}{\Delta x}\int_{C_i} \mathbf{q}(x,t^n)\,dx - \frac{1}{\Delta x}\left[\int_{t^n}^{t^{n+1}} \mathbf{f}\left(\mathbf{q}(x_{i+1/2},t)\right)\,dt - \int_{t^n}^{t^{n+1}} \mathbf{f}\left(\mathbf{q}(x_{i-1/2},t)\right)\,dt\right].\end{aligned} \tag{1.42}$$

This tells us exactly how one should update the cell averages $\bar{\mathbf{q}}$ in one time step. However, in general we cannot directly evaluate the integrals on the right hand side because $\mathbf{q}$ varies with time along each edge of the cell, and the exact solution for $\mathbf{q}$ is unknown. We may rewrite (1.42) using cell averages as follows:

$$\bar{\mathbf{q}}_i^{n+1} = \bar{\mathbf{q}}_i^n - \frac{1}{\Delta x}\left[\int_{t^n}^{t^{n+1}} \mathbf{f}\left(\mathbf{q}(x_{i+1/2},t)\right)\,dt - \int_{t^n}^{t^{n+1}} \mathbf{f}\left(\mathbf{q}(x_{i-1/2},t)\right)\,dt\right]. \tag{1.43}$$

We now see that the issue lies in approximating the flux functions. In fact, the decision on how to approximate the integrals in (1.43) is what gives rise to finite volume methods. From (1.43), we see that we are interested in studying numerical schemes of the form

$$Q_i^{n+1} = Q_i^n - \frac{\Delta t}{\Delta x}\left(F_{i+1/2}^n - F_{i-1/2}^n\right), \tag{1.44}$$

where

$$F_{i+1/2}^n \approx \frac{1}{\Delta t}\int_{t^n}^{t^{n+1}} \mathbf{f}(\mathbf{q}(x_{i+1/2},t))\,dt. \tag{1.45}$$

One key advantage in working with grid averages rather then pointwise values for $\mathbf{q}(x,t)$ is the ease of mimicking certain useful properties associated with conservation laws. In particular, by considering grid averages, one may ensure that a numerical method is *conservative* in the sense that the total mass within the computation domain will be preserved. This is true since the sum $\sum_{i=1}^N Q_i^n \Delta x$ approximates the integral of $\mathbf{q}$ over the interval $[a,b]$, and thus if our scheme is conservative, then the discrete sum given above will be altered only due to the fluxes at the boundary points. The method that we describe below is an example of a conservation form which is useful for capturing shock solutions.

In choosing how to approximate the fluxes given in (1.45), one should take into account the convergence of the resulting numerical scheme. That is, we require that the numerical solution, generated from applying a finite volume method, should converge to the true solution of the differential equation as the grid is refined (i.e. as $\Delta x, \Delta t \to 0$). In analyzing the convergence of a numerical scheme, we are typically concerned with satisfying the following two conditions:

- The finite volume method should be *consistent* with the differential equation. That is, the method approximates the solution well locally.
- The finite volume method should be *stable*. That is, small errors made in each time step do not grow too fast in later time steps.

Regarding consistency, we locally measure the accuracy of the numerical method in

approximating the solution. That is, we require that the local truncation error go to 0 as $\Delta x, \Delta t \to 0$. We also require that our method be stable. By stable, we mean that small changes in the initial data will result in small changes in the numerical approximation. That is, small errors in each time step should not grow too quickly. To analyze these properties further, we use the hyperbolicity of the equation to write the scheme in a manner that is more convenient for us to study. Since we expect information to propagate in a finite amount of time, one may assume that the fluxes $F^n_{i-1/2}$ can be obtained by the cell averages on either side of the grid, Q^n_i and Q^n_{i-1}. With this assumption,the fluxes may be approximated by a function of the form

$$F^n_{i-1/2} = \mathscr{F}\left(Q^n_i, Q^n_{i-1}\right), \tag{1.46}$$

where $\mathscr{F}$ is some numerical flux function. This allows us to recast our numerical scheme as

$$Q^{n+1}_i = Q^n_i - \frac{\Delta t}{\Delta x}\left(\mathscr{F}\left(Q^n_i, Q^n_{i+1}\right) - \mathscr{F}\left(Q^n_i, Q^n_{i-1}\right)\right). \tag{1.47}$$

To determine if a numerical scheme is consistent, we need to check the accuracy of the approximation of the integrals given in (1.45). We observe that if $\mathbf{q}(x,t) = \bar{\mathbf{q}}$ is constant in x, then the integral in (1.45) simply reduces to $\mathbf{f}(\bar{\mathbf{q}})$. Thus, if $Q^n_{i-1} = Q^n_i = \bar{\mathbf{q}}$, then the numerical flux function also reduces down to $\mathbf{f}(\bar{\mathbf{q}})$, so we require

$$\mathscr{F}(\bar{\mathbf{q}}, \bar{\mathbf{q}}) = \mathbf{f}(\bar{\mathbf{q}}), \tag{1.48}$$

for any such value $\bar{\mathbf{q}}$. We also generally expect continuity in $\mathscr{F}$ as Q_i and Q_{i-1} vary, so that $\mathscr{F}\left(Q_{i-1}, Q_i\right) \to \mathbf{f}\left(\bar{\mathbf{q}}\right)$ as $Q_{i-1}, Q_i \to \bar{\mathbf{q}}$. Thus, we would also like to enforce a Lipschitz continuity condition. That is, we require the existence of a constant $L > 0$ so that

$$\left|\mathscr{F}\left(Q^n_i, Q^n_{i-1}\right) - \mathbf{f}(\bar{\mathbf{q}})\right| \leq L \max\left(\left|Q_i - \bar{\mathbf{q}}\right|, \left|Q_{i-1} - \bar{\mathbf{q}}\right|\right). \tag{1.49}$$

Recall that, for hyperbolic problems, information propagates along the characteristics at finite speed. Thus, the domain of dependence for a fixed point is necessarily a bounded set. The bounds of this set are determined by the eigenvalues of the flux of the Jacobian $\mathbf{f}'\left(\mathbf{q}\right)$. In order for the numerical method to be stable, it must necessarily satisfy the Courant-Friederichs-Lewy (CFL) condition which states that the numerical domain of

dependence must contain the actual domain of dependence of the PDE. This is obviously necessary, since if there exists information contributing to the evaluation of a quantity that is not being considered by the numerical method, then a change in the initial data outside the numerical domain of dependence would not affect the approximation, while the true solution would change. We remark that the CFL condition is a necessary, but not a sufficient condition for stability. In what follows, we discuss how one may approximate the fluxes to derive a finite volume method for the numerical simulation of systems of conservation laws.

Godunov Schemes

In numerical analysis and computational fluid dynamics, Godunov's scheme is a conservative numerical scheme, suggested by S. K. Godunov in 1959, for solving partial differential equations. This important class of finite volume methods solves exact, or approximate, Riemann problems at each inter-cell boundary. In its basic form, Godunov's scheme is first order accurate in both space, and time, yet can be used as a base scheme for developing higher-order methods. In [65], the information available at time t^n is reconstructed using a piecewise polynomial function over the cell averages. To update the information to time t^{n+1}, we must solve a corresponding Riemann problem that results from this reconstruction.We remark that the solutions to Riemann problems are not easily accessible nor necessarily available, thus limiting the types of problems to which the method may be applied. For systems of conservation laws, because waves may propagate in different directions, solutions to the Riemann problem are even more complicated. In general, his method can be interpreted as the following *REA algorithm*:

1. **Reconstruct** a piecewise polynomial function $\tilde{\mathbf{q}}^n(x, t^n)$ from the cell averages Q_i^n. In the simplest case, $\tilde{\mathbf{q}}^n(x, t_{n+1})$ is a piecewise constant on each grid cell:

$$\tilde{\mathbf{q}}^n(x, t^n) = Q_i^n, \quad \text{for all } x \in C_i.$$

2. **Evolve** the hyperbolic equation with this initial data to obtain $\tilde{\mathbf{q}}^n(x, t^{n+1})$.

3. **Average** this function over each grid cell to obtain new cell averages.

$$Q_i^{n+1} = \frac{1}{\Delta x} \int_{C_i} \tilde{\mathbf{q}}^n(x, t^{n+1})\, dx. \tag{1.50}$$

Generally, the piecewise reconstruction is given as:

$$\mathbf{q}(x, t^n) \approx \mathbf{p}_i^n(x), \quad \text{for } x \in C_i, \tag{1.51}$$

which is typically discontinuous at the cell interfaces $x = x_{i\pm 1/2}$.

The stability of the finite volume method is, in general, guaranteed when (1.51) is non-oscillatory, which is accomplished by the use of slope limiters. A library of non-oscillatory reconstructions is available, (see e.g., [1, 36, 64, 71, 72, 91, 97, 106]). A more detailed description of the linear piecewise reconstruction is provided in the section describing the semi-discrete central upwind scheme, which is a special class of FV methods. We note that this piecewise reconstruction allows one to obtain an exact evolution of the solution. This solution is given by a finite set of waves traveling at constant speeds. Typically, depending on the type of grid cells used in the derivation of the scheme, Godunov's method requires the solutions to the Riemann problems that arise at the grid interfaces.

In what follows, we discuss a few possibilities for calculating the numerical flux functions in terms of the cell averages available on either side of the flux interface. To this extent, we will consider two ways to determine the control volumes over which the flux function is integrated. These two methods for constructing numerical approximations to the flux functions divide Godunov schemes into two distinct classes: upwind schemes and central schemes.

Upwind Schemes Versus Central Schemes

Recall that for hyperbolic problems, we expect the information to propagate with a finite speed. That is, the waves generated by solving the hyperbolic problem travel at finite speeds. A major goal of upwind methods is to use information about how a solution behaves at previous time steps to determine the numerical flux functions. Upwind methods anticipate the arrival of information along the characteristics on which they travel. Because of this, upwind methods are typically able to produce numerical solutions that are less diffusive.

If we consider the 1-D conservation law given by (1.32), then using upwind schemes, one may update the cell averages at $t = t^{n+1}$ by approximating the integrals on the right hand side of (1.45). One significant disadvantage involved in using upwind schemes is that since the piecewise polynomial reconstruction is usually discontinuous at the interfaces $x = x_{j\pm\frac{1}{2}}$, one must approximate the solution to the Riemann problems that arise there.

As mentioned earlier, this is typically a costly, complicated task. For more information regarding Riemann solvers and upwind schemes, we refer the reader to [5, 9, 36, 64, 65, 91, 104, 141].

Central schemes are usually easier to implement in comparison to upwind schemes, and hence are more applicable to a wide range of problems in a melange of fields. A hallmark feature of central schemes, is that no information about the solution is required to implement the scheme successfully. While the central scheme is easier to implement than the upwind scheme, it is more prone to the development of spurious oscillations during the propagation of the solution. To evolve the solution via a central scheme, one may use the following formula which incorporates a staggered grid:

$$\begin{aligned} \bar{\mathbf{q}}_{i+1/2}^{n+1} &= \frac{1}{2\Delta x}\left(\int_{x_{j-1/2}}^{x_{j+1/2}} \mathbf{q}_j^n(x)\,dx + \int_{x_{j-1/2}}^{x_{j+1/2}} \mathbf{q}_{j+1}^n(x)\,dx\right) \\ &- \frac{1}{\Delta x}\left[\int_{t^n}^{t^{n+1}} \mathbf{f}\left(\mathbf{q}(x_{i+1},t)\right)\,dt - \int_{t^n}^{t^{n+1}} \mathbf{f}\left(\mathbf{q}(x_{i+1},t)\right)\,dt\right]. \end{aligned} \tag{1.52}$$

In contrast to the upwind schemes, the solution is smooth in a neighborhood of the points $\{x_j\}$. Thus, by using an appropriate quadrature formula, one may approximate the flux integrals given in (1.52). For more information regarding central schemes, we refer the reader to [2, 6, 85, 104, 106, 109, 112, 115, 122, 125, 126, 134].

Semidiscrete Central Upwind Scheme

The semi-discrete central upwind scheme considered in [48, 92, 93, 96, 98, 99, 100], combines the advantages of both central schemes and upwind schemes. The main advantages of central upwind schemes are the high resolution, due to the smaller amount of numerical dissipation–a key advantage of the upwind method, and the ease of use–a hallmark feature for central schemes. There are no Riemann solvers to consider and thus this makes central upwind schemes a universal tool for a wide variety of applications. In fact, semidiscrete central upwind schemes have been used to solve a variety of partial differential equations–in particular for systems of hyperbolic conservation laws and Hamilton-Jacobi equations.We remark that much like upwind schemes, central upwind schemes consider the directions for which a wave propagates during its evolution. In what follows, we consider a one dimensional system of N strictly hyperbolic conservation laws and follow

the methods of [94, 96] to develop a semi-discrete central upwind scheme for the considered equations. We recall the 1-D system of N strictly hyperbolic conservation laws given by (1.30).To construct a semi-discrete central upwind scheme, we use the following equivalent integral form for (1.30)

$$\begin{aligned}&\overline{\mathbf{q}}(x,t+\Delta t)\\ =&\overline{\mathbf{q}}(x,t)-\frac{1}{\Delta x}\left[\int_t^{t+\Delta t}\mathbf{f}\left(\mathbf{q}\left(x+\frac{\Delta x}{2},\tau\right)\right)\,d\tau-\int_t^{t+\Delta t}\mathbf{f}\left(\mathbf{q}\left(x-\frac{\Delta x}{2},\tau\right)\right)\,d\tau\right].\end{aligned} \tag{1.53}$$

Here we denote the cell average (the sliding averages of $\mathbf{q}(\cdot,t)$ over the interval $\left(x-\frac{\Delta x}{2},x+\frac{\Delta x}{2}\right)$), $\overline{\mathbf{q}}(x,t)$ as

$$\overline{\mathbf{q}}(x,t):=\frac{1}{\Delta x}\int_{I(x)}\mathbf{q}(\xi,t)\,d\xi,\quad I(x)=\left\{\xi:|\xi-x|<\frac{\Delta x}{2}\right\}. \tag{1.54}$$

For a particular choice of time, say $t=t^n$, we consider (1.53), coupled with a piecewise polynomial initial condition

$$\tilde{\mathbf{q}}(x,t^n)=\mathbf{p}_j^n(x)\qquad x_{j-1/2}<x<x_{j+1/2}\text{ for all }j, \tag{1.55}$$

where $x_i=i\Delta x$ and is obtained from the cell averages, computed at the previous time step. We then evolve this reconstruction according to (1.53). We note that the order of accuracy for such a method will depend both on the order of accuracy of the piecewise polynomial reconstruction and on the quadrature used to approximate the integrals given in (1.53). For instance, one may use a midpoint quadrature to estimate the integral given in (1.53), and the following piecewise linear polynomial reconstruction:

$$\mathbf{p}_j(x,t)=\overline{\mathbf{q}}(x_j,t)+s(x_j)(x-x_j). \tag{1.56}$$

For the second-order central upwind scheme to be non-oscillatory, one must use a non-linear limiter when computing (1.56). For instance, one could use

$$s(x_j)=\text{minmod}\left(\theta\frac{\overline{\mathbf{q}}_j^n-\overline{\mathbf{q}}_{j-1}^n}{\Delta x},\frac{\overline{\mathbf{q}}_{j+1}^n-\overline{\mathbf{q}}_{j-1}^n}{2\Delta x},\theta\frac{\overline{\mathbf{q}}_{j+1}^n-\overline{\mathbf{q}}_j^n}{\Delta x}\right), \tag{1.57}$$

where $1 \leq \theta \leq 2$ and

$$\text{minmod}(x_1, x_2, \ldots) := \begin{cases} \min_j \{x_j\} & : x_j > 0 \ \ \forall j \\ \max_j \{x_j\} & : x_j < 0 \ \ \forall j \\ 0 & : \text{otherwise} \end{cases}. \tag{1.58}$$

We observe that there may exist discontinuities at the end points for each value of j in our linear piecewise polynomial reconstruction. These possible discontinuities propagate with right- and left sided local speeds, which may be estimated as follows

$$a^+_{j+1/2} = \max\left\{\lambda_N\left(\frac{\partial f}{\partial q}\left(\mathbf{q}^-_{j+1/2}\right)\right)\lambda_N\left(\frac{\partial f}{\partial q}\left(\mathbf{q}^+_{j+1/2}\right)\right), 0\right\}$$
$$a^-_{j+1/2} = \min\left\{\lambda_1\left(\frac{\partial f}{\partial q}\left(\mathbf{q}^-_{j+1/2}\right)\right), \lambda_1\left(\frac{\partial f}{\partial q}\left(\mathbf{q}^-_{j+1/2}\right)\right), 0\right\},$$

where $\lambda_1 < \ldots < \lambda_N$ are the N eigenvalues of the Jacobian $\frac{\partial f}{\partial q}$. Given a piecewise polynomial reconstruction, $\mathbf{p}(x)$, then

$$\mathbf{q}^+_{j+1/2} := \mathbf{p}_{j+1}(x_{j+1/2}) \qquad \text{and} \qquad \mathbf{q}^-_{j+1/2} := \mathbf{p}_j(x_{j+1/2})$$

where $x_{j+1/2} = x_j + \frac{\Delta x}{2}$. The second-order semi-discrete central-upwind scheme is given as

$$\frac{d}{dt}\overline{\mathbf{q}}_j(t) = -\frac{\mathbf{H}_{j+1/2}(t) - \mathbf{H}_{j-1/2}(t)}{\Delta x}. \tag{1.59}$$

The numerical fluxes, $\mathbf{H}_{j+1/2}$ are given by

$$\mathbf{H}_{j+1/2}(t) := \frac{a^+_{j+1/2}\mathbf{f}\left(\mathbf{q}^-_{j+1/2}\right) - a^-_{j+1/2}\mathbf{f}\left(\mathbf{q}^+_{j+1/2}\right)}{a^+_{j+1/2} - a^-_{j+1/2}} + \frac{a^+_{j+1/2}a^-_{j+1/2}}{a^+_{j+1/2} - a^-_{j+1/2}}\left[\mathbf{q}^+_{j+1/2} - \mathbf{q}^-_{j+1/2}\right]. \tag{1.60}$$

We remark that the resulting scheme is a system of time dependent ODEs which may be solved using a high-order (at least second order accuracy) method. For our numerical experiments, we used a third-order SSP (strong stability preserving) Runge-

Kutta method (see e.g. [66]) given as follows

$$\begin{aligned}\mathbf{q}^{(1)} &= \mathbf{q}^n + \Delta t L(\mathbf{q}^{(n)}),\\ \mathbf{q}^{(2)} &= \frac{3}{4}\mathbf{q}^n + \frac{1}{4}\mathbf{q}^{(1)} + \frac{1}{4}\Delta t L(\mathbf{q}^{(1)}),\\ \mathbf{q}^{(n+1)} &= \frac{1}{3}\mathbf{q}^n + \frac{2}{3}\mathbf{q}^{(2)} + \frac{2}{3}\Delta t L(\mathbf{q}^{(2)}),\end{aligned}$$

where

$$\frac{d}{dt}\mathbf{q} = L(\mathbf{q}). \tag{1.61}$$

We also choose Δt adaptively. That is, at each time step, we choose Δt in such a way so that $\Delta t < \frac{\Delta x}{a_{max}}$ where

$$a_{max} := \max_j \left\{ a^+_{j+1/2}, -a^-_{j+1/2} \right\}.$$

We also note that while central-upwind schemes have been originally developed for hyperbolic systems of conservation laws [94, 96, 101], they have been extended and applied to hyperbolic systems of balance laws arising in modeling shallow water flows, see [19, 21, 26, 28, 93, 95, 98, 99].

1.2.2 The Particle Method For Transport Equations

In this section, we briefly describe particle methods in the context of linear transport equations. While in recent years, the use of particle methods have been extended to solve a wider variety of PDEs, see [22, 25, 29, 30, 31, 32, 50, 131], particle methods were first used to solve linear transport equations, see [131]. To this extent, we consider the following 1-D linear transport equation:

$$w_t + (uw)_x + u_0(x,t)\, w = S(x,t). \tag{1.62}$$

Here, $w(x,t)$ is our unknown transported quantity. The velocity, u, coefficient u_0, and our source term $S(x,t)$ are known quantities. The primary goal of the particle method is to seek a solution to (1.62) as a linear combination of Dirac- delta functions which are located at certain points in a given domain. To describe the particle method, we wish to consider the following Cauchy problem as considered in [29, 131]:

$$\begin{aligned} &w_t + (uw)_x + u_0(x,t)\, w = S(x,t), \\ &w(x,0) = w_0(x). \end{aligned} \tag{1.63}$$

We assume that $u_0 \in C(\mathbb{R} \times [0,T))$. In the particle method, the location and weights of the Dirac- delta functions are chosen in such a way that the initial condition is appropriately approximated. We then evolve these functions in time according to a system of ODEs which can be derived from considering a weak formulation of the transport equation. To define what is meant by a weak solution, we first denote $M(\Omega)$ as the space of measures defined on $\Omega \subset \mathbb{R}$ which is the dual space of continuous functions from $\Omega \to \mathbb{R}$ with compact support (denoted by $C_0^0(\Omega)$). In this context, we may define a weak solution as defined in [29].

Definition 1.2.1. *A function $w \in M(\mathbb{R} \times [0,T))$ is called a weak solution to (1.63) if*

$$\begin{aligned} &-\int_{\mathbb{R}} w_0(x)\phi(x,0)\,dx - \int_0^T \int_{\mathbb{R}} w(x,t)\left[\phi_t(x,t) + u(x,t)\phi_x(x,t)\right] dx\,dt \\ &+ \int_0^T \int_{\mathbb{R}} u_0(x,t)w(x,t)\phi(x,t)dx\,dt = \int_0^T \int_{\mathbb{R}} S(x,t)\phi(x,t)dx\,dt, \end{aligned}$$

holds for any test function, $\phi \in C_0^1(\mathbb{R} \times [0,T))$.

Along with Definition 1.2.1, we need to establish what is meant by a *fundamental solution*. A fundamental solution to a partial differential equation is a solution (not necessarily unique), which satisfies $Lu = \delta$, where L is some linear differential operator. To define a weak solution for the linear transport equation, we consider equation (1.62) equipped with a special initial condition (and $S(x,t) = 0$ for simplicity):

$$\begin{aligned} &w_t + (uw)_x + u_0(x,t)\, w = 0, \\ &w_0(x) = \delta(x - x_0), \end{aligned} \tag{1.64}$$

where δ is the Dirac-delta function. In [131], a weak solution to equation (1.64) is given by

$$w(x,t) = \alpha(t)\delta(x - x(t)), \tag{1.65}$$

where

$$\begin{aligned} \frac{dx(t)}{dt} &= u(x(t),t), \qquad & x(0) = x_0, \\ \frac{d\alpha(t)}{dt} &+ u_0(x,t)\alpha(t) = 0, \qquad & \alpha(0) = 1. \end{aligned} \tag{1.66}$$

To verify this weak solution, it suffices to show that the solution as given in (1.65) satisfies our definition for a weak solution to (1.62). Using the definition of a weak solution, we obtain:

$$-\phi(x(0),0) - \int_0^T \alpha(t)\left[\phi_t(x(t),t) + u(x(t),t)\phi_x(x(t),t)\right] dt$$

$$+ \int_0^T \alpha(t)u_0(x(t),t)\phi(x(t),t)\,dt = 0.$$

Now, we add and subtract $\displaystyle\int_0^T \alpha(t)\frac{dx}{dt}\phi_x(x(t),t)\,dt$ in the equation given above. We also use the fact that along a particular curve $x = x(t)$,

$$\frac{d\phi(x(t),t)}{dt} = \phi_t(x(t),t) + \frac{dx}{dt}\phi_x(x(t),t).$$

(via the chain rule). Combining these two facts yields the following equation:

$$-\phi(x(0),0) - \int_0^T \alpha(t)\frac{d\phi(x(t),t)}{dt}\,dt$$

$$-\int_0^T \alpha(t)\left[u(x(t),t) - \frac{dx}{dt}\right]\phi_x(x(t),t)\,dt + \int_0^T \alpha(t)u_0(x(t),t)\phi(x(t),t)\,dt = 0.$$

If we integrate the second term by parts and combine like terms, we obtain:

$$-\int_0^T \alpha(t)\left[u(x(t),t) - \frac{dx}{dt}\right]\phi_x(x(t),t)\,dt$$

$$+\int_0^T \frac{d\alpha}{dt} + \alpha(t)u_0(x(t),t) = 0.$$

Now, we recall the system of differential equations that $x(t)$ and $\alpha(t)$ satisfy (i.e. (1.66)). Because this equation holds for all test functions ϕ, we may conclude that equations (1.65) and (1.66) form a weak solution to the transport equation. We note that by using the superposition principle for ODES, we may derive a similar result for any initial data that is a linear combination of δ functions. Given in [29], we state the following proposition:

Proposition 1.2.2. *Consider the following Cauchy problem:*

$$\begin{aligned} w_t + (uw)_x + u_0(x,t)\, w = 0, \\ w_0(x) = \sum_{i=1}^{N} \alpha_i(0)\delta(x - x_i(0)), \end{aligned} \tag{1.67}$$

where $\alpha_i(0)$ are given coefficients and $x_i(0)$ are the initial locations of the δ functions. If we assume that $u_0 \in C(\mathbb{R} \times [0,T))$, then a weak solution of the Cauchy problem given in equations (1.67) *is:*

$$w^N(x,t) = \sum_{i=1}^{N} \alpha_i(t)\delta(x - x_i(t)), \tag{1.68}$$

where

$$\begin{aligned} \frac{dx_i(t)}{dt} &= u(x_i(t),t), \\ \frac{d\alpha_i(t)}{dt} + u_0(x_i(t),t)\alpha_i(t) &= 0, \\ i &= 1,\ldots,N. \end{aligned} \tag{1.69}$$

If $S \neq 0$, then when using a particle method, we must account for the contribution given by this source term. This is done by considering the following particle approximation for $S(x,t)$:

$$S(x,t) \approx S^N(x,t) := \sum_{i=1}^{N} \beta_i(t)\delta(x - x_i(t)),$$

where

$$\beta_i(t) = \int_{\Omega_i(t)} S(x,t)\, dx \approx S(x_i(t),t)|\Omega_i(t)|, \tag{1.70}$$

where $\Omega_i(t)$ is the domain that includes the ith particle. Here, the size of $\Omega_i(t)$ is usually obtained by solving the following ODE:

$$\frac{d}{dt}|\Omega_i(t)| = |\Omega_i(t)| u_x(x_i(t),t). \tag{1.71}$$

Once $\beta_i(t)$ has been determined, we solve the associated system of ODES for the transport

equation with a source:

$$\frac{dx_i(t)}{dt} = u(x_i(t), t), \quad \frac{d\alpha_i(t)}{dt} + u_0(x_i(t), t)\alpha_i(t) = \beta_i(t). \tag{1.72}$$

Solutions given by equation (1.68) are called particle solutions–that is, solutions which are linear combinations of Dirac- delta functions which are then evolved in time through solving an associated system of differential equations. We observe that as long as the initial condition can be described as a linear combination of Dirac-delta functions, then equations (1.68) and (1.69) represent an exact solution to the transport equation. Generally, we will need to approximate the initial condition, w_0, by a linear combination of Dirac-delta functions. Because of this, our particle solution will be an approximation to the true solution. A natural question that arises when dealing with particle methods is how an arbitrary initial datum w_0 can be approximated by a linear combination of Dirac-delta functions (or equivalently as a collection of particles). That is, we look for $(\alpha_i(0), x_i(0))$ such that $w_0(x)$ is accurately approximated by

$$w_0(x) \approx w_0^N(x) = \sum_{i=1}^{N} \alpha_i(0)\delta(x - x_i(0)). \tag{1.73}$$

This is typically done in the sense of measures, and since we are dealing with the Dirac delta function, we must emphasize the fact that such a comparison is valid only through the sense of distributions. Thus, for any test function, $\phi \in C_0^0(\Omega(0))$, we compare the following quantities:

$$\int_{\Omega(0)} w_0(x)\phi(x)\,dx = \sum_{i=1}^{N} \left(\int_{\Omega_i(0)} w_0(x)\phi(x)\,dx \right), \tag{1.74}$$

with

$$\sum_{i=1}^{N} \alpha_i(0)\phi(x_i(0)) = \sum_{i=1}^{N} \left(\int_{\Omega_i(0)} w_0(x)\,dx \right) \phi(x_i(0)), \tag{1.75}$$

where $\Omega_i(0)$ is chosen so that it is the domain that includes the ith particle and satisfies the following property:

$$\Omega_1(0) \oplus \cdots \oplus \Omega_N(0) = \Omega(0).$$

We observe that equation (1.75) is simply a quadrature for equation (1.74). Thus, we may consider a midpoint rule, as was done in [29], (assuming that the ith particle is placed

in the center of mass for $\Omega_i(0)$) for approximating the integral given in equation (1.75). That is, we may set $\alpha_i(0) = |\Omega_i(0)| w_0(x_i(0))$.

To recover the solution $w(x,t)$ at a particular x for some $t > 0$, we must regularize the particle solution $w^N(x,t)$. Following [29], we may regularize the solution by considering a convolution product with a "cutoff function" $\zeta(x)$ that takes into account the initial tightness of the particle discretization (after a proper scaling). That is, we look at

$$w_\epsilon^N(x,t) = \left(w^N * \zeta_\epsilon\right)(x,t) = \sum_{i=1}^{N} \alpha_i(t)\zeta_\epsilon(x - x_i(t)), \tag{1.76}$$

where the function is taken as a smooth approximation of the δ-function which satisfies

$$\zeta_\epsilon(x) = \frac{1}{\epsilon}\zeta\left(\frac{x}{\epsilon}\right), \quad \text{and} \quad \int_{\mathbb{R}} \zeta(x)\, dx = 1.$$

We remark that the accuracy of the particle method will depend on the choice of the cutoff function. We refer the reader to [35, 49, 70, 131] and references therein for a discussion on possible choices for the cutoff function.

We are now in a position to summarize the process for using a particle method to approximate solutions to the Cauchy problem given by equations (1.62) and (1.63). We begin by first approximating the initial condition according to the discussion given above. That is, we choose $x_i(0)$ and $\alpha_i(0)$ in such a way that the initial condition is accurately approximated. Next, we solve the system of differential equations for $\alpha_i(t)$ and $x_i(t)$, as given by equation (1.69) (if $S = 0$). We can then recover the particle solution for the transport equation, $w^N(x,t)$, at a given time by equation (1.68). Finally, to recover the solution $w(x,t)$ at a particular x for some $t > 0$, we regularize the particle solution $w^N(x,t)$ using (1.76).

Chapter 2

Global Weak Solutions to the b-Family of PDEs

2.1 Introduction

In this chapter, we apply the particle method from [22, 31] to the following family of evolutionary 1+1 PDEs which we introduced in the previous chapter:

$$m_t + m_x u + bmu_x = 0 \qquad u = G * m, \quad x \in \mathbb{R}, \qquad t > 0, \tag{2.1}$$

with $b > 1$ and is considered subject to the initial condition

$$m(x, 0) = m_0(x) \quad x \in \mathbb{R}, \tag{2.2}$$

and propose a new self-contained proof of its convergence for any $b > 1$. To accomplish this goal, we establish bounded variation (BV) estimates for the particle solution and use the associated compactness properties found in [113, 114]. To this end, we assume that the kernel $G(x)$ in (2.1) satisfies the the following properties:

(I) $G(x)$ is an even function, that is, $G(-x) = G(x)$ for any $x \in \mathbb{R}$ and thus $G'(0) = 0$,

(II) $G(x) \in C^1(\mathbb{R}\backslash 0),\ ||G||_\infty = G(0)$,

(III) $G(x), G'(x) \in L^1(\mathbb{R}) \cap BV(\mathbb{R})$, and consequently both $||G||_\infty$ and $||G'||_\infty$ are bounded, see e.g. [10].

From this convergence result, we provide a novel method for obtaining global existence and uniqueness results for (2.1), (2.2) with $b > 1$ and $G(x)$ is given by:

$$G(x) = \frac{1}{2\alpha} e^{-|x|/\alpha} \tag{2.3}$$

and show that the global weak solution of (2.1), (2.2) has stronger regularity properties than those previously established in, e.g., [61].

Chapter 2 is organized as follows. We begin in §2.2 with a brief overview of the particle method applied to (2.1)-(2.2) and some of its main features which are relevant to our discussion. We then show that both the particle solution and its derivative are functions of bounded variation for any $b > 1$ and an arbitrary kernel G satisfying the above properties (I)-(III). §2.3 is dedicated to the special case of IVP (2.1), (2.2) with $b > 1$ and G given by (2.3). In particular, in §2.3.1, we prove that for a relatively wide class of initial data there exists a unique global solution of the particle ODE system. Next, in §2.3.2, we use the compactness results associated with BV functions and verify that both the particle solution and its limit are weak solutions to the b-family of fluid transport equations (b-equations), and complete our study on the convergence analysis. Finally, in §2.3.3, we use our convergence results and the obtained BV estimates to prove the existence of a unique global weak solution for the b-equations (2.1), (2.2) for any $b > 1$.

2.2 Particle Method for the CH Equation

In this section, we describe the particle method and show how it is used to solve the b-equations. We also establish important conservation properties of the corresponding particle system and obtain BV estimates of the particle solution that will allow us to prove (in §2.3) our main result – existence of a global weak solution for the IVP (2.1), (2.2).

2.2.1 Description of the Particle Method for the CH Equation

To solve the b-equations by a particle method, we follow [22, 31] and search for a weak solution of (2.1) as a linear combination of Dirac-delta functions:

$$m^N(x,t) = \sum_{i=1}^{N} p_i(t)\delta(x - x_i(t)). \tag{2.4}$$

Here, $x_i(t)$ and $p_i(t)$ represent the location of the ith particle and its weight, and N denotes the total number of particles. The locations and weights of the particles are then evolved in time according to the following system of ODEs, obtained by substituting (2.4) into a weak formulation of (2.1) (for a detailed derivation of the ODE system we refer the reader to [22]):

$$\begin{cases} \dfrac{dx_i(t)}{dt} = u^N(x_i(t),t), \\ \dfrac{dp_i(t)}{dt} + (b-1)u_x^N(x_i(t),t)p_i(t) = 0. \end{cases} \tag{2.5}$$

Using the special relationship between m and u given in (2.1), one can explicitly compute the velocity u and its derivative, by the convolution $u^N = G * m^N$. Thus we have the following exact expressions for both $u^N(x,t)$ and $u_x^N(x,t)$:

$$u^N(x,t) = \sum_{i=1}^{N} p_i(t)G(x - x_i(t)), \tag{2.6}$$

$$u_x^N(x,t) = \sum_{i=1}^{N} p_i(t)G'(x - x_i(t)). \tag{2.7}$$

With the exception of a few isolated cases, the functions $x_i(t)$ and $p_i(t),\ i = 1,\dots,N$ must be determined numerically and the system (2.5) must be integrated by choosing an appropriate ODE solver. In order to start the time integration, one should choose the initial positions of particles, x_i^0, and the weights, p_i^0, so that (2.4) represents a high-order approximation to the initial data $m_0(x)$ in (2.2), as it is shown in [22, 131]. The latter can be done in the sense of measures on $\mathbb{R}$. Namely, we choose $(x_i(0), p_i(0))$ in such a

way such that for any test function $\phi(x) \in C_0^\infty(\mathbb{R})$, we have that

$$\int_{\mathbb{R}} m_0(x)\phi(x)\,dx \approx \left\langle m^N(\cdot,0), \phi(\cdot)\right\rangle = \sum_{i=1}^{N} p_i(0)\phi(x_i), \tag{2.8}$$

where

$$m^N(x,0) = m_0^N(x) = \sum_{i=1}^{N} p_i(0)\delta(x - x_i(0)). \tag{2.9}$$

Based on (2.8), we observe that determining the initial weights, p_i^0, is exactly equivalent to solving a standard numerical quadrature problem. One way of solving this problem is to first divide the computational domain Ω into N nonoverlapping subdomains Ω_i, such that their union is Ω. We then set the ith particle $x_i(0)$ to be the center of mass Ω_i. For instance, given initial particles $\{x_i(0)\}_{i=1}^N$, we may define Ω_i as

$$\Omega_i = [x_{i-1/2}, x_{i+1/2}] = \left\{x \mid x_{i-1/2} \le x \le x_{i+1/2}\right\}, \quad i = 1, \ldots, N,$$

and by $x_i(0)$ the center of Ω_i. For example, a midpoint quadrature will be then given by setting $p_i(0) = \Delta x\, m_0(x_i(0))$, where $\Delta x = \max\limits_{1\le i\le N} |x_{i+1} - x_i|$.

In general, one can build a sequence of basis functions $\{\sigma_i(x)\}_{i=1}^N$ that will aid in solving the numerical quadrature problem given by (2.8). Indeed, we have the following proposition.

Proposition 2.2.1. *Let $\chi(x)$ be a characteristic function,*

$$\chi_{\Omega_i}(x) = \begin{cases} 1, & \text{when } x \in \Omega_i, \\ 0, & \text{when } x \in X \setminus \Omega_i, \end{cases} \qquad \sum_{i=1}^{N} \chi_{\Omega_i} = 1,$$

and $\sigma(x) \in C_0^\infty(\mathbb{R})$ be a mollifier, that is,

$$\sigma(x) \ge 0, \quad \int_{\mathbb{R}} \sigma(x)\,dx = 1, \quad \lim_{\epsilon\to 0} \sigma_\epsilon(x) = \lim_{\epsilon\to 0} \frac{1}{\epsilon}\sigma(x/\epsilon) = \delta(x).$$

Then

$$1 = 1 * \sigma_\epsilon = \sum_{i=1}^{N} \chi_{\Omega_i} * \sigma_\epsilon = \sum_{i=1}^{N} \sigma_i(x).$$

From here one can approximate the initial data by taking $p_i(0) = \int_{\mathbb{R}} \sigma_i(x)\, dm_0$ in (2.9). We note that the latter makes sense only if $m_0 \in \mathcal{M}(\mathbb{R})$, where $\mathcal{M}(\mathbb{R})$ is the set of Radon measures. Furthermore, one can prove that m_0^N converges weakly to $m_0(x)$ as $N \to \infty$. Indeed, given the above definition for $p_i(0)$, one can show that if m_0^N is given by (2.2) then m_0^N converges weakly to m_0 in the sense of measures.

Proposition 2.2.2. *Let $m_0(x)$ be defined by (2.2) and $m_0^N(x)$ be given by (2.9). Let $h = \max\limits_{1\le i\le N} |x_{i+1} - x_i|$. Then m_0^N converges weakly to $m_0(x)$ in the sense of measures.*

Proof. For any $\phi(x) \in C_0^\infty(\mathbb{R})$, we denote $M_0 = \int\limits_{\mathbb{R}} dm_0$ and have the following:

$$\left| \int\limits_{\mathbb{R}} \phi(x)\, dm_0 - \int\limits_{\mathbb{R}} \phi(x)\, dm_0^N \right| = \left| \sum_{i=1}^{N} \left(\int\limits_{\mathbb{R}} \phi(x)\sigma_i(x)\, dm_0 - \phi(x_i) \int\limits_{\mathbb{R}} \sigma_i(x)\, dm_0 \right) \right|$$
$$= \left| \sum_{i=1}^{N} \int\limits_{\mathbb{R}} \left(\phi(x) - \phi(x_i)\right) \sigma_i(x)\, dm_0 \right| \le Kh \sum_{i=1}^{N} \int\limits_{\mathbb{R}} \sigma_i(x)\, dm_0 = KhM_0 \to 0$$

as $h \to 0$ or equivalently as $N \to \infty$. □

While the system (2.5) may be derived by considering a weak formulation of (2.1) and making an appropriate substitution, if we consider the case where $b = 2$, then one may follow [17, 18] by considering the Hamiltonian structure of (2.1). In particular one may show that $x_i(t)$, and $p_i(t)$ satisfy the canonical Hamiltonian equations:

$$\frac{dx_i}{dt} = \frac{\partial H^N}{\partial p_i}, \qquad \frac{dp_i}{dt} = -\frac{\partial H^N}{\partial x_i}, \qquad i = 1, \ldots, N, \tag{2.10}$$

where $H^N(t)$ is the Hamiltonian function defined as:

$$H^N(t) = \frac{1}{2} \sum_{i=1}^{N} \sum_{j=1}^{N} p_i(t) p_j(t) G(x_i(t) - x_j(t)). \tag{2.11}$$

Also, one can easily establish the following result.

Proposition 2.2.3. *Consider the Hamiltonian function given in (2.11) with $G(x)$ given by (2.3). Then*

$$H^N(t) = \frac{1}{2} \int_{-\infty}^{\infty} (u^N)^2(x,t) + \alpha^2 (u_x^N)^2(x,t)\, dx, \tag{2.12}$$

with $u^N(x,t)$ *and* $u_x^N(x,t)$ *given by* (2.6) *and* (2.7) *respectively.*

Proof. From (2.6) and (2.7), we observe that

$$(u^N)^2(x,t) = \frac{1}{4\alpha^2}\sum_{i=1}^{N}\sum_{j=1}^{N} p_i(t)p_j(t)e^{-|x-x_i(t)|/\alpha-|x-x_j(t)|/\alpha}, \tag{2.13}$$

and

$$\alpha^2(u_x^N)^2(x,t) = \frac{1}{4\alpha^2}\sum_{i=1}^{N}\sum_{j=1}^{N} p_i(t)p_j(t)\mathrm{sgn}(x-x_i(t))\mathrm{sgn}(x-x_j(t))e^{-|x-x_i(t)|/\alpha-|x-x_j(t)|/\alpha}. \tag{2.14}$$

Substituting (2.13) and (2.14) into (2.12), yields

$$\frac{1}{2}\int_{-\infty}^{\infty}(u^N)^2(x,t)+\alpha^2(u_x^N)^2(x,t)\,dx = \frac{1}{8\alpha^2}\sum_{i=1}^{N}\sum_{j=1}^{N}p_i(t)p_j(t)\int_{-\infty}^{\infty}(1+\mathrm{sgn}(x_i(t)-x)\mathrm{sgn}(x_j(t)-x))\,e^{-|x-x_i(t)|/\alpha-|x-x_j(t)|/\alpha}\,dx.$$

Computing the integral in the right-hand side (RHS) of the last equation, we obtain

$$\int_{-\infty}^{\infty}(1+\mathrm{sgn}(x_i(t)-x)\mathrm{sgn}(x_j(t)-x))\,e^{-|x-x_i(t)|/\alpha-|x-x_j(t)|/\alpha}\,dx = 2\alpha e^{-|x_i(t)-x_j(t)|/\alpha},$$

and thus prove the proposition. □

The Hamiltonian nature of the particle system for $b = 2$ and its complete integrability allows one to establish the global existence results for the solution of (2.5) and to show that for a relatively wide class of initial data there are no particle collisions in finite time. In particular, we remark that for positive initial momenta, (2.5) has a unique global solution, and hence $p_i(t) \neq p_j(t)$ for all $i \neq j, t \geq 0$. A similar concept may also be established for the case where $b = 3$. For a general $b > 1$, it can be shown that the time dependent parameters $x_i(t)$ and $p_i(t)$ in (2.5) satisfy the following dynamics equations, [81]:

$$\frac{dx_i}{dt} = \frac{\partial H^N}{\partial p_i}, \qquad \frac{dp_i}{dt} = -(b-1)\frac{\partial H^N}{\partial x_i}, \qquad i = 1,\ldots,N, \tag{2.15}$$

where the function $H^N(t)$ is given by (2.11). Notice that equations (2.10) are canonically

Hamiltonian only for the CH equation (2.1) with $b = 2$.

2.2.2 Properties of the Particle System

We now discuss some general properties of the derived particle method. In particular, we establish conservation laws for the particle momenta and show that the particles propagate with a finite speed.

First, we prove the conservation property of the particle system. Namely,

Proposition 2.2.4. *The total momentum of the particle system* (2.5) *is conserved. That is,*

$$\frac{d}{dt}\left[\sum_{i=1}^{N} p_i(t)\right] = 0. \tag{2.16}$$

Proof. We recall (2.5) and (2.7) to obtain

$$\frac{d}{dt}\left[\sum_{i=1}^{N} p_i(t)\right] = -\sum_{i=1}^{N}\sum_{j=1}^{N}(b-1)p_i(t)p_j(t)G'(x_i(t)-x_j(t)). \tag{2.17}$$

Taking into account the fact that $G'(x)$ is an odd function and $G'(0) = 0$ (see page 29) and the fact that the summation in (2.17) is performed over all $i, j = 1, \ldots, N$, we obtain (2.16) and consequently

$$\sum_{i=1}^{N} p_i(t) = \sum_{i=1}^{N} p_i(0) = M_0. \tag{2.18}$$

□

Next, we assume that $x_1(0) < \cdots < x_N(0)$ and $p_i(0) > 0,\ i = 1, \ldots, N$ and show that these properties are preserved by the flow. We also provide an estimation for the speed of propagation of particles.

Proposition 2.2.5. *Suppose that the initial momenta in* (2.9) *are positive, i.e.* $p_i(0) > 0$ *for all* $i = 1, \ldots, N$. *Then* $p_i(t) > 0$ *for all* $i = 1, \ldots, N$ *and* $t > 0$.

Proof. The proof follows directly from [18], in which one may use the fact that the total momentum is conserved, see (2.18), as well as Gronwall's inequality to obtain

$$p_i(0)e^{-Kt} \le p_i(t) \le p_i(0)e^{Kt}, \qquad i = 1, \ldots, N, \tag{2.19}$$

where $K = (b-1)M_0||G'||_\infty$. We observe that the left inequality prevents $p_i(t)$ from being negative as t goes to 0, while the right inequality prevents $p_i(t)$ from being negative as t goes off to infinity. Hence, $p_i(t) > 0$ for all $i = 1, \ldots, N$ and $t > 0$. □

Proposition 2.2.6. *Suppose that* $\dfrac{dx_i(t)}{dt}$ *is given by* (2.5) *in the interval* $0 \leq t \leq T$. *Then there exists a constant* $0 < C \leq \infty$ *such that*

$$|x_i(t)| < CT. \tag{2.20}$$

Proof. From (2.5), we have the following

$$\left|\frac{dx_i(t)}{dt}\right| = |u^N(x_i(t), t)| = \left|\sum_{j=1}^{N} p_j(t) G(|x_j(t) - x_i(t)|)\right| \leq C. \tag{2.21}$$

The last inequality holds due to the conservation of total momentum (2.18) and the properties (I)–(III) of $G(x)$ stated on page 29. Integrating both sides of (2.21) over $0 \leq t \leq T$ leads us to the desired conclusion (2.20). □

2.2.3 Space and Time BV Estimates

In what follows, we show that the total variations of the particle solution $u^N(x,t)$ and its derivative $u_x^N(x,t)$ are bounded both in space and time. To this end, we recall the definition of the total variation of a function.

Definition 2.2.7. Consider a (possibly unbounded) interval $J \subseteq \mathbb{R}$ and a function $u : J \to \mathbb{R}$. The total variation of u is defined as

$$\text{Tot.Var.}\,\{u\} \equiv \sup\left\{\sum_{j=1}^{N} |u(x_j) - u(x_{j-1})|\right\}, \tag{2.22}$$

where the supremum is taken over all $N \geq 1$ and all $(N+1)$-tuples of points $x_j \in J$ such that $x_0 < x_1 < \cdots < x_N$. If the right hand side of (2.22) is bounded, then we say that u has bounded variation, and write $u \in BV(\mathbb{R})$.

Theorem 2.2.8. *Let* $u^N(x,t)$ *and* $u_x^N(x,t)$ *be functions defined in* (2.6) *and* (2.7), *respectively. Furthermore, assume that* $G(x), G'(x) \in L^1(\mathbb{R}) \cap BV(\mathbb{R})$. *Then, both* $u^N \in BV(\mathbb{R} \times \mathbb{R}_+)$ *and* $u_x^N \in BV(\mathbb{R} \times \mathbb{R}_+)$.

Proof. We begin with showing that

$$\text{Tot. Var.}\left\{u^N(\cdot,t)\right\} \quad \text{and} \quad \text{Tot. Var.}\left\{u_x^N(\cdot,t)\right\}$$

are bounded. Indeed, from the fact that the total momentum of the particle system (2.18) is conserved and the fact that for any two functions f, g and for any constant a

$$\text{Tot.Var.}\{f+g\} \le \text{Tot.Var.}\{f\} + \text{Tot.Var.}\{g\} \quad \text{and} \quad \text{Tot.Var.}\{f(x+a)\} \le \text{Tot.Var.}\{f\},$$

we obtain from (2.6) and (2.7)

$$\text{Tot.Var.}\{u^N(\cdot,t)\} \le \sum_{j=1}^{N} p_j(t)\text{Tot.Var.}\{G(x)\} = M_0\text{Tot.Var.}\{G(x)\}, \tag{2.23}$$

$$\text{Tot.Var.}\{u_x^N(\cdot,t)\} \le \sum_{j=1}^{N} p_j(t)\text{Tot.Var.}\{G'(x)\} = M_0\text{Tot.Var.}\{G'(x)\}. \tag{2.24}$$

Since both the total variation of $G(x)$ and $G'(x)$ is bounded, we conclude that $u^N(x,t)$ and $u_x^N(x,t)$ have bounded variations in space.

In order to prove that $u^N(x,t)$ and $u_x^N(x,t)$ have bounded variation with respect to t as well, it now suffices to show that u^N and u_x^N are both Lipschitz continuous in time in L^1, [10, Theorem 2.6]. To this end, we first consider the expression (2.6) for $u^N(x,t)$ to have

$$\int_{-\infty}^{\infty} |u^N(x,t) - u^N(x,s)|\, dx \le \int_{-\infty}^{\infty} \sum_{i=1}^{N} \Big| p_i(t)G(x - x_i(t)) - p_i(s)G(x - x_i(s)) \Big|\, dx.$$

Next, we add and subtract the term $\int_{-\infty}^{\infty} \sum_{i=1}^{N} p_i(t)G(x - x_i(s))\, dx$ in the RHS of the last inequality and rewrite it as:

$$\begin{aligned}\int_{-\infty}^{\infty} |u^N(x,t) - u^N(x,s)|\, dx \le & \int_{-\infty}^{\infty} \sum_{i=1}^{N} p_i(t)\, |G(x - x_i(t)) - G(x - x_i(s))|\, dx \\ & + \int_{-\infty}^{\infty} \sum_{i=1}^{N} |G(x - x_i(s))||p_i(t) - p_i(s)|\, dx.\end{aligned}$$

Using the results from [10, Lemma 2.3] and the fact that $G \in L^1(\mathbb{R}) \cap BV(\mathbb{R})$, we thus have

$$\int_{-\infty}^{\infty} |u^N(x,t) - u^N(x,s)|\, dx \\ \leq \text{Tot.Var.}\{G(x)\} \sum_{i=1}^{N} p_i(t)|x_i(t) - x_i(s)| + ||G||_{L^1} \sum_{i=1}^{N} |p_i(t) - p_i(s)|. \tag{2.25}$$

The sums in the RHS of (2.25) can now be estimated using the ODE system (2.5) as follows:

$$\begin{aligned} |x_i(t) - x_i(s)| &= \left| \int_s^t \frac{dx_i}{d\tau}\, d\tau \right| \leq \int_s^t |u(x_i(\tau),\tau)|\, d\tau \leq ||G||_\infty \int_s^t \sum_{j=1}^{N} p_j(\tau)\, d\tau \\ &= ||G||_\infty \sum_{j=1}^{N} p_j(0)|t-s| = ||G||_\infty M_0 |t-s|, \end{aligned} \tag{2.26}$$

and

$$\begin{aligned} |p_i(t) - p_i(s)| &= \left| \int_s^t \frac{dp_i}{d\tau}\, d\tau \right| \leq (b-1)||G'||_\infty \int_s^t p_i(\tau) \sum_{j=1}^{N} p_j(\tau)\, d\tau \\ &\leq (b-1)||G'||_\infty \int_s^t p_i(\tau)\, d\tau \sum_{j=1}^{N} p_j(0) = (b-1)||G'||_\infty M_0 \int_s^t p_i\, d\tau. \end{aligned}$$

Also,

$$\sum_{i=1}^{N} |p_i(t) - p_i(s)| \leq (b-1)||G'||_\infty M_0 \int_s^t \sum_{i=1}^{N} p_i(\tau)\, d\tau = (b-1)||G'||_\infty M_0^2 |t-s|. \tag{2.27}$$

Substituting (2.26) and (2.27) into (2.25), yields

$$\int_{-\infty}^{\infty} |u^N(x,t) - u^N(x,s)|\, dx \leq \\ \left(\text{Tot.Var.}\{G(x)\}||G||_\infty + (b-1)||G'||_\infty ||G||_{L^1}\right) M_0^2 |t-s|,$$

proving that u^N is Lipshitz continuous in time in L^1 and thus $u^N \in BV(\mathbb{R}\times\mathbb{R}_+)$, [10, Theorem 2.6].

Similarly, from (2.7) we have:

$$\begin{aligned}\int_{-\infty}^{\infty} |u_x^N(x,t) - u_x^N(x,s)|\,dx \le & \int_{-\infty}^{\infty} \sum_{i=1}^{N} p_i(t)\,|G'(x-x_i(t)) - G'(x-x_i(s))|\,dx \\ & + \int_{-\infty}^{\infty} \sum_{i=1}^{N} |G'(x-x_i(s))||p_i(t)-p_i(s)|\,dx.\end{aligned} \tag{2.28}$$

Substituting (2.26) and (2.27) into (2.28) and using the fact that $G' \in L^1(\mathbb{R}) \cap BV(\mathbb{R})$, we finally conclude that

$$\begin{aligned}&\int_{-\infty}^{\infty} |u_x^N(x,t) - u_x^N(x,s)|\,dx \le \\ &\qquad (\text{Tot.Var.}\{G'(x)\}||G||_\infty + (b-1)||G'||_\infty||G'||_{L^1})\,M_0^2|t-s|,\end{aligned}$$

which together with (2.24) proves that $u_x^N(x,t)$ is a BV function in x,t and also the statement of the theorem. □

2.3 Global Weak Solution and Convergence Analysis

In this section, we propose a new, concise method for showing the convergence of the particle solution to a unique global weak solution of the b-equations. We restrict our attention to the specific case of the IVP (2.1), (2.2) with $b > 1$. In this case, one can explicitly compute the velocity u and its derivative, by the convolutions (2.6) and (2.7), respectively, with G defined by (2.3) and G' is given by

$$G'(x) = -\frac{1}{2\alpha^2}\text{sgn}(x)e^{-|x|/\alpha}. \tag{2.29}$$

One can also easily verify that the functions G and G' defined in (2.3) and (2.29), respectively, satisfy properties (I)–(III) (see page 29) and calculate the total variation of

G and G' explicitly:

$$\text{Tot.Var.}\{G(x)\} = 1/\alpha \quad \text{and} \quad \text{Tot.Var.}\{G'(x)\} = 2/\alpha^2. \tag{2.30}$$

We begin the section by proving that for a relatively wide class of initial data, there are no particle collisions in finite time and as a result there exists a unique global solution of the particle ODE system (2.5) for any $b > 1$. We then show that the particle method applied to the b-equation is a weak solution to (2.1), (2.2). Finally, we state our main convergence result, which is proved using the compactness results generated from the BV estimates established above.

2.3.1 Global Solution of the Particle System

We first prove the following important conservation law.

Proposition 2.3.1. *Consider* (2.5)–(2.7) *for any* $b > 1$ *and* G *and* G' *given by* (2.3) *and* (2.29)*, respectively, and assume that* $p_i(0) > 0,\ i = 1 \dots N$ *and* $x_i(t) < x_{i+1}(t),\ i = 1 \dots N$ *at some time* t*. Then,*

$$P_N(t) = \left(\prod_{k=1}^{N} p_k(t) \right) \left(\prod_{k=1}^{N-1} \Big[G(0) - G(x_k(t) - x_{k+1}(t)) \Big]^{(b-1)} \right) \tag{2.31}$$

is constant of motion.

Proof. To establish the above proposition, it suffices to show that (see also [81, 117])

$$\frac{d}{dt} P_N(t) = 0. \tag{2.32}$$

To this end, we calculate the derivative of $P_N(t)$ and write it in the following form:

$$\frac{d}{dt} P_N(t) = P_N(t) \sum_{k=1}^{N-1} \frac{(b-1) G'(x_k(t) - x_{k+1}(t))(\dot{x}_{k+1}(t) - \dot{x}_k(t))}{G(0) - G(x_k(t) - x_{k+1}(t))} + P_N(t) \sum_{k=1}^{N} \frac{\dot{p}_k(t)}{p_k(t)},$$

where $\dot{x}_k(t)$ and $\dot{p}_k(t)$ denote the derivatives of $x_k(t)$ and $p_k(t)$ with respect to time, respectively. Substituting the expressions for $\dot{x}_k(t))$ and $\dot{p}_k(t)$ from (2.5) and expressions

for G and G' from (2.3) and (2.29) into the above equation, we obtain the following:

$$\begin{aligned}\frac{d}{dt}P_N(t) = &\\ &\frac{b-1}{2\alpha^2}P_N(t)\sum_{k=1}^{N-1}\sum_{i=1}^{N}\frac{e^{(x_k(t)-x_{k+1}(t))/\alpha}\left(p_i(t)e^{-|x_{k+1}(t)-x_i(t)|/\alpha}-p_i(t)e^{-|x_k(t)-x_i(t)|/\alpha}\right)}{1-e^{(x_k(t)-x_{k+1}(t))/\alpha}}\\ &+\frac{b-1}{2\alpha^2}P_N(t)\sum_{k=1}^{N}\sum_{i=1}^{N}p_i(t)\mathrm{sgn}(x_k(t)-x_i(t))e^{-|x_k(t)-x_i(t)|/\alpha}. \qquad (2.33)\end{aligned}$$

By splitting up the summation terms in (2.33) into the intervals $i<k$, $i=k$, and $i>k$, the first sum becomes

$$\begin{aligned}&\sum_{k=1}^{N-1}\sum_{i=1}^{N}\frac{e^{(x_k(t)-x_{k+1}(t))/\alpha}p_i(t)\left(e^{-|x_{k+1}(t)-x_i(t)|/\alpha}-e^{-|x_k(t)-x_i(t)|/\alpha}\right)}{1-e^{(x_k(t)-x_{k+1}(t))/\alpha}}\\ &\quad=\sum_{k=1}^{N-1}\sum_{i<k}\frac{p_i(t)\left(e^{(x_k(t)+x_i(t)-2x_{k+1}(t))/\alpha}-e^{(x_i(t)-x_{k+1}(t))/\alpha}\right)}{1-e^{(x_k(t)-x_{k+1}(t))/\alpha}}\\ &\quad+\sum_{k=1}^{N-1}\frac{e^{(x_k(t)-x_{k+1}(t))/\alpha}p_k(t)\left(e^{(x_k(t)-x_{k+1}(t))/\alpha}-1\right)}{1-e^{(x_k(t)-x_{k+1}(t))/\alpha}}\\ &\quad+\sum_{k=1}^{N-1}\sum_{i>k}\frac{p_i(t)\left(e^{(x_k(t)-x_i(t))/\alpha}-e^{(2x_k(t)-x_i(t)-x_{k+1}(t))/\alpha}\right)}{1-e^{(x_k(t)-x_{k+1}(t))/\alpha}} \qquad (2.34)\\ &\quad=\sum_{k=1}^{N-1}\sum_{i<k}\frac{p_i(t)(e^{(x_k(t)-x_{k+1}(t))/\alpha}-1)e^{(x_i(t)-x_{k+1}(t))/\alpha}}{1-e^{(x_k(t)-x_{k+1}(t))/\alpha}}-\sum_{k=1}^{N-1}p_k(t)e^{(x_k(t)-x_{k+1}(t))/\alpha}\\ &\quad+\sum_{k=1}^{N-1}\sum_{i>k}\frac{p_i(t)(1-e^{(x_k(t)-x_{k+1}(t))/\alpha})e^{(x_k(t)-x_i(t))/\alpha}}{1-e^{(x_k(t)-x_{k+1}(t))/\alpha}}\\ &\quad-\sum_{k=1}^{N-1}\sum_{i<k}p_i(t)e^{(x_i(t)-x_{k+1}(t))/\alpha}-\sum_{k=1}^{N-1}p_k(t)e^{(x_k(t)-x_{k+1}(t))/\alpha} \qquad (2.35)\\ &\quad+\sum_{k=1}^{N-1}\sum_{i>k}p_i(t)e^{(x_k(t)-x_i(t))/\alpha}.\end{aligned}$$

Using properties of the signum function, we also split the second summation term in

(2.33) into the intervals $i < k$, $i = k$, and $i > k$ to obtain

$$\begin{aligned}\sum_{k=1}^{N}\sum_{i=1}^{N} p_i(t)\mathrm{sgn}(x_k(t)-x_i(t))e^{-|x_k(t)-x_i(t)|/\alpha} \\ = \sum_{k=1}^{N}\sum_{i<k} p_i(t)e^{(x_i(t)-x_k(t))/\alpha} - \sum_{k=1}^{N-1}\sum_{i>k} p_i(t)e^{(x_k(t)-x_i(t))/\alpha}.\end{aligned} \tag{2.36}$$

Combining (2.34) and (2.36) and using the fact that

$$\sum_{k=1}^{N}\left(\sum_{i<k} p_i(t)e^{(x_i(t)-x_k(t))/\alpha}\right) - \sum_{k=1}^{N-1}\left(\sum_{i<k} p_i(t)e^{(x_i(t)-x_{k+1}(t))/\alpha}\right) = \sum_{k=1}^{N-1} p_k(t)e^{(x_k(t)-x_{k+1}(t))/\alpha},$$

the derivative in (2.33) simplifies to

$$\begin{aligned}\frac{d}{dt}P_N(t) = \frac{b-1}{2\alpha^2}P_N(t)\left(\sum_{k=1}^{N-1}\sum_{i>k} p_i(t)e^{(x_k(t)-x_i(t))/\alpha}\right. \\ \left. - \sum_{k=1}^{N-1}\sum_{i<k} p_i(t)e^{(x_i(t)-x_{k+1}(t))/\alpha} - \sum_{k=1}^{N-1} p_k(t)e^{(x_k(t)-x_{k+1}(t))/\alpha}\right) \\ + \frac{b-1}{2\alpha^2}P_N(t)\left(\sum_{k=1}^{N}\sum_{i<k} p_i(t)e^{(x_i(t)-x_k(t))/\alpha} - \sum_{k=1}^{N-1}\sum_{i>k} p_i(t)e^{(x_k(t)-x_i(t))/\alpha}\right) = 0,\end{aligned}$$

which establishes the proposition. □

Using Propositions 2.2.4–2.2.6 and 2.3.1, we can now show that, for a class of initial data, particles cannot cross and thus establish global existence of the solution to the ODE system given by (2.5).

Lemma 2.3.2. *Consider the system* (2.5) *with initial data* $p_i(0) > 0$ *and* $x_i(0) < x_{i+1}(0)$ *for any* $i = 1 \dots N$. *Then, for all* $t > 0$, $x_i(t) \neq x_{i+1}(t)$ *for any* $i = 1 \dots N$ *and for all.*

Proof. Suppose on the contrary that there exist time $t^* > 0$ and number k such that

$$\lim_{t \to t^*} x_k(t) - x_{k+1}(t) = 0. \tag{2.37}$$

Then, using the fact that $P_N(0) > 0$ by our choice of initial data, we have

$$\lim_{t \to t^*} \prod_{i=1}^{N} p_i(t) = \infty, \tag{2.38}$$

which contradicts the conservation property (2.18). Hence no two particles may cross in finite time. □

We finally present the following global existence result for (2.5) (the proof follows directly from the Propositions 2.2.4–2.2.6, 2.3.1 and Lemma 2.3.2):

Theorem 2.3.3. *If the initial momenta in the system* (2.5) *are positive, i.e.* $p_i(0) > 0$*, and* $x_i(0) < x_{i+1}(0)$ *for any* $i = 1 \dots N$*, then the solution of system* (2.5) *exists uniquely for all* $t \in (0, \infty)$*.*

Remark 2.3.4. We do have a proof for an arbitrary (non-smooth) kernel $G(x)$ satisfying properties (I)–(III). However, if G is smooth, the existence and uniqueness of a global solution to system (2.5) follows from standard ODE theory. In particular, if G in non-smooth, one may regularize a general kernel G to obtain a blob particle/vortex method as was done in [113, 114]. From here, one can apply similar techniques to establish global weak solutions for a general kernel $G(x)$.

Remark 2.3.5. We would also like to note that similar results have been established in [18] and [117] for the special cases of the CH equation (equation (2.1) with $b = 2$) and the DP equation (equation (2.1) with $b = 3$), respectively, for which equation (2.1) is proven to be completely integrable (see, e.g., [53, 57, 129]). The latter property and the Hamiltonian structure of (2.1) was used in [18] to obtain the desired result for the CH equation. The no cross property for the N-peakon solution to the CH equation was proved in [18] by the iso-spectral property associated to the Lax pair.

2.3.2 Consistency of the Particle Method

Throughout this section, we shall assume that the initial momenta are positive and that there are no particle collisions in finite time, that is, the statement of Theorem 2.3.3 holds.

We begin the section with a definition of a weak solution to the IVP (2.1), (2.2) and then show that the particle solution (m^N, u^N) given by (2.4), (2.6) is indeed a weak solution to the IVP.

Definition 2.3.6. $u(x,t) \in C(0,T;H^1(\mathbb{R})), m(x,t) = u(x,t) - \alpha^2 u_{xx}(x,t)$ is said to be a weak solution of (2.1), (2.2) if

$$\begin{aligned}
&\int_{-\infty}^{\infty} \phi(x,0)m(x,0)\,dx + \int_0^{\infty}\int_{-\infty}^{\infty} \left[\phi_t(x,t) - \alpha^2\phi_{txx}(x,t)\right] u(x,t)\,dxdt \\
&\quad + \int_0^{\infty}\int_{-\infty}^{\infty} \left[\frac{b+1}{2}\phi_x(x,t) - \frac{\alpha^2}{2}\phi_{xxx}(x,t)\right] u^2(x,t)\,dxdt \\
&\quad - \int_0^{\infty}\int_{-\infty}^{\infty} \frac{\alpha^2(b-1)}{2}\phi_x(x,t)u_x^2(x,t)\,dxdt = 0
\end{aligned} \tag{2.39}$$

for all $\phi \in C_0^{\infty}(\mathbb{R}\times\mathbb{R}_+)$.

Before showing that the particle solution $(m^N(x,t), u^N(x,t))$ given by (2.4), (2.6) is a weak solution of the problem (2.1), (2.2), we first establish the following propositions.

Proposition 2.3.7. *Suppose that $G(x)$ and $G'(x)$ are given by* (2.3) *and* (2.29)*, respectively. Then the following relation is true for any $\phi(x) \in C_0^{\infty}(\mathbb{R})$:*

$$\begin{aligned}
G(x_1 - x_2)\left(\phi'(x_1) + \phi'(x_2)\right) = 2\int_{-\infty}^{\infty} G(x-x_1)G(x-x_2)\left(\phi'(x) - \frac{\alpha^2}{2}\phi'''(x)\right)dx \\
+ 2\alpha^2\int_{-\infty}^{\infty} G'(x-x_1)G'(x-x_2)\phi'(x)\,dx.
\end{aligned} \tag{2.40}$$

Proof. We consider both the cases where $x_1 = x_2$ and $x_1 < x_2$. If $x_1 = x_2$, then (2.40) reduces to the following:

$$\frac{1}{\alpha}G(0)\phi'(x_1) = 2\int_{-\infty}^{\infty} G^2(x-x_1)\left(\phi'(x) - \frac{\alpha^2}{2}\phi'''(x)\right)dx + 2\alpha^2\int_{-\infty}^{\infty}(G'(x-x_1))^2\phi'(x)\,dx.$$

Splitting the above integrals into two regions ($x < x_1$ and $x > x_1$), integrating the term

containing $\phi'''(x)$ twice, and combining like terms, proves the equality.

We now consider the case where $x_1 < x_2$. We split the integrals into three regions ($x < x_1$, $x_1 < x < x_2$, and $x > x_2$) and integrate the term containing $\phi'''(x)$ by parts twice to obtain

$$\begin{aligned} -\alpha^2 \int_{-\infty}^{\infty} & G(x-x_1)G(x-x_2)\phi'''(x)\,dx \\ &= \frac{1}{2\alpha}e^{(x_1-x_2/\alpha)}\phi'(x_1) - \frac{1}{\alpha^2}\int_{-\infty}^{x_1} e^{(x-x_1)/\alpha+(x-x_2)/\alpha}\phi'(x)\,dx \\ &\quad + \frac{1}{2\alpha}e^{(x_1-x_2)/\alpha}\phi'(x_2) - \frac{1}{\alpha^2}\int_{x_2}^{\infty} e^{(x_1-x)/\alpha+(x_2-x)/\alpha}\phi'(x)\,dx. \end{aligned} \tag{2.41}$$

We also have the following:

$$\begin{aligned} 2\int_{-\infty}^{\infty} G(x-x_1)G(x-x_2)\phi'(x)\,dx &= \frac{1}{2\alpha^2}\int_{-\infty}^{x_1} e^{-(x_1-x)/\alpha-(x_2-x)/\alpha}\phi'(x)\,dx \\ &\quad + \frac{1}{2\alpha^2}\int_{x_1}^{x_2} e^{(x_1-x)/\alpha-(x_2-x)/\alpha}\phi'(x)\,dx + \frac{1}{2\alpha^2}\int_{x_2}^{\infty} e^{-(x-x_1)/\alpha-(x-x_2)/\alpha}\phi'(x)\,dx \end{aligned} \tag{2.42}$$

and

$$\begin{aligned} 2\alpha^2\int_{-\infty}^{\infty} G'(x-x_1)G'(x-x_2)\phi'(x)\,dx &= \frac{1}{2\alpha^2}\int_{-\infty}^{x_1} e^{-(x_1-x)/\alpha-(x_2-x)/\alpha}\phi'(x)\,dx \\ &\quad + \frac{1}{2\alpha^2}\int_{x_1}^{x_2} e^{(x_1-x)/\alpha-(x_2-x)/\alpha}\phi'\,dx + \frac{1}{2\alpha^2}\int_{x_2}^{\infty} e^{-(x-x_1)/\alpha-(x-x_2)/\alpha}\phi'(x)\,dx. \end{aligned} \tag{2.43}$$

Combining (2.41), (2.42), and (2.43), we obtain

$$\frac{1}{2\alpha}e^{(x_1-x_2)/\alpha}\phi'(x_1) + \frac{1}{2\alpha}e^{(x_1-x_2)/\alpha}\phi'(x_2) = G(x_1-x_2)\left(\phi'(x_1)+\phi'(x_2)\right),$$

and hence the proposition is proven. □

Proposition 2.3.8. *Suppose that $G(x)$ and $G'(x)$ are given by* (2.3) *and* (2.29)*, respec-*

tively. Then the following relation is true for any $\phi(x) \in C_0^\infty(\mathbb{R})$:

$$\begin{aligned} &G'(x_1 - x_2)(\phi(x_1) - \phi(x_2)) = \\ &\int_{-\infty}^{\infty} \left[\alpha^2 G'(x - x_1)G'(x - x_2) - G(x - x_1)G(x - x_2)\right] \phi'(x)\, dx. \end{aligned} \tag{2.44}$$

Proof. As before, we first consider the case where $x_1 = x_2$. Then the problem reduces to showing

$$\int_{-\infty}^{\infty} \left[\alpha^2 \left(G'(x - x_1)\right)^2 - \left(G(x - x_1)\right)^2\right] \phi'(x)\, dx = 0. \tag{2.45}$$

Indeed, by definition of $G(x)$ and its derivative in (2.3) and (2.29), we have

$$\begin{aligned} &\int_{-\infty}^{\infty} \left[\alpha^2 \left(G'(x - x_1)\right)^2 - \left(G(x - x_1)\right)^2\right] \phi'(x)\, dx \\ &\qquad = \frac{1}{4\alpha^2} \int_{-\infty}^{\infty} \left[e^{-2|x-x_1|/\alpha} - e^{-2|x-x_1|/\alpha}\right] \phi'(x)\, dx = 0. \end{aligned}$$

We now consider the case where $x_1 < x_2$, and split the integrals as follows:

$$\begin{aligned} -\int_{-\infty}^{\infty} G(x - x_1)G(x - x_2)\phi'(x)\, dx &= -\frac{1}{4\alpha^2} \int_{-\infty}^{x_1} e^{-(x_1-x)/\alpha-(x_2-x)/\alpha} \phi'(x)\, dx \\ &+ \frac{1}{4\alpha^2} \int_{x_1}^{x_2} e^{-(x-x_1)/\alpha-(x_2-x)/\alpha} \phi'(x)\, dx + \frac{1}{4\alpha^2} \int_{x_2}^{\infty} e^{-(x-x_1)/\alpha-(x-x_2)/\alpha} \phi'(x)\, dx \end{aligned} \tag{2.46}$$

and

$$\begin{aligned} \alpha^2 \int_{-\infty}^{\infty} G'(x - x_1)G'(x - x_2)\phi'(x)\, dx &= \frac{1}{4\alpha^2} \int_{-\infty}^{x_1} e^{-(x_1-x)/\alpha-(x_2-x)/\alpha} \phi'(x)\, dx \\ &- \frac{1}{4\alpha^2} \int_{x_1}^{x_2} e^{-(x-x_1)/\alpha-(x_2-x)/\alpha} \phi'(x)\, dx + \frac{1}{4\alpha^2} \int_{x_2}^{\infty} e^{-(x-x_1)/\alpha-(x-x_2)/\alpha} \phi'(x)\, dx. \end{aligned} \tag{2.47}$$

By combining (2.46) and (2.47) and integrating once, we obtain

$$-\frac{1}{2\alpha^2}e^{-(x_2-x_1)/\alpha}\left(\phi(x_2)-\phi(x_1)\right)=G'(x_1-x_2)\left(\phi(x_1)-\phi(x_2)\right).$$

This proves the proposition. □

Proposition 2.3.9. *Suppose that $m^N(x,t)$, $u^N(x,t)$, and $u_x^N(x,t)$ are given by* (2.4), (2.6), *and* (2.7), *respectively. Then relations* (2.48)–(2.50) *are true for any $\phi(x,t)\in C_0^\infty\left(\mathbb{R}\times\mathbb{R}_+\right)$.*

Proof. To begin, we first prove the relation (2.48), which implies that

$$m^N(x,t)=u^N(x,t)-\alpha^2u_{xx}^N(x,t)$$

in the sense of distributions. Indeed for any $\phi(x,t)\in C_0^\infty\left(\mathbb{R}\times\mathbb{R}_+\right)$, we have the following relation by direct substitution of (2.4) into the left-hand side (LHS) of (2.48) and integration by parts:

$$\left\langle u^N-\alpha^2u_{xx}^N,\phi_t\right\rangle=\left\langle u^N,\phi_t\right\rangle+\alpha^2\left\langle u_x^N,\phi_{tx}\right\rangle.$$

Using (2.6) and (2.7) and integrating by parts once again, we prove (2.48):

$$\begin{aligned}\left\langle u^N-\alpha^2u_{xx}^N,\phi_t\right\rangle&=\int_0^\infty\sum_{i=1}^N p_i(t)\int_{-\infty}^\infty G(x-x_i(t))\phi_t(x,t)\,dxdt\\&\quad+\alpha^2\int_0^\infty\sum_{i=1}^N p_i(t)\int_{-\infty}^\infty G'(x-x_i(t))\phi_{tx}(x,t)\,dxdt\\&=\int_0^\infty\sum_{i=1}^N p_i(t)\int_{-\infty}^\infty G(x-x_i(t))\left(\phi_t(x,t)-\alpha^2\phi_{txx}(x,t)\right)\,dxdt\\&=\langle u^N,\phi_t-\alpha^2\phi_{txx}\rangle.\end{aligned}$$

Next, we verify (2.49) as follows. Direct substitution shows that

$$\left\langle m^Nu^N,\phi_x\right\rangle=\int_0^\infty\sum_{i=1}^N\sum_{j=1}^N p_i(t)p_j(t)G(x_i(t)-x_j(t))\phi_x(x_i(t),t)\,dt.$$

Using Propositions 2.3.7 and the fact that $G(x)$ is an even function (see page 29), we find that

$$\begin{aligned}
&\left\langle m^N u^N, \phi_x \right\rangle \\
&= \frac{1}{2} \int_0^\infty \sum_{i=1}^N \sum_{j=1}^N p_i(t) p_j(t) G(x_i(t) - x_j(t)) \left(\phi_x(x_i(t), t) + \phi_x(x_j(t), t) \right) \, dt \\
&= \int_0^\infty \sum_{i=1}^N \sum_{j=1}^N p_i(t) p_j(t) \left[\int_{-\infty}^\infty G(x - x_i(t)) G(x - x_j(t)) \left(\phi_x(x,t) - \frac{\alpha^2}{2} \phi_{xxx}(x,t) \right) \, dx \right. \\
&\left. + \alpha^2 \int_{-\infty}^\infty G'(x - x_i(t)) G'(x - x_j(t)) \phi_x(x,t) dx \right] dt \\
&= \left\langle (u^N)^2, \phi_x - \frac{\alpha^2}{2} \phi_{xxx} \right\rangle + \alpha^2 \left\langle (u_x^N)^2, \phi_x \right\rangle .
\end{aligned}$$

Finally, in order to prove (2.50), we proceed in a similar manner as above by first observing that

$$\left\langle m^N u_x^N, \phi \right\rangle = \int_0^\infty \sum_{i=1}^N \sum_{j=1}^N p_i(t) p_j(t) G'(x_i(t) - x_j(t)) \phi(x_i(t), t) \, dt.$$

We use Proposition 2.3.8 and the fact that $G'(x)$ is an odd function (see page 29)), to obtain

$$\begin{aligned}
&\left\langle m^N u_x^N, \phi \right\rangle \\
&= \frac{1}{2} \int_0^\infty \sum_{i=1}^N \sum_{j=1}^N p_i(t) p_j(t) G'(x_i(t) - x_j(t)) \left(\phi(x_i(t), t) - \phi(x_j(t), t) \right) dt \\
&= \frac{1}{2} \int_0^\infty \sum_{i=1}^N \sum_{j=1}^N p_i(t) p_j(t) \left[- \int_{-\infty}^\infty G(x - x_i(t)) G(x - x_j(t)) \phi_x(x,t) \, dx \right. \\
&\left. + \frac{\alpha^2}{2} \int_{-\infty}^\infty G'(x - x_i(t)) G'(x - x_j(t)) \phi_x(x,t) \, dx \right] dt = \left\langle \frac{\alpha^2 (u_x^N)^2 - (u^N)^2}{2}, \phi_x \right\rangle .
\end{aligned}$$

□

Theorem 2.3.10. *Assume that $m_0 \in \mathcal{M}(\mathbb{R})$, then the particle solution*

$$(m^N(x,t), u^N(x,t)),$$

given by (2.4), (2.6) *is a weak solution of the problem* (2.1), (2.2).

Proof. Let $m^N(x,0), m^N(x,t)$ and $u^N(x,t), u^N_x(x,t)$ be given by formulae (2.9), (2.4) and (2.6), (2.7), respectively and $\phi \in C_0^\infty(\mathbb{R}\times\mathbb{R}_+)$ be a test function. Then, the following relations are true for any ϕ (see 2.3.9):

$$\langle m^N, \phi_t\rangle = \langle u^N, \phi_t - \alpha^2\phi_{txx}\rangle, \tag{2.48}$$

$$\langle m^N u^N, \phi_x\rangle = \left\langle (u^N)^2, \phi_x - \frac{\alpha^2}{2}\phi_{xxx}\right\rangle + \alpha^2\left\langle (u^N_x)^2, \phi_x\right\rangle, \tag{2.49}$$

$$\left\langle m^N u^N_x, \phi\right\rangle = \left\langle \frac{\alpha^2(u^N_x)^2 - (u^N)^2}{2}, \phi_x\right\rangle, \tag{2.50}$$

where $\langle\cdot,\cdot\rangle$ denotes a scalar product in $\mathbb{R}\times\mathbb{R}_+$, i.e., $\langle m^N, \phi_t\rangle = \int\limits_0^\infty\int\limits_{-\infty}^{\infty} m^N(x,t)\phi_t(x,t)\,dxdt$, etc.

Using (2.48)–(2.50) and substituting $m^N(x,t)$ as defined by (2.4) into (2.39), yields

$$\sum_{i=1}^N p_i(0)\phi(x_i(0),0) + \int_0^\infty \sum_{i=1}^N p_i(t)\phi_t\left(x_i(t),t\right)dt + \int_0^\infty \sum_{i=1}^N p_i(t)u^N(x_i(t),t)\phi_x\left(x_i(t),t\right)dt$$
$$- (b-1)\int_0^\infty \sum_{i=1}^N p_i(t)u^N_x\left(x_i(t),t\right)\phi\left(x_i(t),t\right)dt = 0. \tag{2.51}$$

We now add and subtract $\displaystyle\sum_{i=1}^N \int_0^\infty p_i(t)\,\frac{dx_i}{dt}\phi_x(x_i(t),t)\,dt$ into the last equation, use the fact that

$$\frac{d\phi(x_i(t),t)}{dt} = \phi_x(x_i(t),t)\frac{dx_i(t)}{dt} + \phi_t(x_i(t),t)$$

and rewrite (2.51) as follows:

$$\begin{aligned}
&\sum_{i=1}^{N} p_i(0)\phi(x_i(0),0) + \int_0^{\infty} \sum_{i=1}^{N} p_i(t) \frac{d\phi(x_i(t),t)}{dt}\, dt \\
&\int_0^{\infty} \sum_{i=1}^{N} p_i(t) \left[u^N(x_i(t),t) - \frac{dx_i(t)}{dt} \right] \phi_x\left(x_i(t),t\right)\, dt \\
&- (b-1) \int_0^{\infty} \sum_{i=1}^{N} p_i(t) u_x^N\left(x_i(t),t\right) \phi\left(x_i(t),t\right)\, dt = 0.
\end{aligned} \tag{2.52}$$

Integrating by parts the second term in the first row in (2.52), and rearranging other terms, we finally obtain:

$$\begin{aligned}
&\int_0^{\infty} \sum_{i=1}^{N} p_i(t) \left[\frac{dx_i(t)}{dt} - u^N(x_i(t),t) \right] \phi_x\left(x_i(t),t\right)\, dt \\
&+ \int_0^{\infty} \sum_{i=1}^{N} \left[\frac{dp_i(t)}{dt} + (b-1) p_i(t) u_x^N\left(x_i(t),t\right) \right] \phi(x_i(t),t)\, dt = 0.
\end{aligned} \tag{2.53}$$

Since the functions $x_i(t)$ and $p_i(t)$ satisfy the system (2.5), the last equation holds for any ϕ implying that m^N, u^N defined by (2.4), (2.6) is a weak solution of (2.1), (2.2). This completes the proof. □

2.3.3 Compactness and Convergence

We are now in a position to establish a convergence result for the particle method applied to equation (2.1). Using the BV estimates for $u^N(x,t)$ and $u_x^N(x,t)$, and the fact that the particle solution satisfies the equation in the sense of distributions, we may establish the following convergence result, which in turn proves the existence of a unique global weak solution to the b-equation (2.1) with any $b > 1$. Once again, we assume that the statement of Theorem 2.3.3 holds.

Theorem 2.3.11. *Suppose that $(m^N(x,t), u^N(x,t))$ is a particle solution of (2.4), (2.5) with initial approximation $m^N(\cdot,0) \overset{*}{\rightharpoonup} m_0$, $m_0 \in \mathcal{M}_+(\mathbb{R})$. Then there exist functions $u(x,t) \in BV(\mathbb{R}\times\mathbb{R}_+)$ and $m(x,t) \in \mathcal{M}_+(\mathbb{R}\times\mathbb{R}_+)$ such that $m^N(x,t)$ and $u^N(x,t)$*

converge to $m(x,t)$ and $u(x,t)$, respectively in the sense of distributions as $N \to \infty$. Furthermore, the limit (u,m) is the unique weak solution of (2.1), (2.2) for any $b > 1$ with the regularity $u \in C(0,T;H^1(\mathbb{R}))$, $u_x \in BV(\mathbb{R}\times\mathbb{R}_+)$.

Proof. Using BV estimates for $u^N(x,t)$ and $u_x^N(x,t)$, we refer to the compactness property in [10, Theorem 2.4] and conclude that there exist functions $u(x,t)$ and $u_x(x,t)$ and a subsequence (still labeled as $u^N(x,t)$) such that

$$\lim_{N\to 0} ||u^N - u||_{L^1_{\text{loc}}(\mathbb{R}\times\mathbb{R}_+)} = 0, \qquad \lim_{N\to 0} ||u_x^N - u_x||_{L^1_{\text{loc}}(\mathbb{R}\times\mathbb{R}_+)} = 0. \tag{2.54}$$

From Proposition 2.3.10, we know that the particle solution (m^N, u^N) is a weak solution of (2.1) and thus satisfy

$$\begin{aligned}
&\int_{-\infty}^{\infty} \phi(x,0) m^N(x,0)\,dx + \int_0^{\infty}\int_{-\infty}^{\infty} \left[\phi_t(x,t) - \alpha^2 \phi_{txx}(x,t)\right] u^N(x,t)\,dxdt \\
&\quad + \int_0^{\infty}\int_{-\infty}^{\infty} \left[\frac{b+1}{2}\phi_x(x,t) - \frac{\alpha^2}{2}\phi_{xxx}(x,t)\right] (u^N)^2(x,t)\,dxdt \\
&\quad + \int_0^{\infty}\int_{-\infty}^{\infty} \frac{\alpha^2(b-1)}{2}\phi_x(x,t)(u_x^N)^2(x,t)\,dxdt = 0.
\end{aligned} \tag{2.55}$$

To complete the proof, we need to show that each terms in (2.55) converges to that of the limit solution (m,u) in (2.39).

Indeed, by the construction of the initial approximation and Proposition 2.2.2, we have

$$\lim_{N\to\infty} \int_{-\infty}^{\infty} \phi(x,0) m^N(x,0)\,dx = \int_{-\infty}^{\infty} \phi(x,0) m(x,0)\,dx. \tag{2.56}$$

Furthermore, from (2.54) and the fact that $u^N \in \text{BV}(\mathbb{R}\times\mathbb{R}_+)$ and $u_x^N \in \text{BV}(\mathbb{R}\times\mathbb{R}_+)$ it follows that

$$\Big| \int_0^{\infty}\int_{-\infty}^{\infty} \left(u^N(x,t)^2 - u(x,t)^2\right) \phi(x,t)\,dxdt \Big|$$

$$= \Big| \int_0^\infty \int_{-\infty}^\infty (u^N(x,t) + u(x,t))(u^N(x,t) - u(x,t))\phi(x,t)\,dxdt \Big|$$
$$\leq \|\phi\|_{L^\infty}(\|u^N\|_{L^\infty} + \|u\|_{L^\infty}) \iint\limits_{(x,t)\in \mathrm{supp}\{\phi\}} \big|u^N(x,t) - u(x,t)\big|\,dxdt$$

holds for any $\phi \in C_0^\infty(\mathbb{R}\times\mathbb{R}_+)$, and thus

$$\big\langle (u^N)^2, \phi \big\rangle \to \big\langle u^2, \phi \big\rangle \quad \text{as} \quad N \to \infty. \tag{2.57}$$

Similarly, for any $\phi \in C_0^\infty(\mathbb{R}\times\mathbb{R}_+)$ we have

$$\big\langle (u_x^N)^2, \phi \big\rangle \to \big\langle u_x^2, \phi \big\rangle \quad \text{as} \quad N \to \infty, \tag{2.58}$$

and therefore

$$\langle u^N, \phi_t - \alpha^2\phi_{txx}\rangle \to \langle u, \phi_t - \alpha^2\phi_{txx}\rangle \tag{2.59}$$
$$\left\langle (u^N)^2, \phi_x - \frac{\alpha^2}{2}\phi_{xxx} \right\rangle \to \left\langle (u)^2, \phi_x - \frac{\alpha^2}{2}\phi_{xxx} \right\rangle, \tag{2.60}$$
$$\left\langle \frac{\alpha^2(u_x^N)^2 - (u^N)^2}{2}, \phi_x \right\rangle \to \left\langle \frac{\alpha^2(u_x)^2 - (u)^2}{2}, \phi_x \right\rangle, \tag{2.61}$$

as $N \to \infty$. This shows that the limit (m, u) is indeed a weak solution to the b-equation (2.1).

It should be observed that since $G, G' \in L^1(\mathbb{R}) \cap BV(\mathbb{R})$, then $G, G' \in L^2(\mathbb{R})$ and thus with the bounds (2.18), we have $u \in L^\infty(0,T;H^1(\mathbb{R}))$ and $u, u_x \in \mathrm{BV}(\mathbb{R}\times\mathbb{R}_+)$. The latter implies that (see, e.g., [10])

$$\int_{\mathbb{R}} |u(x,t) - u(x,s)|\,dx \leq C_1|t-s|, \quad \int_{\mathbb{R}} |u_x(x,t) - u_x(x,s)|\,dx \leq C_2|t-s|,$$

and thus

$$||u(\cdot,t)||^2_{H^1} - ||u(\cdot,s)||^2_{H^1} \leq \int_{\mathbb{R}} |u(x,t)-u(x,s)|^2 + |u_x(x,t)-u_x(x,s)|^2\,dx$$
$$\leq 2||u||_\infty \int_{\mathbb{R}} |u(x,t)-u(x,s)|\,dx + 2||u_x||_\infty \int_{\mathbb{R}} |u_x(x,t)-u_x(x,s)|\,dx \leq C|t-s|,$$

proving that $u \in C(0,T;H^1(\mathbb{R}))$.

Finally, we remark that the weak solution for the b-equation (2.1), (2.2) is unique in the obtained class of functions. The result has been proven in [46] for the CH equation ($b=2$), by direct estimations for the equation recast in the following conservative form:

$$u_t + uu_x + G' * \left[u^2 + \frac{1}{2}u_x^2\right] = 0, \tag{2.62}$$

where G' is given by (2.29), as before. The proof of the uniqueness result for any $b>1$ follows directly from [46] by rewriting (2.1) as

$$u_t + uu_x + G' * \left[\frac{b}{2}u^2 + \frac{3-b}{2}u_x^2\right] = 0. \tag{2.63}$$

□

Remark 2.3.12. We also note that for the special case of CH equation ($b=2$), the convergence of the particle method to a smooth solution has been verified in [17, 18].

Chapter 3

A Practical Implementation of the Particle Method to the Camassa-Holm Equation

3.1 Introduction

In this chapter, we investigate the dynamics of the interaction among peakon solutions for the 1D Camassa-Holm (CH) equation as well as showcase the merits of using particle methods to simulate solutions to the CH equation using arbitrary smooth initial data. To this extent, we recall that the CH equation is given by

$$m_t + um_x + 2mu_x = 0, \quad m = u - \alpha^2 u_{xx}, \tag{3.1}$$

which is subjected to the following initial data:

$$m(x, 0) = m_0(x). \tag{3.2}$$

We apply the particle method for the numerical solution of the CH equation in order to study the elastic collisions among peakon solutions. Using the particle method developed in Chapter 2 for solving the CH equation, we begin this chapter by reviewing some important properties of the particle method that will be pertinent to our study. In Section 3.2 we provide an analytical discussion about the behavior of peakon interactions for two positive peakons. In Section 3.3, we present several numerical experiments which

showcases both the complex interactions among peakon solutions, as well as the merits of using a particle method to simulate such solutions.

It should be instructive to review some of the general properties of the particle system which are pertinent to our study on the investigation of elastic collisions of peakons. For a more detailed description of the following properties including their proofs, we refer the reader to Chapter 2.

- We begin by observing that the functions $x_i(t)$ and $p_i(t)$ given by (2.5) satisfy the following canonical Hamiltonian equations:

$$\frac{dx_i}{dt} = \frac{\partial H^N}{\partial p_i}, \qquad \frac{dp_i}{dt} = -\frac{\partial H^N}{\partial x_i}, \quad i = 1, \ldots, n, \tag{3.3}$$

  where the Hamiltonian $H^N(t)$ is given as follows:

$$H^N(t) = \frac{1}{2} \sum_{i=1}^{N} \sum_{j=1}^{N} p_i(t) p_j(t) G\left(x_i(t) - x_j(t)\right), \tag{3.4}$$

  and G is the Green's function associated with the modified 1D Helmholtz operator which relates the momentum m with velocity u.

  We note that $H^N(t)$ is conserved, i.e, $H^N(t) = H^N(0)$ for all $t > 0$.

- Another important conservation law for the particle system (2.5) is the conservation of the total momentum, i.e.,

$$\frac{d}{dt}\left[\sum_{i=1}^{N} p_i(t)\right] = 0. \tag{3.5}$$

- Finally, if the initial momenta given in (2.5) are positive, i.e., $p_i(0) > 0$ for all $i = 1, \ldots, N$, then $p_i(t) > 0$ for all $i = 1, \ldots, N$ and $t > 0$. If, in addition, $x_i(0) < x_{i+1}(0)$ $i = 1, \ldots, N$, then the particles never cross, i.e., $x_i(t) < x_{i+1}(t)$ for any $i = 1, \ldots, N$ and for all t. This important property was proved in [17] by using a Lax-Pair formulation. It can also be proved by using a conservation law,

$$\frac{dP_N(t)}{dt} := \frac{d}{dt}\left(\prod_{k=1}^{N} p_k(t) \prod_{k=1}^{N-1} \Big[G(0) - G(x_k(t) - x_{k+1}(t))\Big]\right) = 0,$$

as it has been done in Chapter 2. We will show in the next section that peakons , generated by solving the CH equation, indeed elastically bounce back after becoming close to each other.

3.2 Elastic Collisions Among Peakon Solutions

In this section, we take a close look at the dynamics and interactions of the peakon solutions (2.6) associated with CH equation. In particular, we study the soliton-type behavior of peakons and their elastic collisions. An elastic collision is an encounter between two bodies in which the total kinetic energy and momentum of the two bodies after the encounter are equal to their total kinetic energy and momentum before the encounter. That is, both momentum and kinetic energy are conserved. By conservation of momentum, we mean that the sum of the momenta of all the objects of a system under consideration cannot be changed by the interactions within the system. Additionally, the total energy of a system remains constant at all times under the conservation of energy principle. Using these principal conservation properties, we begin by showing analytically that any collisions among peakons for the case where the initial weights are assumed to be positive are elastic. That is, the collision is through the interaction potential in the Hamiltonian given in (3.3) rather than a head on collision.

3.2.1 Analysis of Two-Peakon Interactions

Since the interaction of peakons is local, it is sufficient to investigate the interactions among two peakons. To this extent, we consider a two-peakon system with weights $p_1(t)$, $p_2(t)$ and locations $x_1(t)$, $x_2(t)$ that evolve in time according to the following system of ODEs (see (2.5)):

$$\begin{cases} \dfrac{dx_1(t)}{dt} = \dfrac{1}{2\alpha}p_1(t) + \dfrac{1}{2\alpha}p_2(t)e^{-|x_2(t)-x_1(t)|/\alpha}, \\ \dfrac{dx_2(t)}{dt} = \dfrac{1}{2\alpha}p_2(t) + \dfrac{1}{2\alpha}p_1(t)e^{-|x_1(t)-x_2(t)|/\alpha}, \\ \dfrac{dp_1(t)}{dt} = \dfrac{1}{2\alpha^2}p_1(t)p_2(t)\mathrm{sgn}(x_1(t)-x_2(t))e^{-|x_1(t)-x_2(t)|/\alpha}, \\ \dfrac{dp_2(t)}{dt} = \dfrac{1}{2\alpha^2}p_1(t)p_2(t)\mathrm{sgn}(x_2(t)-x_1(t))e^{-|x_2(t)-x_1(t)|/\alpha}. \end{cases} \tag{3.6}$$

We assume that there are two times, say t_{before} and t_{after} such that

$$|x_1(t_{\text{before}}) - x_2(t_{\text{before}})| = |x_1(t_{\text{after}}) - x_2(t_{\text{after}})|,$$

with $x_1(t) \neq x_2(t)$ for any finite time t. Here t_{before} is some time t before the two peakons interact, and t_{after} is some time t after the peakons undergo a nonlinear exchange of momentum.

We begin by recalling the two conservation properties of the particle system: the conservation of the Hamiltonian (see (3.3)):

$$H^N(t) = p_1^2(t) + p_2^2(t) + 2p_1(t)p_2(t)e^{-|x_1(t)-x_2(t)|/\alpha} = H^N(0), \quad \forall t > 0, \tag{3.7}$$

and the conservation of momentum (see (3.5)):

$$p_1(t) + p_2(t) = p_1(0) + p_2(0), \quad \forall t > 0. \tag{3.8}$$

From (3.7) and (3.8), we observe that $2\left(p_1p_2\right)_{\text{before}} = 2\left(p_1p_2\right)_{\text{after}}$. Indeed if we square both sides of (3.8) and subtract (3.7), we obtain

$$\begin{aligned} &2p_1(t_{\text{before}})p_2(t_{\text{before}})(1 - e^{-|x_1(t_{\text{before}})-x_2(t_{\text{before}})|/\alpha}) \\ &= 2p_1(t_{\text{after}})p_2(t_{\text{after}})(1 - e^{-|x_1(t_{\text{after}})-x_2(t_{\text{after}})|/\alpha}). \end{aligned}$$

From here, we use the fact that $|x_1(t_{\text{before}}) - x_2(t_{\text{before}})| = |x_1(t_{\text{after}}) - x_2(t_{\text{after}})|$ to conclude that $2\left(p_1p_2\right)_{\text{before}} = 2\left(p_1p_2\right)_{\text{after}}$. This observation along with the conservation of momentum property (see (3.8)) allows us to obtain the following system of equations:

$$\begin{aligned} p_1^2(t_{\text{before}}) + p_2^2(t_{\text{before}}) &= p_1^2(t_{\text{after}}) + p_2^2(t_{\text{after}}), \\ p_1(t_{\text{before}}) + p_2(t_{\text{before}}) &= p_1(t_{\text{after}}) + p_2(t_{\text{after}}). \end{aligned} \tag{3.9}$$

The only possible solutions to the system of equations given above are,

$$p_1(t_{\text{before}}) = p_1(t_{\text{after}}), \quad p_2(t_{\text{before}}) = p_2(t_{\text{after}}), \tag{3.10}$$

and

$$p_1(t_{\text{before}}) = p_2(t_{\text{after}}), \quad p_2(t_{\text{before}}) = p_1(t_{\text{after}}). \tag{3.11}$$

The solution given by (3.10) implies that the peakons do not interact, which is not possible. Hence, the solution to (3.9) is given by (3.11) which shows that the momentum is exchanged after the collision. This explicitly shows the elastic collision behavior among peakon solutions generated by solving (3.1) via a particle method. Below, we illustrate an example of the interaction among two peakons which exhibits the elastic collision behavior as described above.

An Illustration of the Two Positive Peakons Interaction

In this illustration, we begin by considering an interaction among two positive peakons generated from solving the CH equation given in (3.1). To this extent, we consider two positive peakons, which are initially placed at $x_1(0) = 0$, and $x_2(0) = 5$ with initial weights $p_1(0) = 4$ and $p_2(0) = 1$, and move them exactly in time according to (3.6) with $\alpha = 1$ on the domain $[a, b] = [-10, 30]$. We observe that the peakon defined by its initial values at (x_1, p_1) has a bigger weight and will hence move faster than the peakon defined by (x_2, p_2). Thus, we expect that as the two peakons move closer to each other, they will undergo a complex interaction which involves the exchange of momentum.

In Figure 3.1, we provide snapshots of the solution u at different times. To plot the velocity profile, we introduce a uniform grid of size Δx^p, i.e., $x_j^p = j\Delta x^p,\ \Delta x^p = \frac{b-a}{N_p},\ j = 1, \dots N_p$, and compute the values of $u(x_j^p, t),\ j = 1, \dots N_p$, according to formula (2.6) with $\alpha = 1$, i.e., $u^N(x_j^p, t) = \frac{1}{2}\sum_{i=1}^{N_p} p_i(t)e^{-|x_j^p - x_i(t)|}$. As one can see, the peakons emerge unscathed with the exception of a phase shift as predicted by the underlying integrable system. In Figure 3.2, we also show the trajectories of each particle and its momentum as functions of time. From this figure, we see that the particles do not cross; rather, they exchange momentums as they undergo a complex nonlinear interaction with each other.

To gain a better understanding of the elastic collision behavior among two peakon solutions, we compare the particle method (3.6), in which each particle represents a peakon with the multi-particle approach for simulating the evolution of two peakons. The latter case assumes a simple form as well. We follow the method presented in [22] and consider a suitably refined initial grid of particles to represent the two peakons, in which the initial weights, p_i, of the particles are all zero except for two particles that have weights $p_{n_1}(0) = 4$ and $p_{n_2}(0) = 1$ and are placed at $x_{n_1}(0) = 0$ and $x_{n_2}(0) = 5$, respectively. In this case, it follows from (2.5) that $dp_i/dt = 0$ for each $i \neq n_1, n_2$, and thus the weights of all of the weightless particles will remain constant in time. However, the

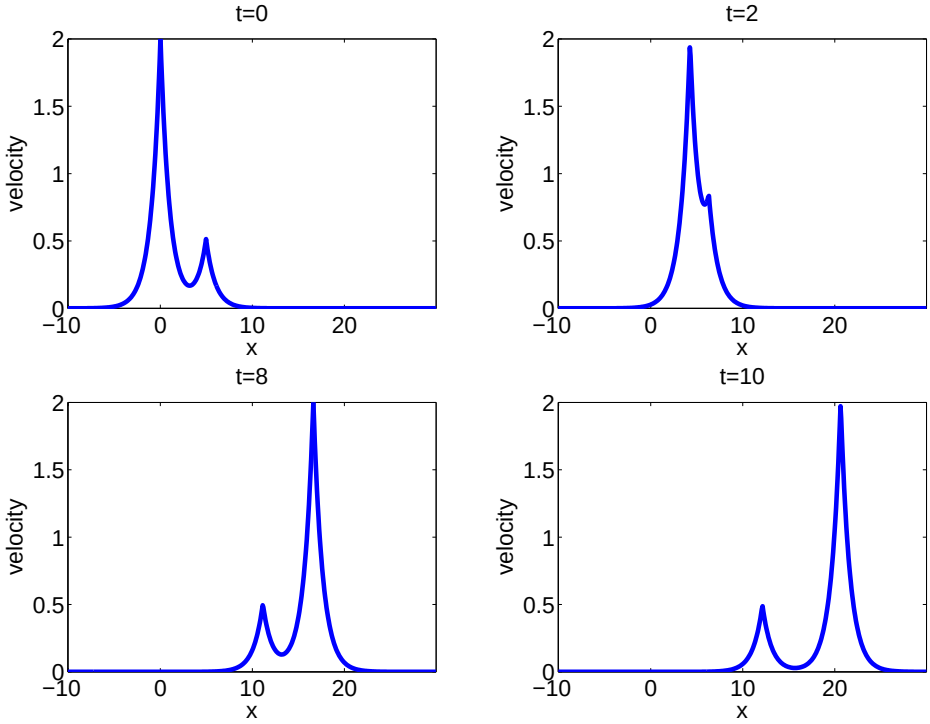

Figure 3.1: Two positive peakon interaction for the CH equation (3.1) for various times.

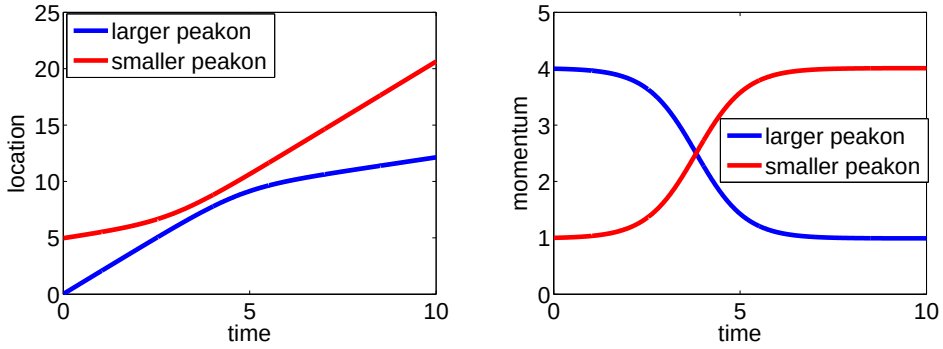

Figure 3.2: Location and momentum trajectories for the two positive peakon interaction.

locations of these particles may change in time since the velocity of the particles depend explicitly on (2.6) which is not necessarily zero. From (2.5) and (2.6), we observe that the $u(x_i(t), t)$ depends solely on $x_{n_1}(t), x_{n_2}(t)$ and $p_{n_1}(t), p_{n_2}(t)$, and thus it is sufficient to evolve the same ODEs for non-zero particles as before.

To rectify the issue of particles clustering around each other, we implement a swapping algorithm, in which the particles are switched once a certain distance threshold is met. In particular, if as before we let Δx^p be the distance between each equidistant point on a computational grid, then we switch the weights, $p_{i+1}(t) \leftrightarrow p_i(t)$, if $x_{i+1}(t) - x_i(t) < \min(\frac{1}{2}(x_i(t) - x_{i-1}(t)), \frac{1}{2}\Delta x^p)$, and $p_i(t) \geq p_{i+1}(t)$. Physically, this algorithm allows peakons to undergo a complex, nonlinear interaction for which there is an exchange of momentum. The results are shown in Figures 3.3–3.6 below – the blue lines correspond to the solution (location trajectories) obtained by running the two particle system (3.6), while the the red ones correspond to the solution computed using the multi-particle approach according to system (2.5). Once again, to plot the computed solution $u(x, t)$, we recover its values on a uniform grid using (2.6). As one can see, the trajectory paths with many particles agree with the trajectory paths for the solution in which we consider only two particles. This shows that even when we consider the interaction among many particles in a peakon simulation, the particles will never cross; rather, they exchange momentums as the particles move closer to each other.

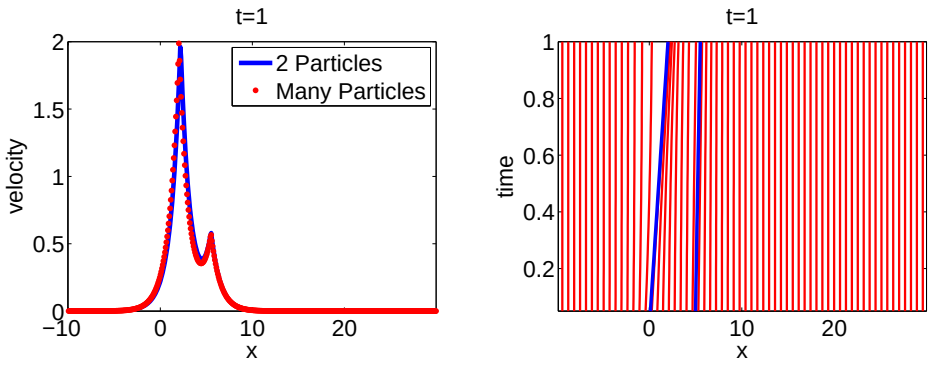

Figure 3.3: The velocity u for the CH equation (3.1) at t=1, and the associated particle location trajectories.

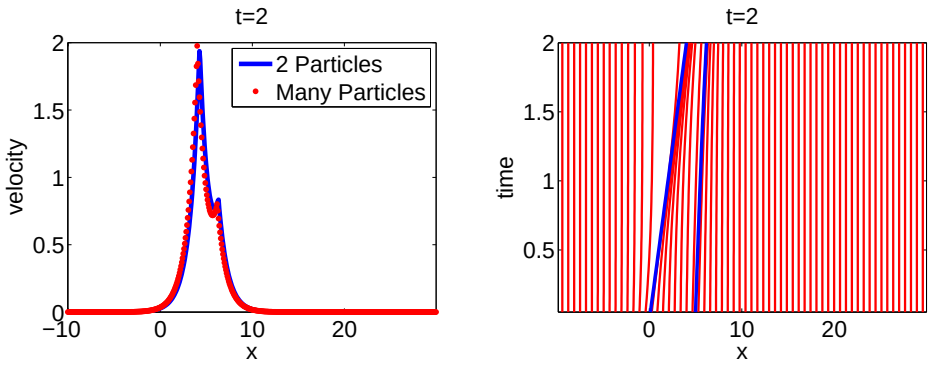

Figure 3.4: The velocity u for the CH equation (3.1) at t=2, and the associated particle location trajectories.

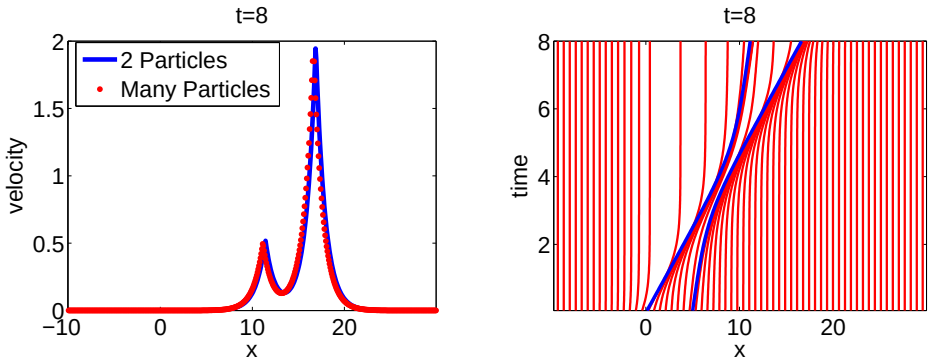

Figure 3.5: The velocity u for the CH equation (3.1) at t=8, and the associated particle location trajectories.

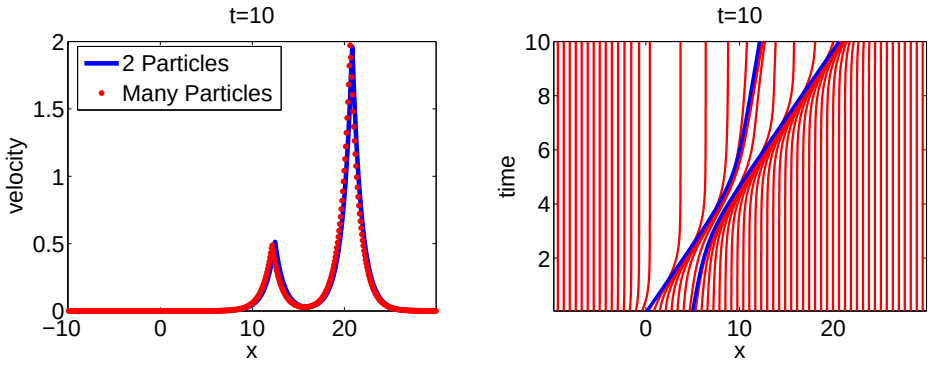

Figure 3.6: The velocity u for the CH equation (3.1) at t=10, and the associated particle location trajectories.

An Illustration of the Peakon-Antipeakon Interaction

One may also observe this no crossing behavior in the peakon-antipeakon case. In this illustration, the peakon and antipeakon (a peakon with a negative initial weight) are initially located at $x_{n_1}(0) = -10$ and $x_{n_2}(0) = 10$ and have momenta of equal magnitude but opposite signs so that the total momentum is zero, i.e., $p_{n_1}(0) = 2$ and $p_{n_2}(0) = -2$. We move the peakons exactly in time according to (3.6) with $\alpha = 1$ on the domain $[a, b] = [-30, 30]$. During the simulation, the total momentum remains zero, however the magnitudes grow very large as the peakon traveling from the left to the right approaches the antipeakon traveling in the opposite direction (see Figure 3.8). At some finite time, t^*, the peakon and antipeakon will collide. Since the total momentum of the system is zero, we expect that the solution will be zero at the collision time t^*. However, due to the inherent symmetry of the problem, $u(x, t) \to -u(-x, -t)$, (c.f, [22] and references therein), peakons may develop after the collision time and propagate in opposite directions, thus exhibiting the elastic collison properties discussed in the previous section. To implement this numerically, we allow particles to exchange momentum, if the particles associated with the nonzero weights are sufficiently close to each other, i.e. $|x_{n_1} - x_{n_2}| < d^*$ where d^* is some prescribed small distance. In our examples, $d^* = \frac{1}{2}\Delta x^p$. To recover the solution $u(x, t)$ as shown below , we once again calculate its values on a uniform grid according to (2.6) (as before, we take $x_j^p = j\Delta x^p,\ \Delta x^p = \frac{b-a}{N_p}$). In Figures 3.8 and 3.9, we plot the location and momentum trajectories for the peakon and antipeakon as a function of time. Here, we observe that similar to the two positive peakon example, the collision between the peakon and antipeakon is elastic in the sense that it involves the exchange of momentum.

If we consider the example where the peakon and antipeakon do not have weights with the same magnitude (say , $p_{n_1}(0) = 1$ and $p_{n_2}(0) = -1.5$), then one may also observe the no crossing behavior for which the peakons exchange momentum. We solve the problem exactly as above with the only change being in the initial weights. With this change, the total momentum is no longer 0; rather, it is -0.5. Similar to the example above, the magnitudes grow very large as the peakon traveling from the left to the right approaches the antipeakon traveling in the opposite direction. Once again, at some finite time, t^*, the peakon and antipeakon will collide. This time, however, the two peakons merge into one antipeakon with a weight -0.5 which is to be expected. Taking advantage of the inherent symmetry built into the problem (see above), we know that peakons may develop after

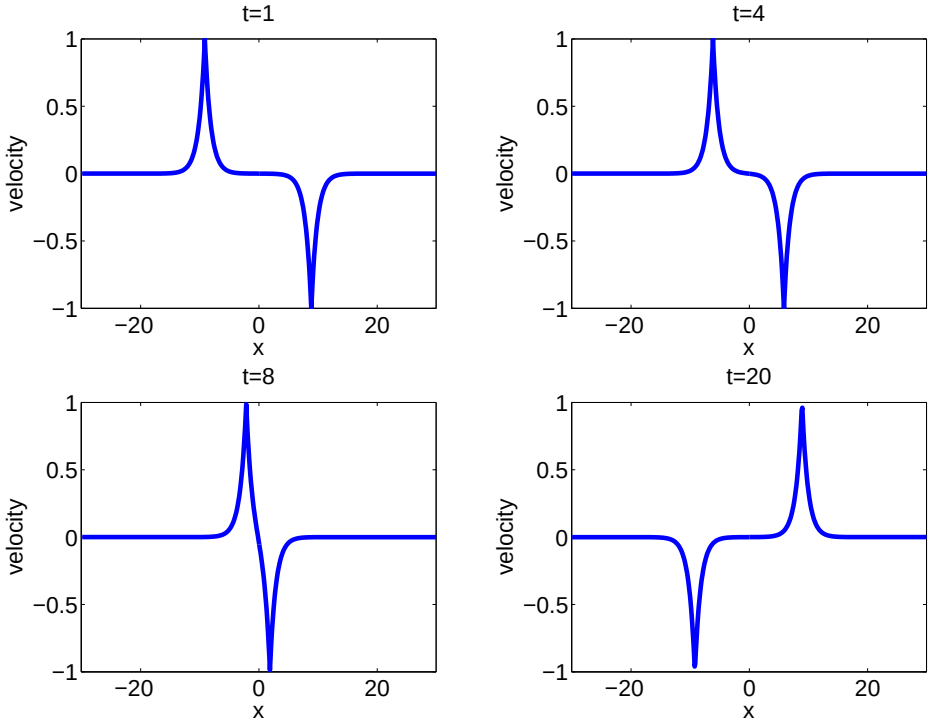

Figure 3.7: An Illustration of the peakon-antipeakon phenomenon at various times.

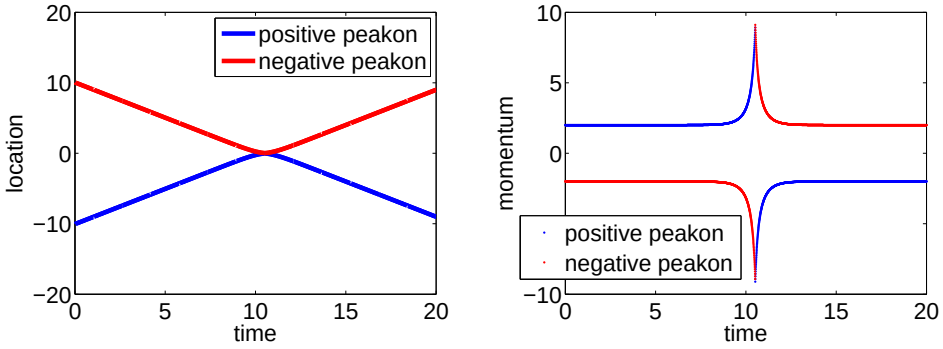

Figure 3.8: Location and momentum trajectories for the peakon-antipeakon interaction.

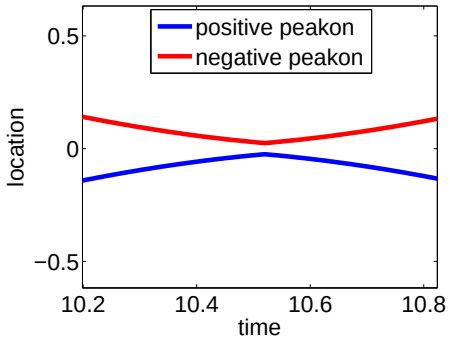

Figure 3.9: (Zoomed) Location trajectories for the peakon-antipeakon interaction.

the collision and propagate in different directions. Using the same numerical strategy as the first peakon-antipeakon case, we observe that the collision between the peakon and antipeakon is elastic in the sense that it involves the exchange of momentum, even when the initial weights have different magnitudes.

3.3 Numerical Experiments

In this section, we perform several numerical simulations, which solve the CH equation under a wide range of initial data. We illustrate that the peakons' behavior is reminiscent of the soliton paradigm as the peakon represents a self-reinforcing solitary wave that maintains its shape while it travels at a constant finite speed. Peakons also exhibit a remarkable stability as their identity is retained through strong nonlinear interactions. The presented numerical examples do not only corroborate the analytical results, but also demonstrate some of the practical advantages that the particle method holds over other numerical methods. In particular, we consider both peakon solutions and solutions arising from arbitrary smooth initial data. In all cases, we compare the results obtained by the particle method (PM) with those obtained using a finite volume (FV) approach, in particular, a semi-discrete central upwind scheme (CU) described in Chapter 1.

CU Scheme for the CH Equation

To apply the CU scheme to the CH equation, we first rewrite the CH equation in the equivalent conservative form:

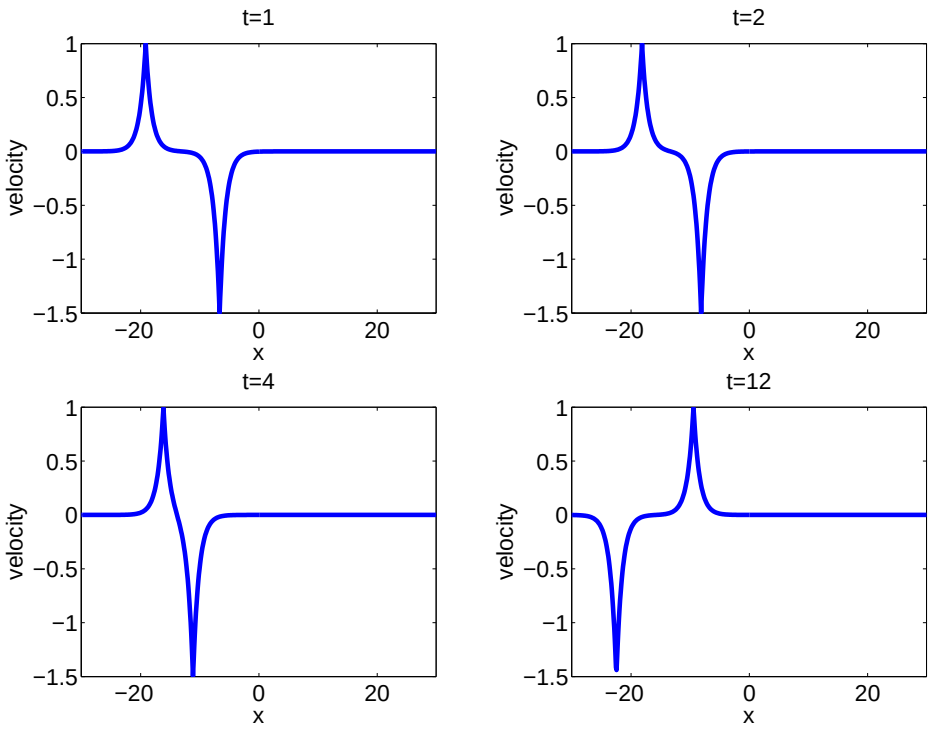

Figure 3.10: An Illustration of the peakon-antipeakon (with different magnitudes) phenomenon at various times.

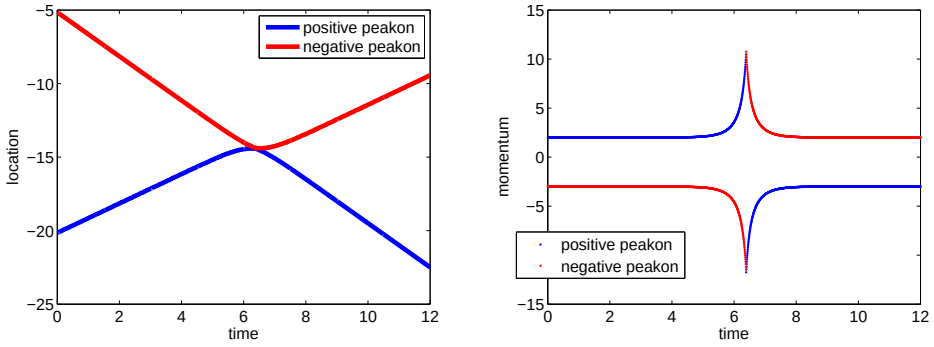

Figure 3.11: Location and momentum trajectories for the peakon-antipeakon (with different magnitudes) interaction.

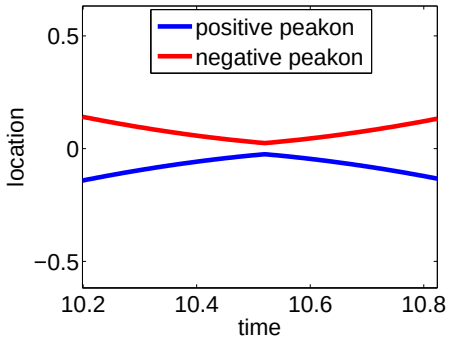

Figure 3.12: (Zoomed) Location trajectories for the peakon-antipeakon (with different magnitudes) interaction.

$$m_t + f(m,u)_x = 0, \quad f(m,u) := um + \frac{1}{2}u^2 - \frac{\alpha^2}{2}u_x^2, \quad m = u - \alpha^2 u_{xx}. \tag{3.12}$$

According to the description in Chapter 1, the second-order CU scheme is then given as

$$\frac{d}{dt}\overline{m}_j(t) = -\frac{H_{j+1/2}(t) - H_{j-1/2}(t)}{\Delta x^c}, \tag{3.13}$$

where the numerical fluxes, $H_{j+1/2}$, are

$$H_{j+1/2}(t) = \frac{a^+_{j+1/2} f\left(m^-_{j+1/2}\right) - a^-_{j+1/2} f\left(m^+_{j+1/2}\right)}{a^+_{j+1/2} - a^-_{j+1/2}} + \frac{a^+_{j+1/2} a^-_{j+1/2}}{a^+_{j+1/2} - a^-_{j+1/2}}\left[m^+_{j+1/2} - m^-_{j+1/2}\right]. \tag{3.14}$$

In (3.13), $\overline{m}_j(t)$ denote the cell averages of m and are given by

$$\overline{m}_j(t) := \frac{1}{\Delta x^c}\int_{C_j} m(x,t)\,dx, \tag{3.15}$$

where $C_j = [x_{j-\frac{1}{2}}, x_{j+\frac{1}{2}}]$. $m^{\pm}_{j+1/2}$ are the point values at $x_{j\pm1/2} = x_j \pm \frac{\Delta x^c}{2}$ to the solution m at each cell interface, given a piecewise polynomial reconstruction (1.56). That is,

$$\begin{aligned} m^+_{j+1/2} &= \overline{m}_{j+1}(t) + (m_x)_{j+1}\left(x_{j+1/2} - x_j\right), \\ m^-_{j+1/2} &= \overline{m}_j(t) + (m_x)_j\left(x_{j+1/2} - x_j\right), \end{aligned}$$

where $(m_x)_j$ is calculated using (1.57).

We recall from Chapter 1 that there may exist discontinuities at the end points for each value of j in our linear piecewise polynomial reconstruction. These possible discontinuities propagate with right- and left sided local speeds, which may be estimated as follows

$$a^+_{j+1/2} = \max\left\{u^-_{j+1/2}, u^+_{j+1/2}, 0\right\},$$
$$a^-_{j+1/2} = \min\left\{u^-_{j+1/2}, u^+_{j+1/2}, 0\right\},$$

where $u^{\pm}_{j+1/2}$ are the values of the velocity at cell interfaces. We recall that the momentum and velocity in the CH equation (3.1) are related through the modified Helmholtz equation, which we may solve by transforming the PDE to an algebraic equation in another (i.e. frequency) domain, via a Fourier transform. To this extent, we recall that the Fourier transform of a continuous function is given by

$$\mathscr{F}[u] = F(\xi) = \frac{1}{\sqrt{2\pi}}\int_{-\infty}^{\infty} u(x)e^{-i\xi x}\,dx. \tag{3.16}$$

For sufficiently smooth functions, the following property is particularly useful for transforming PDEs to algebraic equations:

$$\mathscr{F}\left[u^{(n)}\right] = \frac{1}{\sqrt{2\pi}}\int_{-\infty}^{\infty} u^{(n)}e^{-i\xi x}\,dx = (i\xi)^n\mathscr{F}[u]. \tag{3.17}$$

For instance, if $\mathscr{F}[u] = \hat{u}$, then one has the following expression:

$$m = u - \alpha^2 u_{xx} \implies \hat{u} = \frac{\hat{m}}{1+\alpha^2\xi^2}. \tag{3.18}$$

One can then compute the inverse Fourier transform given by

$$\mathscr{F}^{-1}[\hat{u}] = u = \frac{1}{\sqrt{2\pi}}\int_{-\infty}^{\infty} \hat{u}(\xi)e^{i\xi x}\,d\xi. \tag{3.19}$$

to recover u. Numerically, one can use a Fast Fourier Transform (and an Inverse Fast Fourier Transform) to carry out these calculations. This technique is used to first solve the modified Helmholtz equation (3.18) to recover the cell center values $\{u_j\}$ from $\{\overline{m}_j\}$ (in the performed numerical experiments, we have used periodic boundary conditions). The cell interface values $u^{\pm}_{j+\frac{1}{2}}$ are then computed from $\{u_j\}$ using the minmod limiter

(1.58).

We remark that the resulting scheme (3.13), (3.14) is a system of time dependent ODEs which should be solved using a high-order (at least second order accuracy) method. For our numerical experiments, we used a third-order SSP (strong stability preserving) Runge-Kutta method (see e.g. [68]) with an adaptive time step $\Delta t < \frac{\Delta x^c}{2a_{\max}}$, where

$$a_{\max} := \max_j \left\{ a^+_{j+1/2}, -a^-_{j+1/2} \right\}.$$

The results shown below demonstrate the advantages that the particle method holds over the CU scheme. In all of the examples that follow, we take $\alpha = 1$ and $\theta = 1.5$ in (1.58) associated with the CU scheme.

3.3.1 Peakon Initial Data

Single Peakon. We begin by considering a single peakon solution and implementing the multi-particle approach described in Section 3.2.1 in the context of two particles. To this extent, we place $N_p = 500$ equidistant particles in the interval $[-30, 30]$ at $t = 0$ such that $p_i = 0$ for $i \neq q$ and $p_q = 1$. As we discussed before, the weights of all of the zero particles in consideration will remain constant in time. Their locations will change in time according to the values of the velocity $u(x_i(t), t)$, which in this case depends solely on $x_q(t)$ and $p_q(t)$, and therefore can be computed explicitly:

$$u(x_i(t), t) = \frac{1}{2} p_q(t) e^{-|x_q(t) - x_i(t)|}, \quad x_q(t) = \frac{1}{2} p_q(0) t + x_q(0). \tag{3.20}$$

This remarkable simplicity in integrating the ODE as well as recovering the solution at any $t > 0$ is one advantage that the particle method holds over say a finite volume approach. To illustrate this, we compare the results generated from the particle method to those obtained by applying a second-order CU scheme to the CH equation (3.1). In the finite volume setting, we use a uniform grid $x_j = j\Delta x^c$ with $\Delta x^c = 0.12$ (i.e., $N_c = 500$) on the same interval $[-30, 30]$. To compare the FV solution with the PM solution we run the simulations until $t = 1$ and $t = 10$ (initially we place particles at the middle of each finite volume cell). The solutions obtained by both methods are presented in Figure 3.13. As one can see, the particle solution generates a more accurate approximation to the solution of (3.1) due to the minimal effects of numerical diffusion. We observe that the

maximum height of the "peak" generated from the CU scheme becomes noticeably smaller as time progresses. This is due to the numerical diffusion introduced by the FV scheme which is a result of its Eulerian nature. In contrast, the particle method is Lagrangian in nature, and hence is generally resistant to the numerical diffusion introduced in the approximation of the solution. In Figure 3.14 we show that the FV solution converges to the particle solution through an appropriate grid refinement study. In this figure, we take $N_c = 3000$ in the FV simulations while the number of particles remains $N_p = 500$ as before.

Remark 3.3.1. We would like to remark that the examples considered in this chapter are comparable with [146], in which the authors solved the CH equation with both peakon initial data and non-peakon initial data. There, they considered a local discontinuous Galerkin method to numerically solve the CH equation.

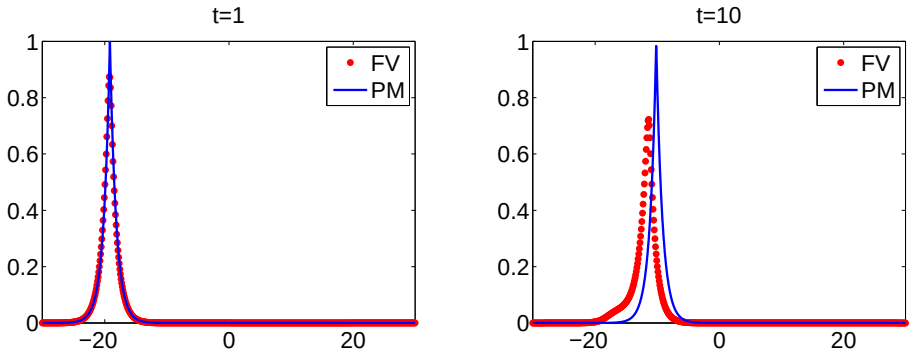

Figure 3.13: The velocity u obtained by both PM and FV at times $t = 1, 10$ with $N_p = N_c = 500$.

Two Peakons. Next, we return to the two-peakon problem discussed in Section 3.2.1 and perform a comparison against a CU scheme. Similar to the previous example, for the FV method, we use a uniform grid $x_j = j\Delta x^c$ with $\Delta x^c = 0.12$ (i.e., $N_c = 500$) on the same interval $[-10, 30]$. As in the one peakon case, we see in Figure 3.15 that the peak associated with the FV solution is shorter than that of the PM solution which is a direct consequence of the numerical diffusion introduced into the problem. Due to this dampening of the peakon's height from the FV method, we expect that as the peakons

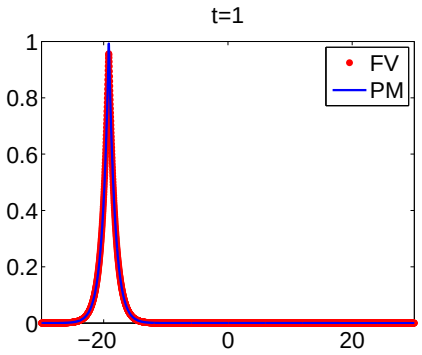

Figure 3.14: The velocity u obtained by both PM and FV at times $t = 1$ with $N_p = 500, N_c = 3000$.

propagate in time, the error between the CU scheme and particle method grows. One can reduce this error between the simulations by considering a finer computational grid for the CU scheme. In Figure 3.16, we consider such a refinement by taking $N_c = 3000$ while still having $N_p = 500$. This shows that the particle method is able to capture complicated nonlinear interactions among peakon solutions for (3.1) with considerably fewer points compared to FV methods. We also see that as in the single peakon example, the solution generated from the FV method will converge to the particle method.

3.3.2 Arbitrary Smooth Initial Data

If we do not consider an initial condition in the form of a linear combination of peakon solutions, then we are no longer guaranteed that the particle method will yield an exact solution to (3.1).To this extent, we consider the following smooth initial data:

$$m(x,0) = \begin{cases} 3\cos^2\left(\frac{1}{4}x\right) & : |x| \leq 2\pi, \\ 0 & : |x| > 2\pi. \end{cases} \tag{3.21}$$

To simulate solutions using a particle method, we place $N_p = 500$ equidistant particles in the interval $[-10, 30]$ at $t = 0$, with the initial weights given by $p_i(0) = \Delta x^p m(x_i(0), 0)$ where $\Delta x^p = \frac{4}{50}$. We then evolve the locations and weights of the particles according to the system of ODEs given by (2.5). As usual, we recover the velocity $u(x,t)$ at some final time t by computing its values on a uniform grid according to (2.6) (here we take the

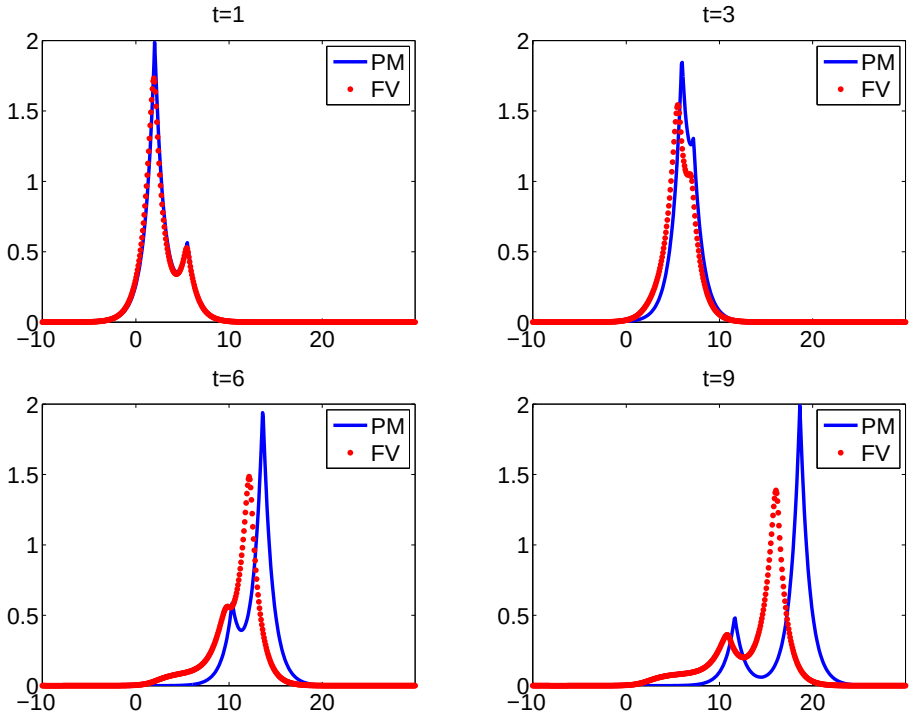

Figure 3.15: The velocity u for the CH equation obtained by FV and PM at various times with $N_p = N_c = 500$.

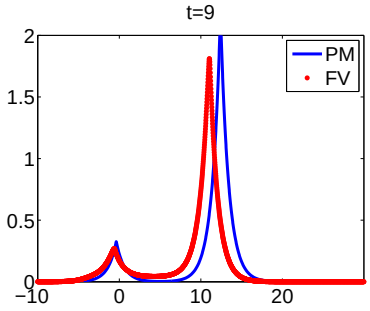

Figure 3.16: The velocity u for the CH equation at t=9 with $N_p = 500, N_c = 3000$.

same Δx^p used in the initial placement of the particles). To simulate solutions via a CU scheme, we use a uniform grid $x_j = j\Delta x^c$ with $\Delta x^c = \Delta x^p$ on the same interval $[-10, 30]$. For clarity purposes, at further times ($t > 4$), we extend the computation domain so that one may clearly see the "peakon train" that forms as we simulate the solution for longer periods of time.

In Figure 3.17, we show that the PM solution generates a more accurate approximation to the solution of (3.1) due to its low numerical diffusion. We observe a "steepening behavior" as was described in [16, 17] and the formation of peakons from arbitrarily smooth data. This is due to the complete integrability of (3.1). In fact, we expect peakons to form after a finite time for any smooth arbitrary initial data.

The accuracy of both the particle and finite volume method may be visualized by performing a grid refinement study as is done in Figure 3.18. Similar to the peakon simulations in 3.3.1, we observe that the maximum height of the "peak" generated from the CU scheme becomes noticeably smaller as time progresses. Finally, in Figure 3.19, we show that the FV solution converges to the PM solution with a suitably refined grid. Here we consider $N_c = 7000$ compared to the original $N_p = 500$ particles placed in a uniform grid for the particle method. This shows once again that the particle method is able to resolve the solution to (3.1) under a suitable class of smooth initial data, with less points than a a FV method.

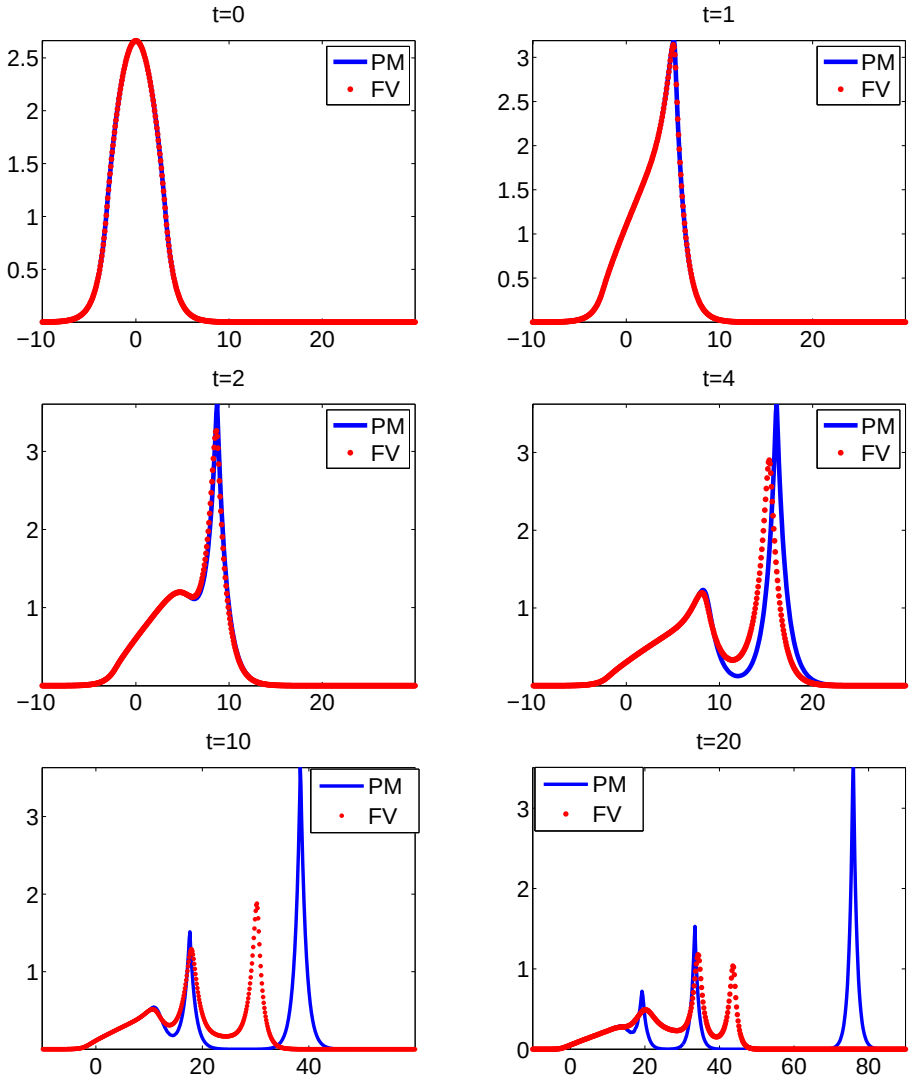

Figure 3.17: The velocity u for the CH equation obtained by FV and PM at various times with $N_c = N_p = 500$.

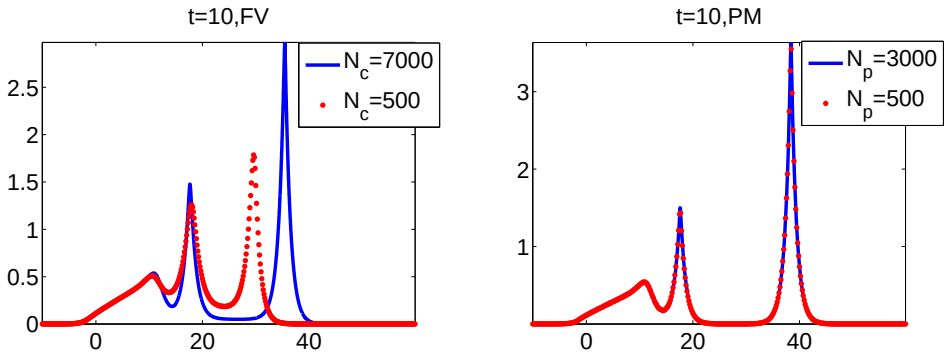

Figure 3.18: Grid refinement analysis for both FV and PM at $t = 10$.

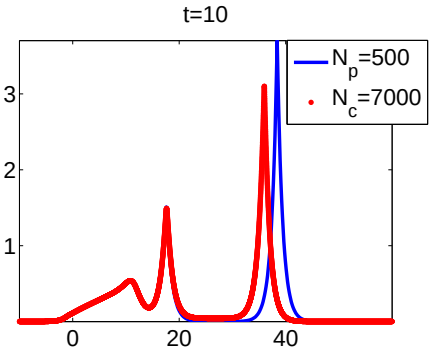

Figure 3.19: The velocity u for the CH equation obtained by FV and PM at $t = 10$, $N_c = 7000$ and $N_p = 500$.

Chapter 4

Long Time Tsunami Wave Propagation

4.1 Introduction

Due to the potential tragic nature of tsunami waves, there is a need for the scientific understanding and modeling of this complicated phenomenon in order to reduce unwanted destruction and prevent unnecessary deaths from this natural disaster. Tsunami waves are caused by the displacement of a large volume of a body of water, typically in an ocean or a large lake, see, e.g., [15, 124, 127]. They do not resemble other sea waves and are instead characterized by having relatively low amplitude (wave height) offshore, large wavelength, and large characteristic wave speed. This characterization is what prevents tsunami waves from being felt at sea. Tsunami waves grow in height as they reach shallowing water, in what is known as a *wave shoaling* process. In this process, the wave slows down, the wavelength decreases, and a very high and powerful wave arrives on the shore and may cause massive destruction.

There have been many attempts to create accurate models and corresponding numerical methods for simulating tsunami waves. One popular model in shallow water wave theory is the classical Saint-Venant system [52], which reasonably approximates the behavior of real ocean waves and is a depth-averaged system that can be derived from the Navier-Stokes equations, see, e.g., [87, 105, 130]. The Saint-Venant system is a very good simplification for lakes, rivers, and coastal areas in which the typical time and space scales of interest are relatively short. Because the Saint-Venant system is quite difficult to

solve, it is sometimes simplified in a number of ways, including linearization, in which the velocity of water particles is taken to be the gradient of a scalar potential. Taking various asymptotic limits of the inviscid Euler equations result in a host of integrable and nearly integrable equations such as the Korteweg-de Vries (KdV) equation, the Camassa-Holm (CH) equation,the nonlinear Schrödinger equation, and so on, see, e.g., [90, 129, 139, 144].

Tsunami waves form in deep water and travel very long distances (thousands of kilometers) before coming to shore. Over long time, solutions of the Saint-Venant system break down, dissipate in an unphysical manner, develop shock waves, and fail to capture small, trailing waves that are seen in nature and laboratory experiments. Thus, it is necessary to use a more sophisticated model in order to preserve the wave characteristics over long time simulations.

Non-hydrostatic models (such as the celebrated Green-Naghdi equations [69] and several others, see, e.g., [4, 7, 8] and references therein) work well for the long-time propagation of tsunami-type waves because they allow the wave to travel for long distances without changing the shape or decaying in amplitude. In addition, since these systems are dispersive, they give rise to trailing waves that are observed to follow tsunamis in nature. However, it is necessary to achieve some balance between the dispersion observed with a non-hydrostatic model and the dissipation seen in the classical Saint-Venant system.

One attempt to achieve such a balance has been recently made in [13, 14], where the non-hydrostatic Saint-Venant system has been rigorously derived from the Green-Naghdi equations. As has been demonstrated in [26], the non-hydrostatic Saint-Venant system is capable of accurately modeling long-time propagation of tsunami-type waves. However, the system is quite complicated and developing highly accurate, robust and efficient numerical methods for computing its solutions is a highly non-trivial task.

Another system that has been derived from the Green-Naghdi equations is a two-component generalization of the CH equation, for which the integrability property associated with the CH equation has been combined with compressibility, see, e.g., [42, 84, 135]. Compared with the original CH equation, the two-component Camassa-Holm (2CH) equation contains an additional continuity equation for the scalar density ρ, and the momentum (velocity) equation contains a pressure term involving density:

$$\rho_t + (\rho u)_x = 0, \tag{4.1a}$$

$$m_t + um_x + 2mu_x = -\frac{g}{2}(\rho^2)_x, \quad m = u - \alpha^2 u_{xx}. \tag{4.1b}$$

Similar to the CH equation, $m(x,t)$ is the momentum related to the fluid velocity $u(x,t)$ through the modified Helmholtz equation, the density $\rho(x,t)$ is related to the total depth of the water column, $\alpha > 0$ is a length scale, and $g > 0$ is the gravitational constant.

In this chapter, we develop a new numerical method in an attempt to solve the 2CH equation under the context of tsunami waves dynamics using appropriate initial data. The preliminary results shown in this chapter serve as an impetus for the eventual goal of showing that the 2CH equation could become a viable model for the long time propagation of tsunami-type waves. To begin, we first consider the finite-volume central-upwind (CU) scheme for solving the system (4.1). To apply the (CU) scheme to the system (4.1), we rewrite equations (4.1a) and (4.1b) in the following conservative form:

$$\begin{aligned} &\rho_t + (\rho u)_x = 0, \\ &m_t + \left(um + \frac{1}{2}u^2 - \frac{\alpha^2}{2}u_x^2 + \frac{1}{2}g\rho^2 \right)_x = 0, \end{aligned} \tag{4.2}$$

and then implement the CU scheme for system (4.2) in quite a straightforward manner as it was described in Chapter 1.

Even though the designed finite-volume (FV) method is robust and efficient, it suffers from excessive numerical dissipation in the same manner for which the CU scheme for the original CH equation did (as was shown in Chapter 3). To reduce the amount of numerical diffusion, we follow the idea presented in [23, 24, 27] and derive a hybrid finite-volume-particle (FVP) method for the system (4.1). In the hybrid approach, the density equation (4.1a) is solved using the CU scheme, while the momentum equation and velocity equation (4.1b) are solved by a deterministic particle method. Particle methods were originally introduced for solving linear transport equations (see, e.g., [49, 131]), but in recent years have also been used for approximating solutions to a variety of time-dependent PDEs, see, e.g., [25, 29, 30, 56, 111].

Finally, in §4.4, we perform several numerical experiments to study the effect of the bifurcation parameter α in (4.1b) and to compare the performance of the CU scheme and hybrid FVP method. The obtained results demonstrate that for certain choices of

α, the amplitude and speed of the wave, generated by solving (4.1a)–(4.1b), is preserved for longer times than those solved by the classical Saint-Venant system.

4.2 A Derivation of the Two Component Camassa-Holm System

In this section, we follow a process as described in [42, 86] for deriving the 2CH equation in the context of shallow water waves. To this extent, we begin with a reduced version of the celebrated Green-Naghdi (GN) equations, which are derived from Euler's equations, under a particular set of assumptions. For instance, one may consider the motion of shallow water over a flat surface, which is located at $z = 0$. One may also assume that the motion is in the x-direction and that the physical variables do not depend on y. If we let h be the mean level of water, a the typical wavelength amplitude of the wave and λ the typical wavelength of the wave then we can introduce the following dimensionless parameters $\epsilon = a/h$ and $\delta = h/\lambda$, which are assumed to be small in shallow water wave dynamics. If we let $u(x,t)$ describe the horizontal velocity of the fluid and $\eta(x,t)$ describe the horizontal deviation of the surface from equilibrium, then the reduced form of the GN equations (in the context of 1D wave motion over a flat, horizontal bed) are given as

$$\begin{aligned} &u_t + \epsilon u u_x + \eta_x = \frac{\delta^2/3}{1+\epsilon\eta}\left[(1+\epsilon\eta)^3\left(u_{xt} + \epsilon u u_{xx} - \epsilon u_x^2\right)\right]_x = 0, \\ &\eta_t + \left[u\left(1+\epsilon\eta\right)\right]_x = 0. \end{aligned} \tag{4.3}$$

These equations are obtained under the assumption that at leading order, u is not a function of z. While this is not correct at $O(\epsilon)$, this approximation is valid for the leading order problem (see e.g. [86]). In fact, this assumption is equivalent to the simplifying approximation used by Green and Naghdi ([69]). Using this assumption as well as the pressure term's derivative in Euler's equation, the authors in [86] were able to deduce the following condition for the pressure term in Euler's equation:

$$p = \eta - \frac{1}{2}\delta^2\left\{(1+\epsilon\eta)^2 - z^2\right\}\left(u_{xt} + \epsilon u u_x - \epsilon u_x^2\right). \tag{4.4}$$

A leading order expansion with respect to the variables ϵ and δ^2 yields the following system of equations

$$\left(u - \tfrac{\delta^2}{3}u_{xx}\right)_t + \epsilon u u_x + \eta_x = 0, \tag{4.5}$$

$$\eta_t + \left[u\left(1 + \epsilon\eta\right)\right]_x = 0. \tag{4.6}$$

To derive the 2CH equation, we follow the process given in [42] and consider a function of u and η in the form

$$\rho(u, \eta) = \rho_0 + B\epsilon\eta - C\epsilon^2\left(u^2 + \eta^2\right), \tag{4.7}$$

where ρ_0, B, C are arbitrary constants. One may expand ρ in the same order of ϵ as in ρ^2 to obtain

$$\rho^2 = \rho_0^2 + 2B\rho_0\epsilon\eta + \epsilon^2\left(B^2 - 2C\rho_0\right)\eta^2 - 2C\rho_0\epsilon^2u^2. \tag{4.8}$$

We observe that

$$\left(\rho^2\right)_x = 2B\rho_0\epsilon\eta_x + \epsilon^2\left(2B^2 - 4C\rho_0\right)\eta\eta_x - 4C\rho_0\epsilon^2uu_x,$$

and when comparing this to (4.5), we take $2B^2 - 4C\rho_0 = 0$ or $B = \sqrt{2C\rho_0}$. This yields the following

$$\frac{1}{\epsilon}\left(\rho^2\right)_x = 2\sqrt{2C\rho_0}\rho_0\eta_x - 4C\rho_0\epsilon uu_x. \tag{4.9}$$

Thus, we may rewrite (4.5) as follows

$$\left(u - \frac{\delta^2}{3}u_{xx}\right)_t + \left(1 + \sqrt{\frac{2C}{\rho_0}}\right)\epsilon uu_x + \frac{1}{2\epsilon\sqrt{2C\rho_0}\rho_0}\left(\rho^2\right)_x = 0. \tag{4.10}$$

We may further simplify (4.10), by taking $m = u - \frac{\delta^2}{3}u_{xx}$ and using the following relations (taking ϵ as the highest order):

$$\epsilon mu_x \approx \epsilon uu_x,$$

$$\epsilon um_x \approx \epsilon uu_x.$$

This allows us to rewrite (4.10) as follows:

$$m_t + \frac{1}{2\epsilon\sqrt{2C\rho_0}\rho_0}\left(\rho^2\right)_x + D\epsilon mu_x + E\epsilon um_x = 0, \tag{4.11}$$

where $D+E=1+\sqrt{\frac{2C}{\rho_0}}$. From (4.3), we have the following approximations: $u_t \approx -\eta_x$ and $\eta_t \approx -u_x$. Thus, we can write

$$\rho_t = \sqrt{2C\rho_0}\epsilon\eta_t + 2C\epsilon^2\left(uu_t + \eta\eta_t\right) = \sqrt{2C\rho_0}\epsilon\eta_t + 2C\epsilon^2\left(\eta u\right)_x.$$

Using the fact that $\rho \approx \rho_0 + \sqrt{2C\rho}\epsilon\eta$, we obtain

$$\begin{aligned}(\rho u)_x &= \rho u_x + u\rho_x \\ &= \left(\rho_0 + \sqrt{2C\rho}\epsilon\eta\right)u_x + u\left(\sqrt{2C\rho}\epsilon\eta_x\right) \\ &= \rho_0 u_x + \sqrt{2C\rho_0}\epsilon\left(\eta u\right)_x.\end{aligned}$$

Using the two facts above, we obtain

$$\rho_t + \sqrt{\frac{2C}{\rho_0}}\epsilon\left(\rho u\right)_x = \sqrt{2C\rho_0}\epsilon\left(\eta_t + u_x + \frac{4C}{\sqrt{2C\rho_0}}\epsilon\left(\eta u\right)_x\right) = 0, \tag{4.12}$$

if we take $\frac{4C}{\sqrt{2C\rho_0}} = 1$ or $C = \frac{1}{8}\rho_0$ (by (4.6)). We remark that this implies that

$$\rho = \rho_0 + \frac{1}{2}\rho_0\epsilon\eta - \frac{1}{8}\rho_0\epsilon^2\left(u^2+\eta^2\right),$$

and hence $\rho \to \rho_0$ as $|x| \to \infty$. We also note that if the local size of ϵ is about the same size of δ^2, then one may achieve a balance between nonlinearity and dispersion. The scalings that allow one to achieve such a balance are given by

$$x = \frac{\delta}{\sqrt{\epsilon}}\hat{x}, \quad t = \frac{\delta}{\sqrt{\epsilon}}\hat{t}. \tag{4.13}$$

We can use the following rescaling to eliminate ϵ and ρ_0 from (4.11) and (4.12) : $u \to \frac{2}{\epsilon}u$, $\rho \to \rho_0\rho$. If we let $\alpha^2 = \frac{\delta^2}{3}$, then we obtain the following system of PDEs:

$$\begin{aligned}&m_t + 2Dmu_x + 2Eum_x = -\rho\rho_x, \\ &\rho_t + (\rho u)_x = 0,\end{aligned} \tag{4.14}$$

with $m = u - \alpha^2 u_{xx}$ and $D+E = \frac{3}{2}$. Finally, to add a dependence on g as given by (4.1b), we let $\rho = \sqrt{g}\rho$ to obtain:

$$\begin{aligned} &m_t + 2Dmu_x + 2Eum_x = -g\rho\rho_x, \\ &\rho_t + (\rho u)_x = 0. \end{aligned} \tag{4.15}$$

We remark that if $D = 1$ and $E = 1/2$, then (4.15) reduces to the 2CH equation. If $D = E = 3/4$, then (4.15) reduces to the following conservative form:

$$\begin{aligned} &m_t + \frac{3}{2}(um)_x = -g\rho\rho_x, \\ &\rho_t + (\rho u)_x = 0, \end{aligned} \tag{4.16}$$

Another interesting case is when $\alpha = 0$ or $m = u$ in which the 2CH equation assumes the form

$$\begin{aligned} &u_t + \left(\frac{3}{2}u^2 + g\rho^2\right)_x = 0, \\ &\rho_t + (\rho u)_x = 0. \end{aligned} \tag{4.17}$$

For comparison purposes we note that this case most closely resembles the Saint-Venant system given by

$$\begin{aligned} &h_t + (uh)_x = 0, \\ &(hu)_t + \left(hu^2 + \frac{1}{2}gh^2\right)_x = 0. \end{aligned} \tag{4.18}$$

Here, h is the height (depth) of an incompressible fluid, and hu is the momentum (or discharge) of the system.

An open question is to determine how one may relate (4.17) with (4.18). For instance, is there a way to relate ρ in (4.17) with h in (4.18) algebraically? Is the momentum m given in (4.17) the same momentum as given in (4.18)? One way to gain a better understanding of the possible connection between the 2CH equation (with $\alpha = 0$) and the Saint Venant system is to derive (4.18) in the context of the Green-Nagdhi equations without dispersion (as we have done for the 2CH equation). Indeed, if we consider (4.3) with $h = 1 + \epsilon\eta$ or $\eta = \frac{1}{\epsilon}(h - 1)$ then we may express (4.3) as follows:

$$\begin{aligned} &u_t + \epsilon u u_x + \frac{1}{\epsilon}(h_x) = 0, \\ &\frac{1}{\epsilon}h_t + (hu)_x = 0. \end{aligned} \tag{4.19}$$

(4.19) further simplifies to

$$\begin{aligned} &(\epsilon u)_t + \left(\frac{(\epsilon u)^2}{2} + h \right)_x = 0, \\ &h_t + (h(\epsilon u))_x = 0. \end{aligned} \tag{4.20}$$

Finally, we take $\bar{u} = \epsilon u$ to arrive at an alternative form of the Saint Venant system:

$$\begin{aligned} &\bar{u}_t + \left(\frac{\bar{u}^2}{2} + h \right)_x = 0, \\ &h_t + (h\bar{u})_x = 0. \end{aligned} \tag{4.21}$$

To add a dependence on g and arrive back to the Saint Venant system given in (4.18), we let $h = gh$. We remark that (4.18) is equivalent to (4.21) only under the assumption of smooth solutions. From the derivations of the 2CH equation and the Saint Venant system, we see that a possible relation between h and ρ is

$$\rho \approx \rho_0 + \frac{1}{2}\rho_0(h-1) - \frac{1}{8}\rho_0(h-1)^2.$$

4.3 Numerical Methods for the 2CH Equation

In this section, we present two different numerical methods for the purpose of solving the 2CH equation. We begin our discussion by describing the process for applying a CU scheme (as presented in Chapter 1) to the 2CH equation. We then present a hybrid finite volume-particle (FVP) method, which utilizes the strengths of both the FV and particle method. To this regard, we solve the continuity equation (4.1a) using the CU scheme while simultaneously solving the momentum and velocity equations (4.1b) by a deterministic particle method.

4.3.1 A Semi-discrete Central Upwind Scheme for the 2CH Equation

To apply a semi-discrete central upwind scheme (FV) for the 2CH equation, we follow the approach described in Chapter 1 in quite a straightforward manner by rewriting the

2CH equation in conservative form (see (1.30)) to obtain

$$\boldsymbol{q} = \begin{pmatrix} \rho \\ m \end{pmatrix}, \qquad \boldsymbol{f}(\boldsymbol{q}) = \begin{pmatrix} \rho u \\ mu + \dfrac{1}{2}\,u^2 - \dfrac{\alpha^2}{2}\,u_x^2 + \dfrac{g}{2}\,\rho^2 \end{pmatrix}, \tag{4.22}$$

where u globally depends on m through the modified Helmholtz equation (4.1b). The CU scheme for (4.22) is then given by (1.59)–(1.60) with the local speeds $a^{\pm}_{j\pm1/2}$ that should be estimated from the largest and smallest eigenvalues of the Jacobian $\frac{\partial \boldsymbol{f}}{\partial \boldsymbol{q}}$. In the purely hyperbolic case, that is, when $\alpha = 0$ and thus $u(m) \equiv m$, the right- and left-sided local speeds of propagation can be easily estimated using the largest and smallest eigenvalues of the Jacobian

$$\frac{\partial \boldsymbol{f}}{\partial \boldsymbol{q}} = \begin{pmatrix} m & \rho \\ g\rho & 3m \end{pmatrix} \equiv \begin{pmatrix} u & \rho \\ g\rho & 3u \end{pmatrix}. \tag{4.23}$$

The eigenvalues associated with (4.23) are given by

$$\lambda_{\pm} = 2u \pm \sqrt{u^2 + g\rho^2}, \tag{4.24}$$

and hence we have

$$\begin{aligned} a^{+}_{j+\frac{1}{2}} &= \max\left\{2u^{-}_{j+\frac{1}{2}} + \sqrt{\left(u^{-}_{j+\frac{1}{2}}\right)^2 + g\left(\rho^{-}_{j+\frac{1}{2}}\right)^2},\, 2u^{+}_{j+\frac{1}{2}} + \sqrt{\left(u^{+}_{j+\frac{1}{2}}\right)^2 + g\left(\rho^{+}_{j+\frac{1}{2}}\right)^2},\, 0\right\}, \\ a^{-}_{j+\frac{1}{2}} &= \min\left\{2u^{-}_{j+\frac{1}{2}} - \sqrt{\left(u^{-}_{j+\frac{1}{2}}\right)^2 + g\left(\rho^{-}_{j+\frac{1}{2}}\right)^2},\, 2u^{+}_{j+\frac{1}{2}} - \sqrt{\left(u^{+}_{j+\frac{1}{2}}\right)^2 + g\left(\rho^{+}_{j+\frac{1}{2}}\right)^2},\, 0\right\}. \end{aligned} \tag{4.25}$$

In the dispersive case, that is, when $\alpha \neq 0$, there is a global dependence of u on m and formula (4.25) is not true any more. However, when α is small, we still use (4.25) to estimate the local speeds. In the minmod function (1.58), we take $\theta = 1.3$.

In (4.25), $u^{\pm}_{j+\frac{1}{2}}$ are the values of the velocity at cell interfaces $x = x_{j+\frac{1}{2}}$, which are obtained as follows. Recalling that the momentum m and velocity u of the 2CH equation are related by (4.1b), we recover $u^{\pm}_{j+\frac{1}{2}}$ from m at each time step using a Fast Fourier approach as discussed in Chapter 3.

4.3.2 A Hybrid Finite Volume-Particle Method for the 2CH Equation

To construct a hybrid finite volume-particle (FVP) method for the 2CH equation, let us assume that at some time level t the computed solution is available. As described in Chapter 1, the density ρ is realized in terms of its cell averages, $\{\overline{\rho}_j(t)\}$, and thus it is globally available at all x via the piecewise linear reconstruction,

$$\widetilde{\rho}(x;t) = \overline{\rho}_j(t) + (\rho_x(t))_j(x - x_j), \quad x \in C_j, \tag{4.26}$$

where the cells C_j are given by (1.39) and the slopes $(\rho_x(t))_j$ are computed using the minmod limiter as given by (1.58).

On the other hand, the particle approximation of the momentum m is given in the form of a linear combination of Dirac δ-functions,

$$m^N(x,t) = \sum_{i=1}^{N} w_i(t)\delta(x - x_i^{\mathrm{p}}(t)), \tag{4.27}$$

where $x_i^{\mathrm{p}}(t)$ and $w_i(t)$ represent the location and weight of the ith particle, and N denotes the total number of particles in the computational domain Ω.

Using the special relationship between m and u given in (4.1b), one can directly compute the velocity u from the particle distribution of the momentum (4.27), see Chapter 2. Namely, u can be obtained by taking the convolution product $u = G * m$, where

$$G(|x - y|) = \frac{1}{2\alpha}\, e^{-|x-y|/\alpha},$$

is the Green's function associated with the Helmholtz operator in (4.1b). Thus, we have the following global (in x) approximation of u:

$$u^N(x,t) = \left(G * m^N\right)(x,t) = \frac{1}{2\alpha}\sum_{i=1}^{N} w_i(t)e^{-|x-x_i^{\mathrm{p}}(t)|/\alpha}. \tag{4.28}$$

The solution at the next time level is computed according to the following algorithm.

First, the cell averages $\{\bar{\rho}_j\}$ are evolved using the CU scheme as described in Chapter 1:

$$\frac{d}{dt}\bar{\rho}_j(t) = -\frac{H_{j+\frac{1}{2}}(t) - H_{j-\frac{1}{2}}(t)}{\Delta x}, \tag{4.29}$$

where (after omitting the time dependence of all of the indexed quantities)

$$H_{j+\frac{1}{2}} = \frac{\left(a^+_{j+\frac{1}{2}}\rho^-_{j+\frac{1}{2}} - a^-_{j+\frac{1}{2}}\rho^+_{j+\frac{1}{2}}\right)u_{j+\frac{1}{2}}}{a^+_{j+\frac{1}{2}} - a^-_{j+\frac{1}{2}}} + \frac{a^+_{j+\frac{1}{2}}a^-_{j+\frac{1}{2}}}{a^+_{j+\frac{1}{2}} - a^-_{j+\frac{1}{2}}}\left[\rho^+_{j+\frac{1}{2}} - \rho^-_{j+\frac{1}{2}}\right]. \tag{4.30}$$

Here, $\rho^{\pm}_{j+\frac{1}{2}}$ are the left and right values of the piecewise linear reconstruction (4.26) at $x = x_{j+\frac{1}{2}}$, $u_{j+\frac{1}{2}} = u^N(x_{j+\frac{1}{2}}, t)$ is the velocity obtained from (4.28), and the one-sided local speeds $a^{\pm}_{j+\frac{1}{2}}$ are estimated using (4.25) with $u^+_{j+\frac{1}{2}} = u^-_{j+\frac{1}{2}} = u_{j+\frac{1}{2}}$.

Next, following [22, 31, 33], we substitute (2.4) into a weak formulation of (4.1b) and obtain the following system of ODEs for $x^{\mathrm{p}}_i(t)$ and $w_i(t)$:

$$\begin{cases} \dfrac{dx^{\mathrm{p}}_i(t)}{dt} = u(x^{\mathrm{p}}_i(t), t), \\ \dfrac{dw_i(t)}{dt} + u_x(x^{\mathrm{p}}_i(t), t)\, w_i(t) = \beta_i(t). \end{cases} \tag{4.31}$$

Here, $u_x(x^{\mathrm{p}}_i(t), t)$ are computed from

$$u^N_x(x,t) = \left(G_x * m^N\right)(x,t) = -\frac{1}{2\alpha^2}\sum_{i=1}^{N} w_i(t)\mathrm{sgn}(x - x^{\mathrm{p}}_i(t))e^{-|x-x^{\mathrm{p}}_i(t)|/\alpha}, \tag{4.32}$$

and $\beta_i(t)$ is the contribution associated with the pressure term $-\frac{g}{2}(\rho^2)_x$:

$$\beta_i(t) = -\int\limits_{\Omega_i(t)} \frac{g}{2}(\rho^2)_x\, dx, \tag{4.33}$$

with $\Omega_i(t)$ being a domain that includes the ith particle and satisfies the following properties:

$$w_i(t) = \int\limits_{\Omega_i(t)} m(x,t)\, dx, \quad \Omega_1(t) \oplus \cdots \oplus \Omega_N(t) = \Omega. \tag{4.34}$$

In general, $\Omega_i(t)$ is not known (see, e.g., [25]), but it can be approximated by

$$\Omega_i(t) \approx \left[x^{\mathrm{p}}_{i-\frac{1}{2}}(t), x^{\mathrm{p}}_{i+\frac{1}{2}}(t)\right], \quad x^{\mathrm{p}}_{i+\frac{1}{2}}(t) := \frac{x^{\mathrm{p}}_i(t) + x^{\mathrm{p}}_{i+1}(t)}{2}, \tag{4.35}$$

and thus the integration in (4.33) results in

$$\beta_i(t) = -\frac{g}{2}\left\{\rho^2\big(x^{\mathrm{p}}_{i+\frac{1}{2}}(t)\big) - \rho^2\big(x^{\mathrm{p}}_{i-\frac{1}{2}}(t)\big)\right\}, \tag{4.36}$$

where $\rho\big(x^{\mathrm{p}}_{i+\frac{1}{2}}(t)\big) = \widetilde{\rho}\big(x^{\mathrm{p}}_{i+\frac{1}{2}}(t); t\big)$ are obtained using the piecewise linear reconstruction (4.26). To this end, one needs to find out which cell the point $x^{\mathrm{p}}_{i+\frac{1}{2}}(t)$ is located. This can be efficiently done since by a time step restriction associated with the particle method, every particle can either remain in the same cell or move to the neighboring cell within one time step.

The ODE system (4.29), (4.31) is to be integrated by an appropriate ODE solver. In our numerical experiments, we have used the third-order SSP Runge-Kutta method from [67, 68]. To this end, the initial positions of particles, $x^{\mathrm{p}}_i(0)$, and their weights, $w_i(0)$, are chosen so that

$$m^N(x,0) = \sum_{i=1}^{N} w_i(0)\delta(x - x^{\mathrm{p}}_i(0)),$$

represents a high-order approximation of the initial data $m(x,0)$ at time $t = 0$. One way of obtaining such an approximation is to use (4.34), (4.35) with $t = 0$. For example, a second-order midpoint quadrature applied to the integral in (4.34) will lead to $w_i(0) = |\Omega_i(0)|\, m(x^{\mathrm{p}}_i(0), 0)$.

4.4 Numerical Experiments

In this section, we apply a CU scheme and a hybrid FVP method to the 2CH equation subjected to physically relevant initial data to simulate the propagation of tsunami-type waves.

We are interested in using the 2CH equation as a model for the long time propagation of tsunami waves. To this extent, we consider the initial data generated in [26], for which they consider the situation for which a steep ridge on the bottom of the water body breaks off and causes a submarine landslide using a Savage-Hutter type model. In this scenario, the landslide creates surface waves which propagate in two directions. In one

direction, this yields a "tsunami-like" wave. For more information regarding the Savage-Hutter model, we refer the readers to [63, 143] and references therein. While this model seems sufficient for the generation of these waves, it is incapable of exhibiting the long time behavior of the wave, as the wave dissipates after a short time. To exhibit the long-time propagation of this "tsunami-like" wave, we solve (4.1) using this initial data with $\alpha = 0$ up to $t = .0015$. Here, time is measured in hours. When this simulation is ran, we observe the formation of two waves propagating in opposite directions. To study the dynamics of the propagation of our "tsunami-like" wave, we consider only the portion of the domain which captures the propagation of the right traveling wave. To accomplish this, we adjust the computational domain by removing the portion that does not capture this wave. This new data serves as the initial data used to simulate solutions to (4.1), with $g = 271008\,\mathrm{km/h^2}$ and $\alpha \geq 0$.

In the following numerical examples, we show how the speed and magnitude of the wave is affected by our choice of α. We run each of these simulations with 1024 grid points using a CU scheme with a uniform grid and minmod parameter $\theta = 1.3$. For the time evolution, we use a third-order strong stability preserving Runge-Kutta ODE solver as presented in [68]. The boundary conditions are taken to be periodic and the time steps were chosen adaptively as to satisfy the associated CFL conditions required for both the CU/FV scheme and the particle method.

In what follows, we show the necessity of adding dispersion (in the form of a nonzero α) to preserve the wave's height during longer time intervals. We also show that if we consider the hybrid FVP method for simulating the tsunami dynamics, then we can recover the solution with fewer grid points.

4.4.1 Tsunami Dynamics for $\alpha = 0$

In this example, we consider (4.1) with the initial data described above with $\alpha = 0$.

Recalling our previous discussion, we note that it was shown in [26], that for the classical Saint-Venant system, the modeling of long-time propagation and on-shore arrival of the tsunami-type waves is not feasible as the waves diffuse and decay over time. We expect to see a similar behavior for the $\alpha = 0$ case, given its close resemblance to this system. Indeed, we observe the following behavior in Figure 4.1.

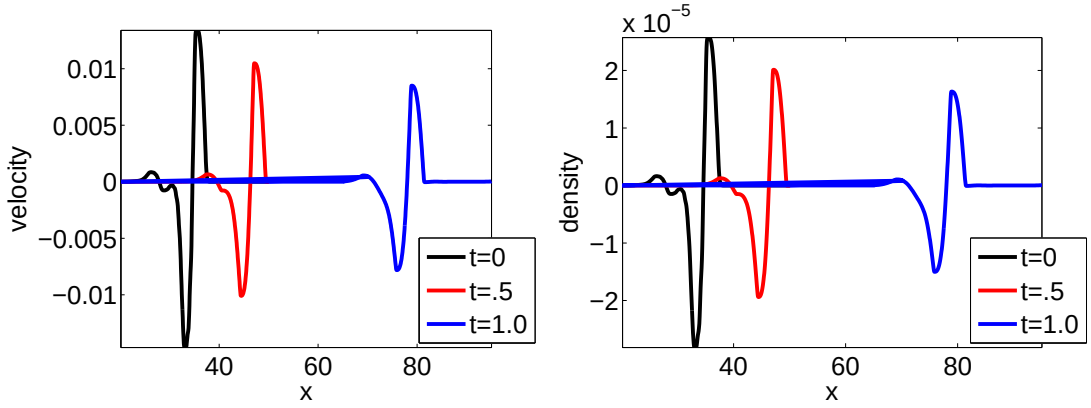

Figure 4.1: The velocity u and density ρ for the 2CH equation at various times with $\Delta x = 0.029$ using the CU scheme.

4.4.2 Tsunami Dynamics for $\alpha \neq 0$

To compensate for this feature, we may introduce dispersion into the equation by choosing a nonzero α. Of course, we must be careful not to add too much dispersion, or the wave profile will be destroyed. Indeed, if we look at Figure 4.2, we see that the height of the traveling tsunami wave is better preserved for a nonzero value of α. Indeed, we run the exact same simulation as the $\alpha = 0$ example with the exception that we consider $\alpha = 0.01$ in order to introduce dispersion into the equation.

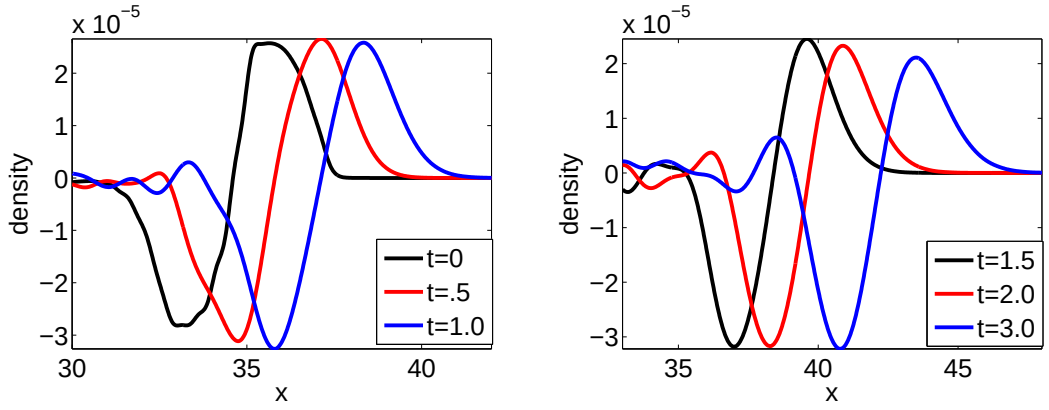

Figure 4.2: The density ρ for the 2CH equation obtained by at various times with $\Delta x = 0.029$, $\alpha = 0.01$ using the CU scheme.

We also see that if we choose α too large, as in Figure 4.3, then the initial tsunami wave decomposes into a train of oscillatory waves, and the profile is destroyed. In Figure 4.3, we take $\alpha = 0.05$, and compare it to the solution at $t = 0$. Here, we consider solutions up to $t = 1$.

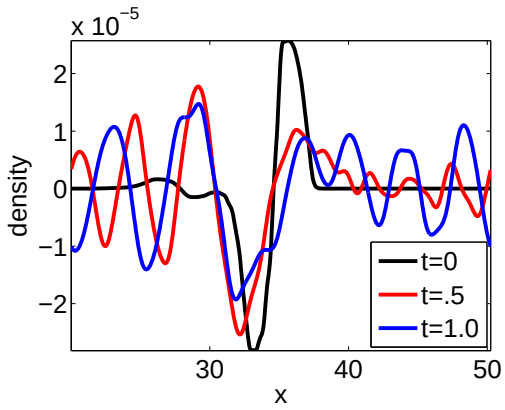

Figure 4.3: The density ρ for the 2CH equation obtained by at various times with $\Delta x = 0.029$, $\alpha = 0.05$ using the CU scheme.

We may tackle the problem of diffusion in another manner. Recall that the hybrid FVP method, presented in the previous section, seeks to combine the advantages of both the particle method and finite volume method to solve (4.1). One of the advantages of using the particle method is its Lagrangian nature which implies that the scheme is generally resistant to the numerical diffusion introduced in the approximation of the solution. Indeed, we see that we may recover the same solution via the FVP method with considerably less grid points, see Figure 4.4. Combining these results allow us to conclude that with a small perturbation of α, using the FVP method on (4.1) can potentially serve as viable model for the long time propagation of tsunami waves.

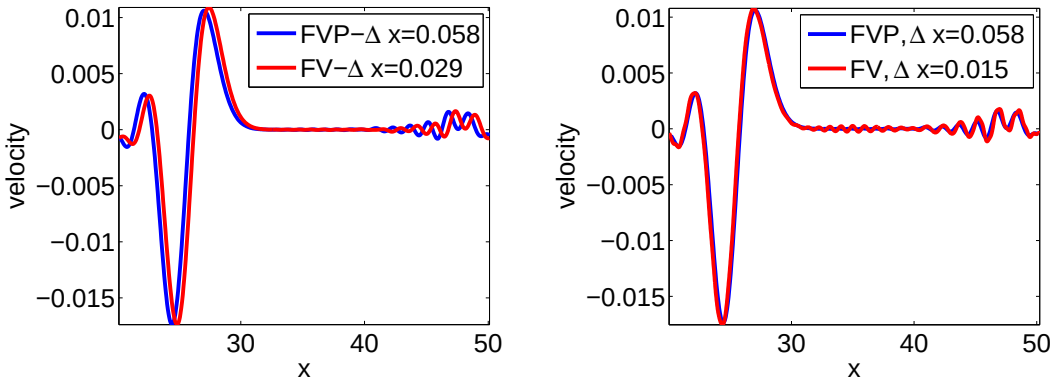

Figure 4.4: The velocity u for the 2CH equation obtained at time $t = 0.02$ using CU/FV scheme and FVP method , $\alpha = 0.1$.

Chapter 5

Conclusion

In this thesis, we established various analytical and numerical properties for a class of evolutionary PDEs. For instance, the concept of functions of bounded variation was used to establish the convergence of the particle method applied to the b-equation (2.1) for a special choice of the convolution kernel G and under a suitable class of initial data. These bounded variation estimates were derived by using conservation properties associated with the particle system. In turn, our convergence results allowed us to provide a novel method for proving the existence of a unique global weak solution to (2.1) for G given by (2.3) and for any $b > 1$.

We also applied a particle method to the CH equation, (3.1) to show that the non-linear interaction among peakon solutions for (3.1) is indeed an elastic collision. This was accomplished by using the conservation of momentum and conservation of kinetic energy associated with the particle system obtained from the particle method applied to the considered equations. We were able to visualize these results through a numerical implementation of the method. Futhermore, we were able to explicitly showcase some of the advantages a particle method holds over other numerical methods, such as a semi-discrete central upwind scheme, in simulating these solutions. For instance, the particle method allowed us to show multiple solutions for the peakon-antipeakon interaction for the CH equation. We were also able to show that the particle method can capture the interaction and dynamics of the solution with a lower resolution than a semi-discrete central upwind method.

Finally, we have introduced two numerical methods for solving a two component generalization of the CH equation, (4.1) which was derived in the context of shallow

water wave theory by considering a reduced form of the Green-Nadghi equations. Using both a semi-discrete central upwind scheme as well as a hybrid finite-volume particle method, we were able to show that for certain values of α, (4.1) may potentially serve as a viable model for the long time propagation of tsunami-like waves. For these values of α, which adds dispersion to (4.1), we have shown that the amplitude and speed of the wave was preserved for longer times than those solved by the classical Saint-Venant system. We were also able to explicitly showcase some of the advantages that a hybrid finite-volume particle method holds over other numerical methods, such as a semi-discrete central upwind scheme, in simulating these solutions. For instance, we are able to resolve the dynamics of the tsunami wave with a coarser grid when compared to the semi-discrete method.

To this extent, we have only provided an analytical and theoretical study of the dynamics and interaction of peakon solutions for (3.1). In the future, numerical experiments will performed on the analogous 2-D version of (3.1), i.e. the EPDiff equation, with arbitrary smooth initial data. We will also analyze the interaction and dynamics of peakon solutions generated from numerically solving the EPDiff equation. We have also only provided an initial study of numerically solving (4.1) from the viewpoint of a model for the propagation of tsunami waves. In the future, further studies will be conducted to better understand the effects of changing the length scale α on the solutions generated from solving (4.1).

REFERENCES

[1] R. Abgrall, *On essentially non-oscillatory schemes on unstructured meshes: analysis and implementation*, J. Comput. Phys., 114 (1994), pp. 45–58.

[2] P. Arminjon, M.-C. Viallon, and A. Madrane, *A finite volume extension of the Lax-Friedrichs and Nessyahu-Tadmor schemes for conservation laws on unstructured grids*, Int. J. Comput. Fluid Dyn., 9 (1997), pp. 1–22.

[3] R. Artebrant and H. Schroll, *Numerical simulation of Camassa-Holm peakons by adaptive upwinding*, Appl. Numer. Math., 56 (2006), pp. 695–711.

[4] E. Barthelemy, *Nonlinear shallow water theories for coastal waves*, Surveys in Geophysics, 25 (2004), pp. 315–337.

[5] M. Ben-Artzi and J. Falcovitz, *Generalized Riemann problems in computational fluid dynamics*, vol. 11 of Cambridge Monographs on Applied and Computational Mathematics, Cambridge University Press, Cambridge, 2003.

[6] F. Bianco, G. Puppo, and G. Russo, *High-order central schemes for hyperbolic systems of conservation laws*, SIAM J. Sci. Comput., 21 (1999), pp. 294–322.

[7] J. L. Bona, M. Chen, and J.-C. Saut, *Boussinesq equations and other systems for small-amplitude long waves in nonlinear dispersive media. I. Derivation and linear theory*, J. Nonlinear Sci., 12 (2002), pp. 283–318.

[8] ——, *Boussinesq equations and other systems for small-amplitude long waves in nonlinear dispersive media. II. The nonlinear theory*, Nonlinearity, 17 (2004), pp. 925–952.

[9] F. Bouchut, *Nonlinear stability of finite volume methods for hyperbolic conservation laws and well-balanced schemes for sources*, Frontiers in Mathematics, Birkhäuser Verlag, Basel, 2004.

[10] A. Bressan, *Hyperbolic systems of conservation laws. The one-dimensional Cauchy problem*, vol. 20 of Oxford Lecture Series in Mathematics and its Applications, Oxford University Press, Oxford, 2000.

[11] A. Bressan and A. Constantin, *Global conservative solutions of the Camassa-Holm equation*, Arch. Ration. Mech. Anal., 183 (2007), pp. 215–239.

[12] A. Bressan and A. Constantin, *Global dissipative solutions of the Camassa-Holm equation*, Anal. Appl. (Singap.), 5 (2007), pp. 1–27.

[13] M.-O. Bristeau, N. Goutal, and J. Sainte-Marie, *Numerical simulations of a non-hydrostatic shallow water model*, Comput. & Fluids, 47 (2011), pp. 51–64.

[14] M.-O. Bristeau and J. Sainte-Marie, *Derivation of a non-hydrostatic shallow water model; comparison with Saint-Venant and Boussinesq systems*, Discrete Contin. Dyn. Syst. Ser. B, 10 (2008), pp. 733–759.

[15] E. Bryant, *Tsunami: the Underrated Hazard*, Cambridge University Press, second ed.

[16] R. Camassa, D. Holm, and J. Hyman, *A new integrable shallow water equation*, Adv. Appl. Mech., 31 (1994), pp. 1–33.

[17] R. Camassa, J. Huang, and L. Lee, *On a completely integrable numerical scheme for a nonlinear shallow-water wave equation*, J. Nonlinear Math. Phys., 12 (2005), pp. 146–162.

[18] ——, *Integral and integrable algorithms for a nonlinear shallow-water wave equation*, J. Comput. Phys., 216 (2006), pp. 547–572.

[19] M. Castro Diaz, Y. Chen, A. Chertock, and Kurganov, *Solving two-mode shallow water equations using finite volume methods*, (2013). Preprint.

[20] S. Chen, C. Foias, D. Holm, E. Olson, E. Titi, and S. Wynne, *Camassa-Holm equations as a closure model for turbulent channel and pipe flow*, Phys. Rev. Lett., 81 (1998), pp. 5338–5341.

[21] A. Chertock, S. Cui, A. Kurganov, and T. Wu, *Well-balanced positivity preserving central-upwind scheme for the shallow water system with friction terms*, (2013). Preprint.

[22] A. Chertock, P. Du Toit, and J. Marsden, *Integration of the EPDiff equation by particle methods*, M2AN Math. Model. Numer. Anal., (2011). to appear.

[23] A. Chertock, E. Kashdan, and A. Kurganov, *Propagation of diffusing pollutant by a hybrid eulerian-lagrangian method*, in Hyperbolic problems: theory, numerics, applications (Lyon 2006), S. Benzoni-Gavage and D. Serre, eds., Springer, 2008, pp. 371–380.

[24] A. Chertock and A. Kurganov, *On a hybrid finite-volume particle method*, M2AN Math. Model. Numer. Anal, 38 (2004), pp. 1071–1091.

[25] ——, *On a practical implementation of particle methods*, Appl. Numer. Math., 56 (2006), pp. 1418–1431.

[26] A. Chertock, A. Kurganov, and J. Miller, *Central-upwind scheme for a non-hydrostatic Saint-Venant system*, submitted.

[27] A. Chertock, A. Kurganov, and G. Petrova, *Finite-volume-particle methods for models of transport of pollutant in shallow water*, J. Sci. Comput., 27 (2006), pp. 189–199.

[28] A. Chertock, A. Kurganov, Z. Qu, and T. Wu, *On a three-layer approximation of two-layer shallow water equations*, (2012). Preprint.

[29] A. Chertock and D. Levy, *Particle methods for dispersive equations*, J. Comput. Phys., 171 (2001), pp. 708–730.

[30] ——, *A particle method for the KdV equation*, J. Sci. Comput., 17 (2002), pp. 491–499.

[31] A. Chertock, J.-G. Liu, and T. Pendleton, *Convergence analysis of the particle method for the Camassa-Holm equation*, in Proceedings of the 13th International Conference on "Hyperbolic Problems: Theory, Numerics and Applications", P. G. Ciarlet and T.-T. Li, eds., Contemporary Applied Mathematics, 2012, pp. 356–373.

[32] A. Chertock, J.-G. Liu, and T. Pendleton, *Convergence of a particle method and global weak solutions of a family of evolutionary PDEs*, SIAM J. Numer. Anal., 50 (2012), pp. 1–21.

[33] A. Chertock, J.-G. Liu, and T. Pendleton, *Elastic collisions among peakon solutions for the camassa-holm equation*, (2013). Preprint.

[34] P. H. Chiu, L. Lee, and T. W. H. Sheu, *A dispersion-relation-preserving algorithm for a nonlinear shallow-water wave equation*, J. Comput. Phys., 228 (2009), pp. 8034–8052.

[35] A. J. Chorin, *Numerical study of slightly viscous flow*, J. Fluid Mech., 57 (1973), pp. 785–796.

[36] B. Cockburn, C. Johnson, C.-W. Shu, and E. Tadmor, *Advanced numerical approximation of nonlinear hyperbolic equations*, vol. 1697 of Lecture Notes in Mathematics, Springer-Verlag, Berlin, 1998. Papers from the C.I.M.E. Summer School held in Cetraro, June 23–28, 1997, Edited by Alfio Quarteroni, Fondazione C.I.M.E.. [C.I.M.E. Foundation].

[37] G. Coclite and K. Karlsen, *On the well-posedness of the degasperis-procesi equation*, J. Funct. Anal., 233 (2006), pp. 60–91.

[38] G. Coclite, K. Karlsen, and N. Risebro, *A convergent finite difference scheme for the Camassa-Holm equation with general H^1 initial data*, SIAM J. Numer. Anal., 46 (2008), pp. 1554–1579.

[39] D. Cohen, B. Owren, and X. Raynaud, *Multi-symplectic integration of the Camassa-Holm equation*, J. Comput. Phys., 227 (2008), pp. 5492–5512.

[40] A. Constantin and J. Escher, *Global existence and blow-up for a shallow water equation*, Ann. Scuola Norm. Sup. Pisa Cl. Sci. (4), 26 (1998), pp. 303–328.

[41] ——, *Global weak solutions for a shallow water equation*, Indiana Univ. Math. J., 47 (1998), pp. 1527–1545.

[42] A. Constantin and R. I. Ivanov, *On an integrable two-component Camassa-Holm shallow water system*, Phys. Lett. A, 372 (2008), pp. 7129–7132.

[43] A. Constantin and B. Kolev, *On the geometric approach to the motion of inertial mechanical systems*, J. Phys. A: Math. Gen., 35 (2002), pp. R51–R79.

[44] ——, *Geodesic flow on the diffeomorphism group of the circle*, Comment. Math. Helv., 78 (2003), pp. 787–804.

[45] A. Constantin and D. Lannes, *The hydrodynamical relevance of the Camassa-Holm and Degasperis-Procesi equations*, Arch. Ration. Mech. Anal., 192 (2009), pp. 165–186.

[46] A. Constantin and L. Molinet, *Global weak solutions for a shallow water equation*, Comm. Math. Phys., 211 (2000), pp. 45–61.

[47] A. Constantin and W. A. Strauss, *Stability of peakons*, Comm. Pure Appl. Math., 53 (2000), pp. 603–610.

[48] L. A. Constantin and A. Kurganov, *Adaptive central-upwind schemes for hyperbolic systems of conservation laws*, in Hyperbolic problems: theory, numerics and applications. I, Yokohama Publ., Yokohama, 2006, pp. 95–103.

[49] G.-H. Cottet and P. D. Koumoutsakos, *Vortex methods*, Cambridge University Press, Cambridge, 2000. Theory and practice.

[50] G.-H. Cottet and S. Mas-Gallic, *A particle method to solve transport-diffusion equations, part 1: the linear case*, Tech. Report 115, Ecole Polytechnique, Palaiseau, France, 1983.

[51] H. Dai, *Model equations for nonlinear dispersive waves in a compressible mooney-rivlin rod*, Acta Mech., 127 (1998), pp. 193–207.

[52] A. de Saint-Venant, *Thèorie du mouvement non-permanent des eaux, avec application aux crues des rivière at à l'introduction des marèes dans leur lit.*, C.R. Acad. Sci. Paris, 73 (1871), pp. 147–154.

[53] A. Degasperis, D. Holm, and A. Hone, *A new integrable equation with peakon solutions*, Teoret. Mat. Phys., 133 (2002), pp. 1463–1474.

[54] A. Degasperis, D. D. Holm, and A. N. W. Hone, *Integrable and non-integrable equations with peakons*, in Nonlinear physics: theory and experiment, II (Gallipoli, 2002), World Sci. Publ., River Edge, NJ, 2003, pp. 37–43.

[55] A. Degasperis and M. Procesi, *Asymptotic integrability*, in Symmetry and perturbation theory (Rome, 1998), World Sci. Publ., River Edge, NJ, 1999, pp. 23–37.

[56] P. Degond and F. Mustieles, *A deterministic approximation of diffusion equations using particles*, SIAM J. Sci. Stat. Comp., 11 (1990), pp. 293–310.

[57] H. Dullin, G. Gottwald, and D. Holm, *An integrable shallow water equation with linear and nonlinear dispersion*, Phys. Rev. Lett., 87 (2001), pp. 194501–194504.

[58] K. El Dika and L. Molinet, *Exponential decay of H^1-localized solutions and stability of the train of N solitary waves for the Camassa-Holm equation*, Philos. Trans. R. Soc. Lond. Ser. A Math. Phys. Eng. Sci., 365 (2007), pp. 2313–2331.

[59] J. Escher, O. Lechtenfeld, and Z. Yin, *Well-posedness and blow-up phenomena for the 2-component Camassa-Holm equation*, Discrete Contin. Dyn. Syst., 19 (2007), pp. 493–513.

[60] J. Escher, Y. Liu, and Z. Yin, *Global weak solutions and blow-up structure for the degasperis-procesi equation*, J. Funct. Anal., 241 (2006), pp. 457–485.

[61] J. Escher and Z. Yin, *Well-posedness, blow-up phenomena, and global solutions for the b-equation*, J. Reine Angew. Math., 624 (2008), pp. 51–80.

[62] B.-F. Feng, K.-i. Maruno, and Y. Ohta, *A self-adaptive moving mesh method for the Camassa-Holm equation*, J. Comput. Appl. Math., 235 (2010), pp. 229–243.

[63] E. D. Fernández-Nieto, F. Bouchut, D. Bresch, M. J. Castro Díaz, and A. Mangeney, *A new Savage-Hutter type model for submarine avalanches and generated tsunami*, J. Comput. Phys., 227 (2008), pp. 7720–7754.

[64] E. Godlewski and P.-A. Raviart, *Numerical approximation of hyperbolic systems of conservation laws*, vol. 118 of Applied Mathematical Sciences, Springer-Verlag, New York, 1996.

[65] S. K. Godunov, *A difference method for numerical calculation of discontinuous solutions of the equations of hydrodynamics*, Mat. Sb. (N.S.), 47 (89) (1959), pp. 271–306.

[66] S. Gottlieb, *On high order strong stability preserving Runge-Kutta and multi step time discretizations*, J. Sci. Comput., 25 (2005), pp. 105–128.

[67] S. Gottlieb, D. Ketcheson, and C.-W. Shu, *Strong stability preserving Runge-Kutta and multistep time discretizations*, World Scientific Publishing Co. Pte. Ltd., Hackensack, NJ, 2011.

[68] S. Gottlieb, C.-W. Shu, and E. Tadmor, *Strong stability-preserving high-order time discretization methods*, SIAM Rev., 43 (2001), pp. 89–112.

[69] A. Green and P. Naghdi, *A derivation of equations for wave propagation in water at variable depth*, J. Fluid Mech., 78 (1976), pp. 237–246.

[70] O. H. Hald, *Convergence of vortex methods*, in Vortex methods and vortex motion, SIAM, Philadelphia, PA, 1991, pp. 33–58.

[71] A. Harten, B. Engquist, S. Osher, and S. R. Chakravarthy, *Uniformly high-order accurate essentially nonoscillatory schemes. III*, J. Comput. Phys., 71 (1987), pp. 231–303.

[72] A. Harten and S. Osher, *Uniformly high-order accurate nonoscillatory schemes. I*, SIAM J. Numer. Anal., 24 (1987), pp. 279–309.

[73] A. Hirani, J. Marsden, and J. Arvo, *Averaged template matching equations*, in EMMCVPR, vol. 2134 of Lecture Notes in Computer Science, Springer, 2001, pp. 528–543.

[74] H. Holden and X. Raynaud, *Convergence of a finite difference scheme for the Camassa-Holm equation*, SIAM J. Numer. Anal., 44 (2006), pp. 1655–1680 (electronic).

[75] ——, *A convergent numerical scheme for the Camassa-Holm equation based on multipeakons*, Discrete Contin. Dyn. Syst., 14 (2006), pp. 505–523.

[76] D. Holm and J. Marsden, *Momentum maps and measure-valued solutions (peakons, filaments, and sheets) for the EPDiff equation*, in The breadth of symplectic and Poisson geometry, vol. 232 of Progr. Math., Birkhäuser Boston, Boston, MA, 2005, pp. 203–235.

[77] D. Holm, J. Ratnanather, A. Trouvé, and L. Younes, *Soliton dynamics in computational anatomy*, NeuroImage, 23 (2004), pp. S170 – S178.

[78] D. Holm, T. Schmah, and C. Stoica, *Geometric mechanics and symmetry*, vol. 12 of Oxford Texts in Applied and Engineering Mathematics, Oxford University Press, Oxford, 2009.

[79] D. Holm and M. Staley, *Interaction dynamics of singular wave fronts.* under "Recent Papers" at http://cnls.lanl.gov/∼staley/.

[80] ——, *Nonlinear balance and exchange of stability of dynamics of solitons, peakons, ramps/cliffs and leftons in a* $1+1$ *nonlinear evolutionary PDE*, Phys. Lett. A, 308 (2003), pp. 437–444.

[81] ——, *Wave structure and nonlinear balances in a family of evolutionary PDEs*, SIAM J. Appl. Dyn. Syst., 2 (2003), pp. 323–380 (electronic).

[82] D. D. Holm, L. Ó Náraigh, and C. Tronci, *Singular solutions of a modified two-component Camassa-Holm equation*, Phys. Rev. E (3), 79 (2009), pp. 016601, 13.

[83] L. Hörmander, *Lectures on nonlinear hyperbolic differential equations*, vol. 26 of Mathématiques & Applications (Berlin) [Mathematics & Applications], Springer-Verlag, Berlin, 1997.

[84] R. Ivanov, *Two-component integrable systems modelling shallow water waves: the constant vorticity case*, Wave Motion, 46 (2009), pp. 389–396.

[85] G.-S. Jiang and E. Tadmor, *Nonoscillatory central schemes for multidimensional hyperbolic conservation laws*, SIAM J. Sci. Comput., 19 (1998), pp. 1892–1917 (electronic).

[86] R. S. Johnson, *Camassa-Holm, Korteweg-de Vries and related models for water waves*, J. Fluid Mech., 455 (2002), pp. 63–82.

[87] R. S. Johnson, *The classical problem of water waves: a reservoir of integrable and nearly-integrable equations*, J. Nonlinear Math. Phys., 10 (2003), pp. 72–92.

[88] H. Kalisch and J. Lenells, *Numerical study of traveling-wave solutions for the Camassa-Holm equation*, Chaos Solitons Fractals, 25 (2005), pp. 287–298.

[89] H. Kalisch and X. Raynaud, *Convergence of a spectral projection of the Camassa-Holm equation*, Numer. Methods Partial Differential Equations, 22 (2006), pp. 1197–1215.

[90] D. Korteweg and G. de Vries, *On the change of form of long waves advancing in a rectangular canal, and on a new type of long stationary waves*, Philosophical Magazine, 39 (1895), pp. 422–443.

[91] D. Kröner, *Numerical schemes for conservation laws*, Wiley-Teubner Series Advances in Numerical Mathematics, John Wiley & Sons Ltd., Chichester, 1997.

[92] A. Kurganov and D. Levy, *A third-order semidiscrete central scheme for conservation laws and convection-diffusion equations*, SIAM J. Sci. Comput., 22 (2000), pp. 1461–1488 (electronic).

[93] ——, *Central-upwind schemes for the Saint-Venant system*, M2AN Math. Model. Numer. Anal., 36 (2002), pp. 397–425.

[94] A. Kurganov and C.-T. Lin, *On the reduction of numerical dissipation in central-upwind schemes*, Commun. Comput. Phys., 2 (2007), pp. 141–163.

[95] A. Kurganov and J. Miller, *Central-upwind scheme for Savage-Hutter type model of submarine landslides and generated tsunami waves*, (2012). Preprint.

[96] A. Kurganov, S. Noelle, and G. Petrova, *Semidiscrete central-upwind schemes for hyperbolic conservation laws and Hamilton-Jacobi equations*, SIAM J. Sci. Comput., 23 (2001), pp. 707–740 (electronic).

[97] A. Kurganov and G. Petrova, *A third-order semi-discrete genuinely multidimensional central scheme for hyperbolic conservation laws and related problems*, Numer. Math., 88 (2001), pp. 683–729.

[98] ——, *A second-order well-balanced positivity preserving central-upwind scheme for the Saint-Venant system*, Commun. Math. Sci., 5 (2007), pp. 133–160.

[99] A. Kurganov and G. Petrova, *A central-upwind scheme for nonlinear water waves generated by submarine landslides*, in Hyperbolic problems: theory, numerics, applications, Springer, Berlin, 2008, pp. 635–642.

[100] A. Kurganov and G. Petrova, *Central-upwind schemes for two-layer shallow water equations*, SIAM J. Sci. Comput., 31 (2009), pp. 1742–1773.

[101] A. Kurganov and E. Tadmor, *New high-resolution central schemes for nonlinear conservation laws and convection-diffusion equations*, J. Comput. Phys., 160 (2000), pp. 241–282.

[102] P. D. Lax, *Integrals of nonlinear equations of evolution and solitary waves*, Comm. Pure Appl. Math., 21 (1968), pp. 467–490.

[103] J. Lenells, *Stability of periodic peakons*, Int. Math. Res. Not., (2004), pp. 485–499.

[104] R. J. LeVeque, *Finite volume methods for hyperbolic problems*, Cambridge Texts in Applied Mathematics, Cambridge University Press, Cambridge, 2002.

[105] R. J. LeVeque, D. L. George, and M. J. Berger, *Tsunami modelling with adaptively refined finite volume methods*, Acta Numer., 20 (2011), pp. 211–289.

[106] D. Levy, G. Puppo, and G. Russo, *Central WENO schemes for hyperbolic systems of conservation laws*, M2AN Math. Model. Numer. Anal., 33 (1999), pp. 547–571.

[107] J. B. Li and Y. S. Li, *Bifurcations of travelling wave solutions for a two-component Camassa-Holm equation*, Acta Math. Sin. (Engl. Ser.), 24 (2008), pp. 1319–1330.

[108] Y. Li and P. Olver, *Well-posedness and blow-up solutions for an integrable nonlinearly dispersive model wave equation*, J. Differential Equations, 162 (2000), pp. 27–63.

[109] K.-A. Lie and S. Noelle, *An improved quadrature rule for the flux-computation in staggered central difference schemes in multidimensions*, J. Sci. Comput., 18 (2003), pp. 69–81.

[110] Z. Lin and Y. Liu, *Stability of peakons for the Degasperis-Procesi equation*, Comm. Pure Appl. Math., 62 (2009), pp. 125–146.

[111] P.-L. Lions and S. Mas-Gallic, *Une méthode particulaire déterministe pour des équations diffusives non linéaires*, C. R. Acad. Sci. Paris Sér. I Math., 332 (2001), pp. 369–376.

[112] S. F. Liotta, V. Romano, and G. Russo, *Central schemes for balance laws of relaxation type*, SIAM J. Numer. Anal., 38 (2000), pp. 1337–1356.

[113] J.-G. Liu and Z. Xin, *Convergence of vortex methods for weak solutions to the 2-D Euler equations with vortex sheets data*, Comm. Pure Appl. Math., 48 (1995), pp. 611–628.

[114] ——, *Convergence of point vortex method for 2-D vortex sheet*, Math. Comp., 70 (2001), pp. 565–606.

[115] X.-D. Liu and E. Tadmor, *Third order nonoscillatory central scheme for hyperbolic conservation laws*, Numer. Math., 79 (1998), pp. 397–425.

[116] Y. Liu and Z. Yin, *Global existence and blow-up phenomena for the degasperis-procesi equation*, Comm. Math. Phys., 267 (2006), pp. 801–820.

[117] H. Lundmark and J. Szmigielski, *Multi-peakon solutions of the Degasperis-Procesi equation*, Inverse Problems, 19 (2003), pp. 1241–1245.

[118] T. Matsuo and Y. Miyatake, *Conservative finite difference schemes for the degasperis-procesi equation*, METR, 23 (2010), p. 17pp.

[119] T. Matsuo and H. Yamaguchi, *An energy-conserving Galerkin scheme for a class of nonlinear dispersive equations*, J. Comput. Phys., 228 (2009), pp. 4346–4358.

[120] R. C. McOwen, *Partial differential equations methods and applications*, Prentice Hall, second ed., 2003.

[121] L. Molinet, *On well-posedness results for Camassa-Holm equation on the line: a survey*, J. Nonlinear Math. Phys., 11 (2004), pp. 521–533.

[122] H. Nessyahu and E. Tadmor, *Nonoscillatory central differencing for hyperbolic conservation laws*, J. Comput. Phys., 87 (1990), pp. 408–463.

[123] P. J. Olver and P. Rosenau, *Tri-Hamiltonian duality between solitons and solitary-wave solutions having compact support*, Phys. Rev. E (3), 53 (1996), pp. 1900–1906.

[124] M. Ortiz, E. Reyes-Gomez, and H. Velez-Munoz, *A fast preliminary estimation model for transoceanic tsunami propagation*, Geofisica International.

[125] L. Pareschi, *Central differencing based numerical schemes for hyperbolic conservation laws with relaxation terms*, SIAM J. Numer. Anal., 39 (2001), pp. 1395–1417 (electronic).

[126] L. Pareschi, G. Puppo, and G. Russo, *Central Runge-Kutta schemes for conservation laws*, SIAM J. Sci. Comput., 26 (2005), pp. 979–999.

[127] E. Pelinovsky, T. Talipova, and C. Kurkin, A.and Kharif, *Nonlinear mechanism of tsunami wave generation by atmospheric disturbances*, Natural Hazard and Earth Sci., 1 (2001), pp. 243–250.

[128] Y. Pinchover and J. Rubinstein, *An introduction to partial differential equations*, Cambridge University Press, Cambridge, 2005.

[129] C. R. and D. Holm, *An integrable shallow water equation with peaked solitons*, Phys. Rev. Lett., 71 (1993), pp. 1661–1664.

[130] M. Rahman, *Water Waves: Relating Modern Theory to Advanced Engineering Practice.*

[131] P.-A. Raviart, *An analysis of particle methods*, in Numerical methods in fluid dynamics (Como, 1983), vol. 1127 of Lecture Notes in Math., Springer, Berlin, 1985, pp. 243–324.

[132] G. Rocca, M. Lombardo, M. Sammartino, and V. Sciacca, *Singularity tracking for Camassa-Holm and Prandtl's equations*, Appl. Numer. Math., 56 (2006), pp. 1108–1122.

[133] G. Rodríguez-Blanco, *On the cauchy problem for the camassa-holm equation*, Nonlinear Anal., 46 (2001), pp. 309–327.

[134] G. Russo, *Central schemes and systems of balance laws*, in Hyperbolic partial differential equations (Hamburg, 2001), Friedr. Vieweg, Braunschweig, 2002, pp. 59–114.

[135] A. Shabat and L. Martínez Alonso, *On the prolongation of a hierarchy of hydrodynamic chains*, in New trends in integrability and partial solvability, vol. 132 of NATO Sci. Ser. II Math. Phys. Chem., Kluwer Acad. Publ., Dordrecht, 2004, pp. 263–280.

[136] M. Shearer, *The Riemann problem for* 2×2 *systems of hyperbolic conservation laws with case I quadratic nonlinearities*, J. Differential Equations, 80 (1989), pp. 343–363.

[137] M. Shearer and S. Schecter, *Undercompressive shocks for nonstrictly hyperbolic conservation laws*, J. Dynamics and Different. Eq., 3 (1989), pp. 199–271.

[138] W. A. Strauss, *Partial differential equations*, John Wiley & Sons Ltd., Chichester, second ed., 2008. An introduction.

[139] C. Sulem and P.-L. Sulem, *The nonlinear Schrödinger equation*, vol. 139 of Applied Mathematical Sciences, Springer-Verlag, New York, 1999. Self-focusing and wave collapse.

[140] J. F. Toland, *Stokes waves*, Topol. Methods Nonlinear Anal., 7 (1996), pp. 1–48.

[141] E. F. Toro, *Riemann solvers and numerical methods for fluid dynamics*, Springer-Verlag, Berlin, third ed., 2009. A practical introduction.

[142] A. Tveito and R. Winther, *Introduction to partial differential equations*, vol. 29 of Texts in Applied Mathematics, Springer-Verlag, Berlin, 2005. A computational approach, Corrected second printing of the 1998 original.

[143] Y. Wang, K. Hutter, and S. P. Pudasaini, *The Savage-Hutter theory: a system of partial differential equations for avalanche flows of snow, debris, and mud*, ZAMM Z. Angew. Math. Mech., 84 (2004), pp. 507–527.

[144] G. B. Whitham, *Linear and nonlinear waves*, Wiley-Interscience [John Wiley & Sons], New York, 1974. Pure and Applied Mathematics.

[145] Z. Xin and P. Zhang, *On the weak solutions to a shallow water equation*, Comm. Pure Appl. Math., 53 (2000), pp. 1411–1433.

[146] Y. Xu and C.-W. Shu, *A local discontinuous Galerkin method for the Camassa-Holm equation*, SIAM J. Numer. Anal., 46 (2008), pp. 1998–2021.

[147] Z. Yin, *On the cauchy problem for an integrable equation with peakon solutions*, Ill. J. Math., 47 (2003), pp. 649–666.

[148] ——, *Global weak solutions for a new periodic integrable equation with peakon solutions*, J. Funct. Anal., 212 (2004), pp. 182–194.

[149] E. C. Zachmanoglou and D. W. Thoe, *Introduction to partial differential equations with applications*, Dover Publications Inc., New York, second ed., 1986.